Strain Distribution in the Tibia as a Function of Applied Loading through a Revision Total Knee Replacement

Wright, Samantha

Award date:
2015

Awarding institution:
University of Bath

Strain Distribution in the Tibia as a Function of Applied Loading through a Revision Total Knee Replacement

Samantha Jane Wright

A thesis submitted for the degree of Doctor of Philosophy

University of Bath

Centre for Orthopaedic Biomechanics

Department of Mechanical Engineering

June 2015

Signed..

Abstract

The growth in primary total knee replacement procedures coupled with changes in patient demographics and life expectancy has led to corresponding growth in revision total knee replacements. Revision components usually include intramedullary stems to aid fixation and manage bone stock deficiencies. Stemmed tibial components are thought to have an adverse effect on load transfer, contributing to complications in revision knee replacement. Current in vitro testing rarely incorporates physiological loading which considers the compartmental load share across the tibial plateau or includes the patellofemoral joint.

A robust experimental test protocol was developed to assess the effect of the applied loading on strain distribution in the tibia for the evaluation of stemmed revision tibial components. A tibiofemoral loading rig was developed to incorporate compartmental load distribution. This increased the confidence in the strain distribution results, but did not include potential effects of the load transfer associated with the patellofemoral joint. A combined loading rig included the force transferred through both the tibiofemoral and patellofemoral joints. It was therefore possible to compare the results from this rig to those of the tibiofemoral rig whilst allowing testing at higher flexion angles.

Investigations were conducted into the effect of applied loading on strain distribution through the tibia. The results demonstrate that implanting a revision tibial component, increasing the flexion angle and including the patellofemoral joint all reduce the principal compressive strains through the tibia. However, below the stem tip the compressive strains significantly increased following implantation of the tibial component. This research has demonstrated the issues with a current component design, which contribute to proximal strain shielding and end of stem pain linked to distal strain concentrations. A novel test methodology has been developed which better simulates physiological loading and can be used in future pre-clinical evaluation of revision total knee implants.

Acknowledgements

I would like to thank everyone who has either contributed to this research or supported me through the successes and the setbacks. I very much appreciate the constant support and wisdom that I have received from my supervisors, Professor Tony Miles and Dr Sabina Gheduzzi. I also wish to acknowledge the Biomechanics laboratory technician, Nick Waywell and colleague Tim Holsgrove who between them have been of great assistance with the experimental work undertaken. I am indebted to all of those who have provided me with the wealth of clinical knowledge and equipment necessary to conduct this research, with a special mention to Sam Horrocks, Gearoid Walsh and Mr Andy Toms. My thanks also go to the Enid Linder Foundation for funding my scholarship which has supported me throughout this journey. Finally, I especially wish to thank Tom Micklewright and the rest of my wonderful family whose endless encouragement and guidance has enabled me to reach this point.

Table of Contents

List of Figures

List of Tables

List of Abbreviations

AORI - Anderson Orthopaedic Research Institute

BW - Body Weight

CMM - Coordinate Measuring Machine

DIC - Digital Image Correlation

FEA - Finite Element Analysis

Fps - Frames per Second

NJR - National Joint Registry

PE - Polyethylene

PFJ - Patellofemoral Joint

RTKR - Revision Total Knee Replacement

RoM - Range of Motion

TFJ - Tibiofemoral Joint

TKR - Total Knee Replacement

1 Introduction

1.1 Background

Total joint replacement is one of the most widely used surgical interventions to treat joint disorders. The operation involves the replacement of the articulating surfaces in the joint by removal of bone from a failed joint and the insertion of an artificial replacement to restore function and alleviate pain. The most common joint replacement operations relate to the hip and knee as these are the joints most affected by arthritis and are exposed to high loads due to their weight bearing nature. It is estimated that there are currently 7.2 million people living with hip or knee replacements in the USA (Maradit-Kremers et al. 2014) which is approximately one in 45 people (United States Census Bureau 2015). This compares to approximately one in 50 people having a hip or knee replacement in the past 10 years in the UK (National Joint Registry 2014a, Office for National Statistics 2015). The overall success of these joint replacements has resulted in increased demand, driven further research and led to the formation of joint registers in the UK and elsewhere. Such developments have improved our understanding of the factors contributing to the patient outcomes associated with these procedures.

Total hip replacements have been performed regularly since the first metal-on-metal prosthesis in 1953 and are widely regarded as the more successful of the joint replacement surgeries (Bourne et al. 2010). Their success can be attributed to the inherent stability of the hip joint ball and socket geometry and relative simplicity compared to the knee joint. Whilst 95.8% patients report joint related improvements following their hip replacement operation, only 91.6% are satisfied with their primary knee replacement (The Health and Social Care Information Centre 2010). Despite this, the number of total knee replacements has now surpassed hip replacements with 676,082 primary knees recorded in the National Joint Registry for England, Wales and Northern Ireland over the past 10 years compared to 620,400 hip replacements (National Joint Registry 2014a). In the UK in 2013, 76,274 primary hips were performed compared to 85,920 primary knees (National Joint Registry 2014a). Recent projections for national life expectancy show a continued rise to 85.7 years for men and 87.6 for women by 2030 (Bennett et al. 2015). Coupled with this, the older generations are increasingly active compared to their predecessors. All of these factors increase the demands on the knee joint and contribute to the growing requirement for replacement. If primary knee replacements are unsuccessful, a revision operation is often performed.

In 2013 there were 5,783 revision total knee replacement (RTKR) procedures performed in the UK (National Joint Registry 2014a). Revision surgery is carried out when the primary component fails, so it follows that the number of revisions are increasing in line with the growth in primary procedures. At the same time a trend for patients undergoing primary knee surgery at a younger age has been observed and therefore they are increasingly outliving the average expected lifetime of the primary components. Revision total knee replacement procedures involve removing the primary components and replacing them with more advanced and more invasive replacement components. The revision components typically utilise stems that insert into the long axis of the bone, providing fixation stability to address the bone stock loss prevalent in failed primary knee replacements.

The implantation of stemmed tibial components during revision total knee replacement surgery is believed to alter the strain distribution through the tibia and may lead to proximal bone resorption and patient reported pain at the stem tip. Thus an understanding of load transfer aspects associated with knee replacement is important to address this. The in vivo use of instrumented tibial components has demonstrated that the compartmental load share across the tibial condyles changes during daily living activities (Mundermann et al. 2008). Despite this, compartmental load share is not directly measured or controlled in typical experimental studies that assess load transfer through the tibia. Importantly, in past research and pre-clinical testing of knee components, the patellofemoral joint is not accounted for when considering the transfer of load through to the tibia.

1.2 Aims

The focus of the research was to address the reported clinical issues with RTKR by developing a methodology to measure strain distribution through the tibia. This included the development of an experimental rig to enable the evaluation of revision tibial components for investigation into the reported bone resorption and pain at the end of the stem region. The study aimed to develop experimental methods to measure the influence of both compartmental loading and the effects of loading associated with the tibiofemoral and patellofemoral joints in the knee. This should aid future implant design parameters, contribute to the development in the methodology and experimental testing for evaluation of RTKR components in the future and ensure optimum pre-clinical testing.

2 The Natural Knee

To understand the concept of replacing the knee joint it is important to appreciate the anatomy and biomechanics of the natural knee. The knee is the largest joint in the human body (Nordin and Frankel 2001) and is located at the intersection with the femur, tibia, fibula and patella as shown in Figure 1. It has six degrees of freedom, three rotational and three translational, as illustrated in Figure 2(a), which are often described based on the planes of motion shown in Figure 2(b). The six degrees of freedom are provided by a combination of two joints within the knee structure, where one of these is the articulation between the tibia and femur (Tibiofemoral joint - TFJ) and the other between the patella and femur (Patellofemoral joint - PFJ) (Figure 3a).

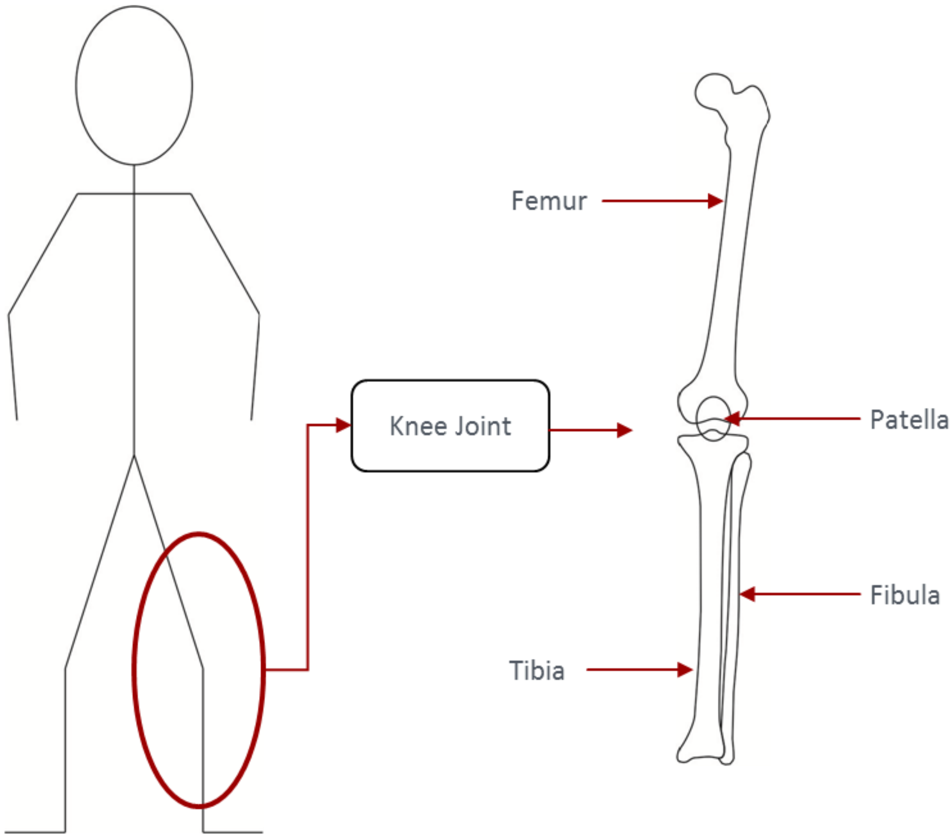

Figure 1 - The bones of the lower limb and the knee joint

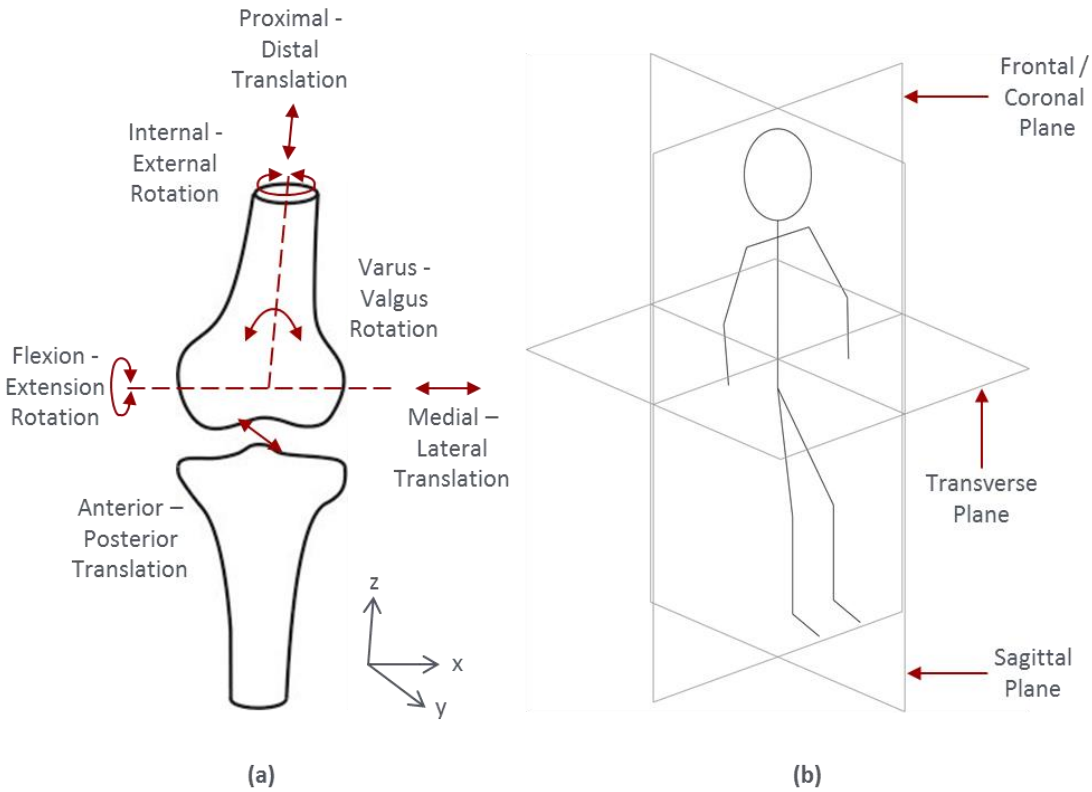

Figure 2 – The six degrees of freedom of the knee joint (a) and the three anatomical planes of motion (b)

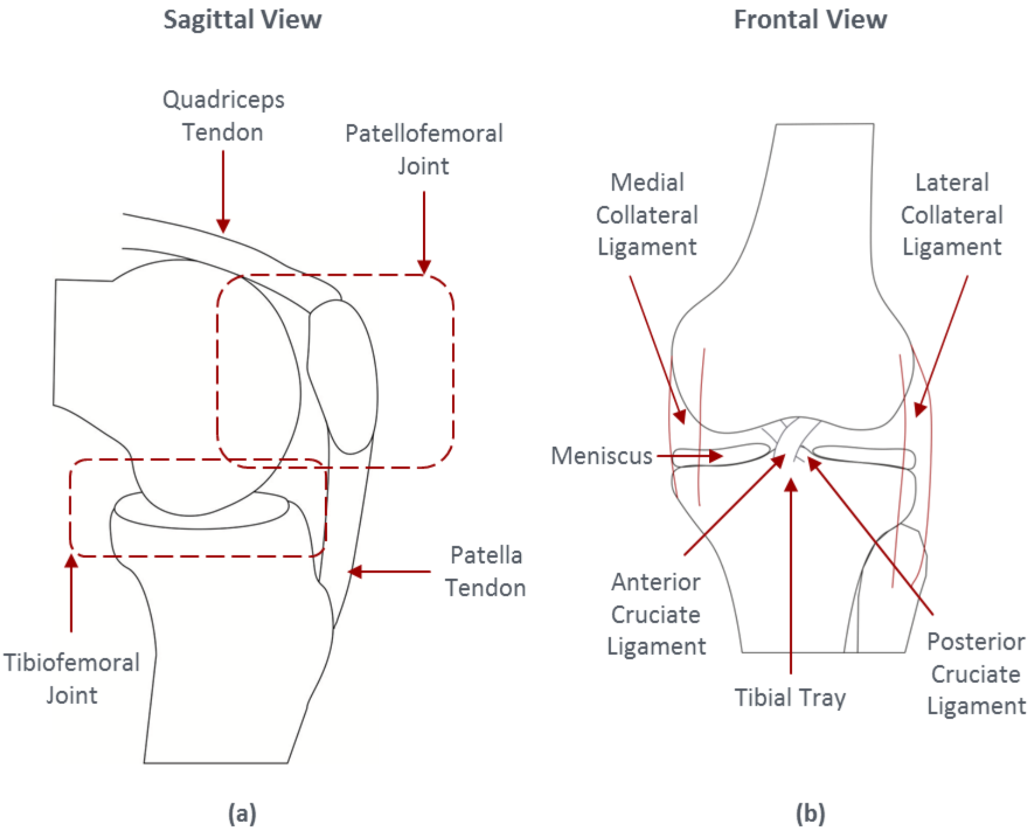

Figure 3 - The two joints and (a) the four main ligaments (b) of the knee

The stability and motions of the knee are aided by the surrounding soft tissues. These include the patella tendon and quadriceps tendon that locate and support the patella to accommodate high extensor forces through the patellofemoral joint (Figure 3a). There are four main ligaments which are illustrated in Figure 3(b) that also act to stabilise the knee and guide motion. The medial and lateral collateral ligaments connect across the outer condyles of the femur and tibia to provide guidance for varus - valgus motion. The anterior and posterior cruciate ligaments, which guide anterior - posterior (A-P) motion, are located in between the femoral condyles at the centre of the tibial tray. The meniscus is a soft tissue structure that sits within the tibiofemoral joint and will be discussed in detail. Lastly, the groups of quadriceps and hamstring muscles act to provide flexion and extension of the knee joint and also contribute to knee stability. The importance of all of the surrounding soft tissues is highlighted in knee surgery as the function and longevity of the procedure is considered to be dependent on the soft-tissue balance achieved and the consequences on the knee kinematics (Eckhoff et al. 2003).

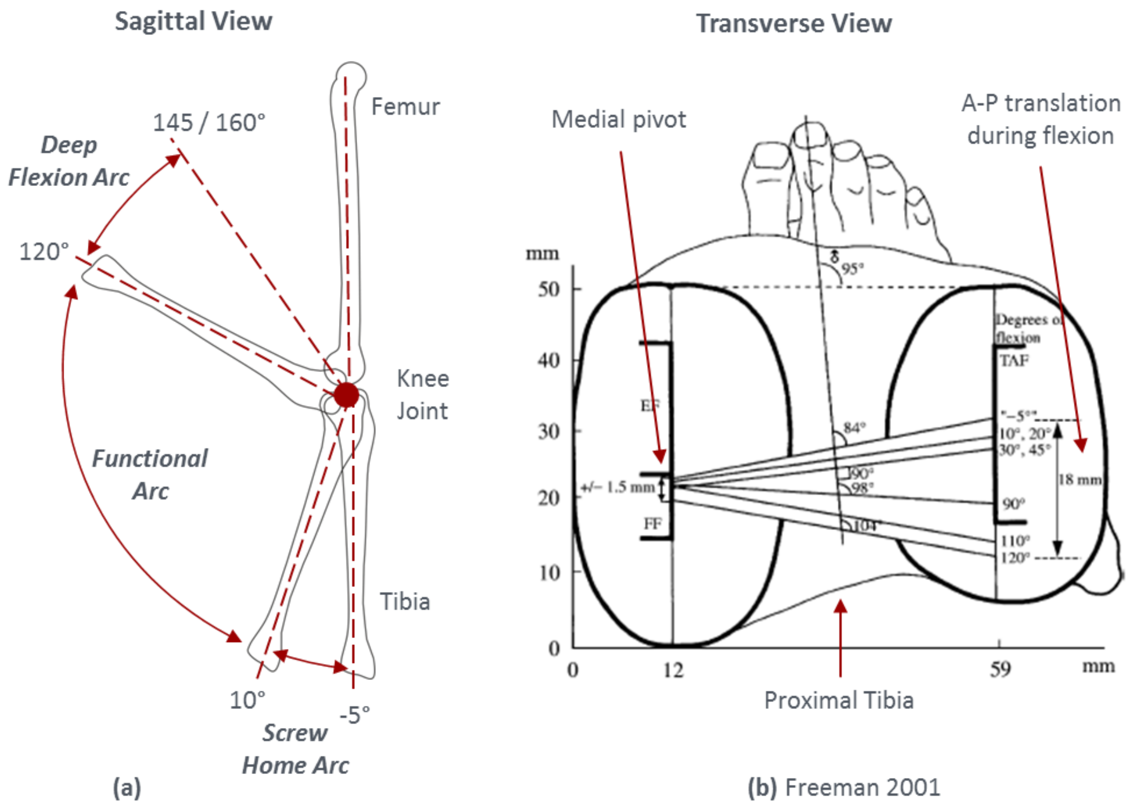

Figure 4 – (a) The knee range of motion and (b) the knee motion in the transverse plane during flexion

In the field of knee replacement surgery, it is important to understand the relative motions of the bones within the natural knee. The surgeon aims to reproduce this with the performance of the implant, specifically the knee kinematics during daily living activities. The modern kinematic theory is based on three fundamental arcs of motion which can be seen in Figure 4(a). The functional arc is the only active motion section and can range between 20-120° (Freeman et al. 2001). The femoral surfaces in the sagittal plane have a circular, single radius within this range (Eckhoff et al. 2003, Hollister et al. 1993). As the knee flexes, the femur rotates about the centre of this circle. During flexion in the transverse plane, the lateral condyle of the femur moves in the anterior to posterior direction causing longitudinal tibial rotation. The medial condyle does not move in the A-P direction during the functional arc (Freeman et al. 2001). The shape of the tibial plateau also contributes to the motion pattern during flexion. The medial compartment is concave in shape and has a fixed meniscus which provides constraint during flexion and extension. The lateral compartment is convex and has a mobile meniscus, therefore offering far less constraint and contributing to the lateral translational movement shown in Figure 4(b). Due to movement on the lateral side and none on the medial side at this stage, the concept is often referred to as the medial pivot and is illustrated in Figure 4(b). The screw home arc, shown in Figure 4(a), is a passive motion requiring little muscle use and serves to lock the knee into position. The deep flexion arc is also a passive motion which takes the knee beyond the functional arc of motion. As discussed, the femur externally rotates with reference to the tibia as the knee flexes and within deep flexion the whole femur also posteriorly rolls back with respect to the tibia.

Two different axes of the lower limb in the frontal plane are commonly referred to; the mechanical axis and the anatomical axis. The mechanical axis is a line connecting the centre of the femoral head to the centre of the knee and the centre of the ankle in the frontal plane (Figure 5). In contrast, the anatomical axis runs through the shafts of the tibia and femur as shown in Figure 5. There is an average of 7° difference between these angles, although this varies greatly between individuals. Other axes include the flexion - extension axis which runs through the single radius of the femoral condyles (Eckhoff et al. 2003) and the longitudinal rotation axis which approximates the anatomical axis of the tibial shaft.

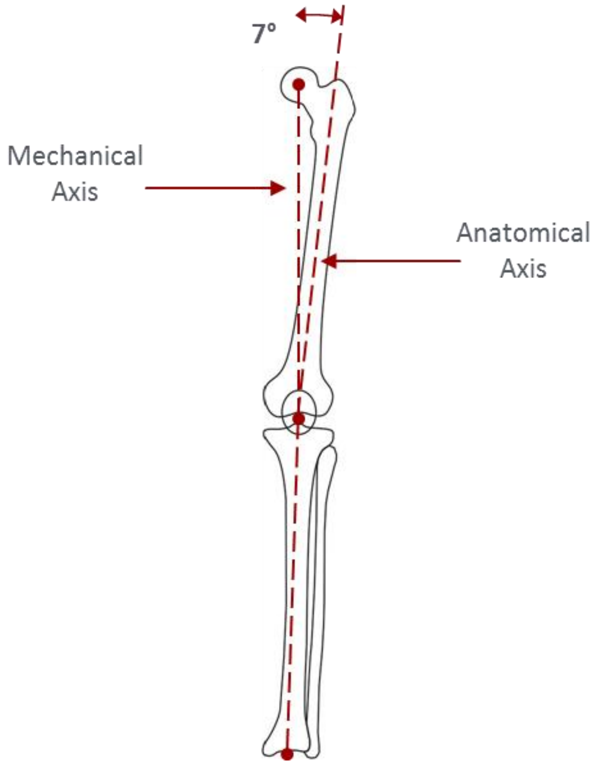

Figure 5 – Illustrating the angle difference between the mechanical and anatomical axis of the lower limbs

2.1 Tibiofemoral joint

The primary role of the tibiofemoral joint is to allow for motion and transmit the body weight force from the femur through to the tibia. It can be seen from the geometry of the knee in Figure 6(a) that the TFJ involves the articulation of the femoral and tibial condyles during knee motion. Due to the high forces and large ranges of motion, the surfaces of the femoral and tibial condyles are covered with articular cartilage. This acts to provide low friction and to spread and transfer physiological forces. It also, with the soft tissues of the knee as discussed, guides the motion and provides stability to the highly loaded joint. A specific type of articular cartilage called the meniscus can be found in the TFJ which is attached to the tibial plateau in the medial and lateral condyles. The menisci are semi-circular structures (as indicated in Figure 6b) which are roughly triangular in cross section and they function to increase the contact area and congruency between the condyles of the femur and tibia (Reilly et al. 1982). This helps to distribute the loads being transferred through the TFJ and protects the tibia, particularly through energy absorption in high loading activities (Rath and Richmond 2000).

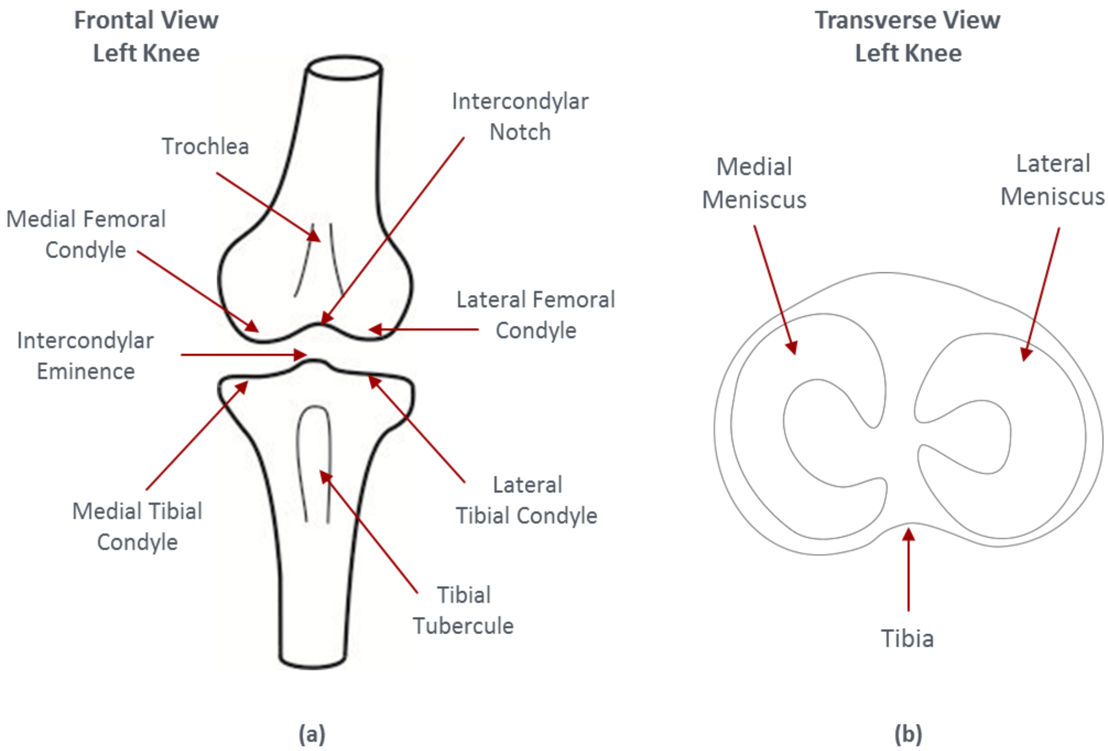

Figure 6 – Detailed annotation of the bones in the TFJ (a) and a typical shape of the knee menisci (b)

2.2 Tibia

The tibia and femur are classified as long weight-bearing bones and are the two largest bones in the human body (Nordin and Frankel 2001). An appreciation of the detailed anatomy of the tibia is important when studying the load transfer characteristics through the bone. The tibia consists of two epiphyses, two metaphyses, and a diaphysis along its length as displayed in Figure 7. These areas of bone correlate with a change in the tibial structure and proportion of cortical to cancellous bone. In the proximal epiphysis, dense platforms of bone can be found across the tibial plateau (Reilly 1982, Scott and Biant 2012). Distal to this thick cortical bone in the tibial plateau is spongy cancellous bone in the metaphysis section. This cancellous bone has a varying density and trabeculae which are small beams of tissue forming a network within the bone. These trabeculae are orientated both perpendicular to the joint surface and also in arch-like orientations radiating from the tibial shaft cortex as illustrated in Figure 8 (Palastanga et al. 2002, Reilly et al. 1982). A thin cortical shell surrounds the cancellous bone in this metaphysis layer, which thickens as it develops into the shaft of the diaphysis (Reilly et al. 1982). Such bone structure exists to allow the tibia to carry out its important weight bearing function in the body.

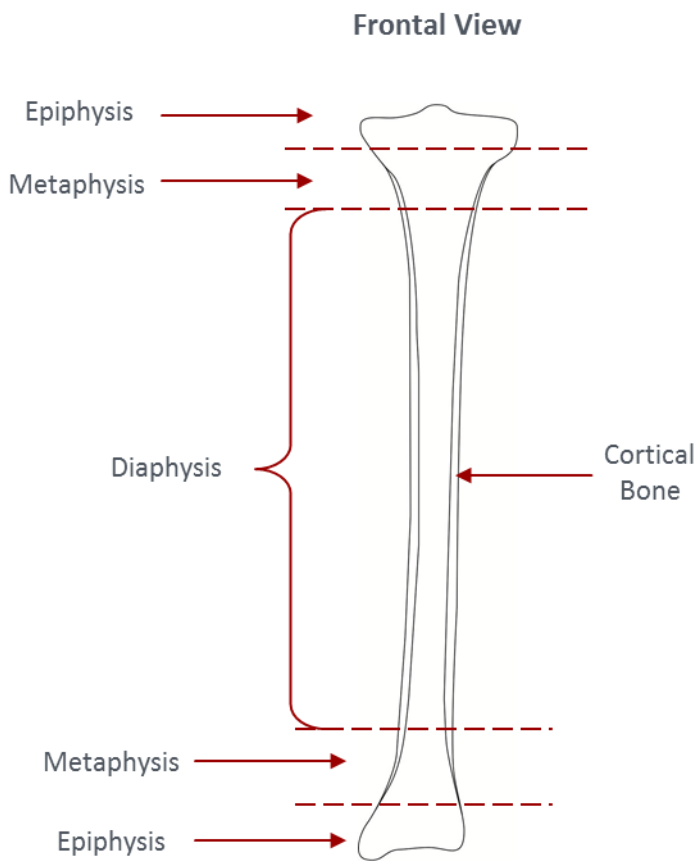

Figure 7 – The overall structure of the tibia

Frontal View

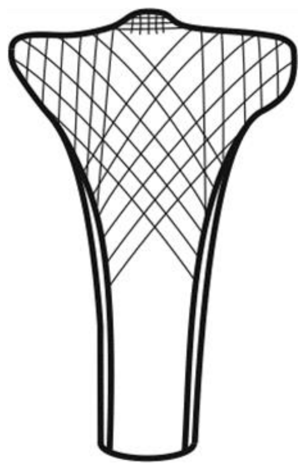

Figure 8 - The trabecular architecture of the tibia showing both perpendicular and arched orientations from the joint surface (adapted from Palastanga et al. 2002 and Weber 1992)

The structure of the tibia derives from the way in which bone can constantly remodel to change its external and internal architecture, in response to applied stress and strain. This theory is commonly termed ‘Wolff’s Law’ as it is traditionally attributed to Julius Wolff. It is strongly debated if it really did belong to Wolff and if it really is a law. This controversy is described in depth by Cowin in his Bone Mechanics Handbook (Cowin 2001). Either way, the concept of ‘functional adaptation’, the adaptive bone remodelling response to strain, is valid. The manner of the remodelling process is determined by the magnitude and direction of the applied strain on the bone. It is believed that the level of strain required for normal remodelling to occur lies within the limits of 50-1500 µstrain. If it is below 50 µstrain then bone resorption is likely to occur, whereas above 1500 µstrain could cause damage to the bone and ultimately failure (Frost 1991). To put these values into context, Aluminium (E = 69GPa, Yield Strength = 95 MPa) has a yield point at approximately 1400 µstrain, with stainless steel (E = 180GPa, Yield Strength = 502 MPa) approximately 2800 µstrain (The Engineering Toolbox 2015).

2.3 Patellofemoral Joint

The patellofemoral joint (PFJ) is historically the understated of the two joints in the knee, with less research conducted to establish its role in knee kinematics and load transfer than the TFJ. The patellofemoral knee joint facilitates flexion and extension by using the patella to provide an increased extension lever arm for the quadriceps tendon (Browne et al. 2005). During normal daily activities, forces of up to 9.7 x body weight (BW) can act through the PFJ (Schindler and Scott 2011). Such force is originated from the quadriceps tendon, with a proportion transmitted through to the tensile patella tendon and the remainder transferred through the contact force of the patella with the trochlea in the femur (Schindler 2012). The force can vary with the angle of flexion and the distance between the PFJ and the centre of gravity. It can be seen from Figure 9 (b) that the moment produced by the PFJ is required for the knee to function. This opposing moment has growing importance as the knee flexion angle increases and any knee model set-up must include some form of counteract to the body weight force through the femur. The contact area of the patella on the femur increases with flexion as the joint forces increase. A diagram of the main components of the PFJ in the sagittal plane can be found in Figure 3, including the femur, patella, quadriceps tendon and patella tendon. Figure 9 (a) illustrates the difference in angle between the patella tendon and quadriceps tendon in the frontal plane, known as the Q angle. The average Q angle has been found to be around 15° (Mizuno et al. 2001, Aglietti et al. 1983) and can have an important influence on knee kinematics (Mizuno et al. 2001). The Q angle has been seen to change with knee flexion; as it travels through the flexion cycle from full extension to 30° flexion, the tibia rotates externally through the screw-home mechanism (Browne et al. 2005). From 30° flexion an internal rotation of the tibia then occurs (Mizuno et al. 2001). It is clear that both the PFJ and TFJ have fundamental roles in knee function. It follows that if either joint becomes damaged or deficient it is likely to affect the normal functioning of the knee coupled with potential pain. In some cases it will be appropriate to perform knee replacement surgery to alleviate this.

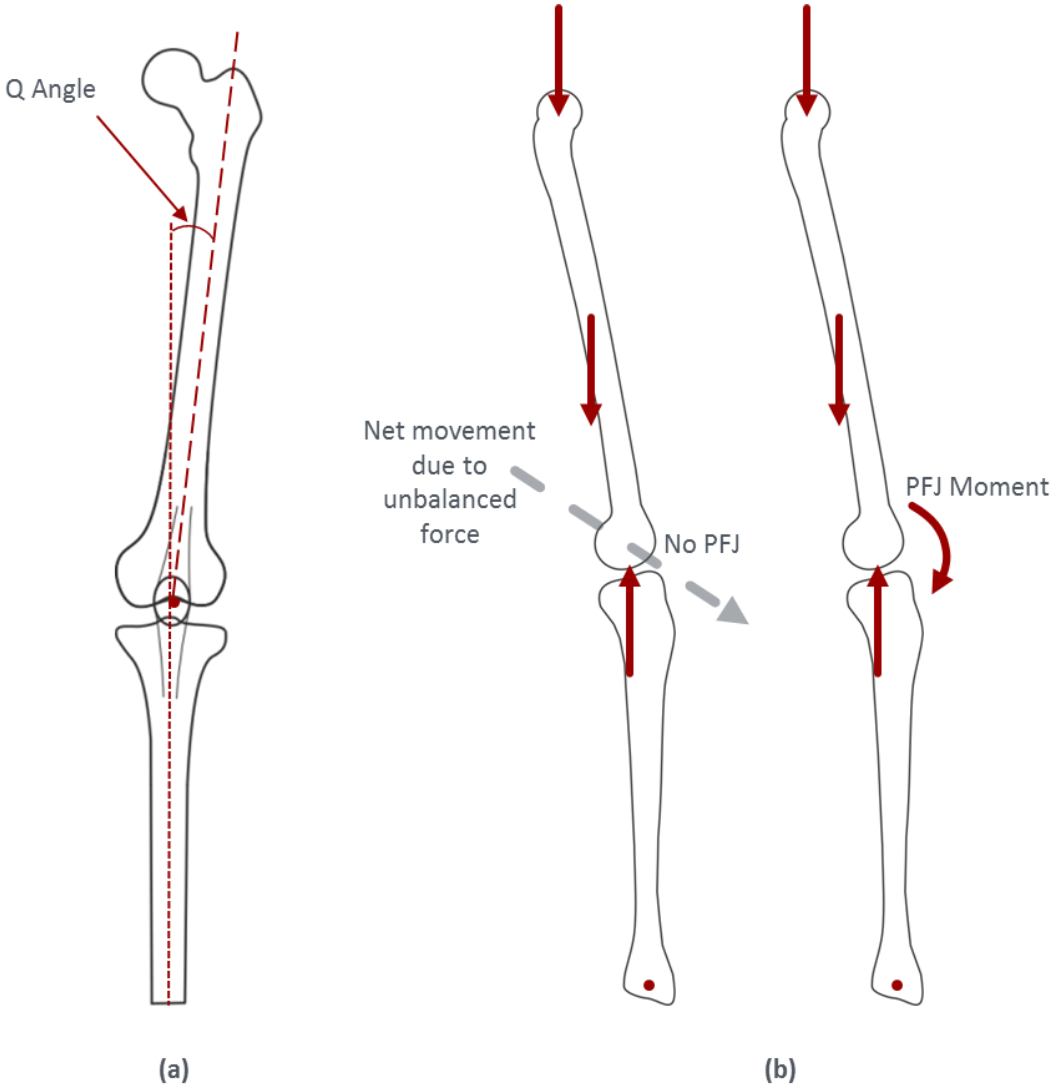

Figure 9 – The Q Angle (a) and the important role of the PFJ (b)

3 The Prosthetic Knee

3.1 Primary Total Knee Replacements (TKR)

The knee joint is one of the most highly loaded joints in the human body and these high forces, coupled with its complexity, cause it to be susceptible to injury and degenerative disease. Treatment is therefore often required to relieve pain and restore function. Primary TKR involves replacing the bearing surfaces of the joint with typically a metal femoral component articulating against a polyethylene tibial component. There were over 85,000 primary procedures recorded in the UK in 2013, which were performed on patients with an average age of 69.28 years (National Joint Registry 2014a). The primary indication for surgery was osteoarthritis, although other indications included rheumatoid arthritis, previous infection or trauma (National Joint Registry 2014a). The prevalence of knee replacements has grown rapidly as the population gets older and the quality of healthcare improves. In the US, the lifetime probability of having a TKR currently lies at 7% and 9.5% for males and females respectively (Mann et al. 2014). The demand for TKR continues to grow and is expected to increase by 673% in the US between 2005 and 2030 (Kurtz et al. 2007). This highly respected estimate is based on regression projections from data between 1990 and 2003 and on population projections. These were updated in 2014 to show that the economic downturns in the 2000s had no influence on the growth trends across the US (Kurtz et al. 2014). The increasing number of TKRs being performed on younger and more active patients with increased life expectancies can subject the implants to greater and prolonged functional demands. It is therefore imperative that the design, manufacture, implantation and outcomes of knee replacements are optimal for the patients, clinicians and companies involved, to avoid complications and keep pace with such growth.

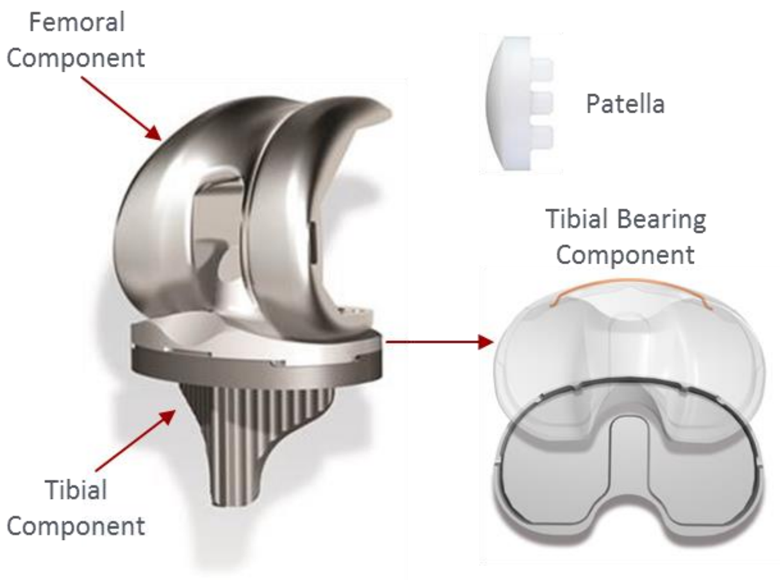

Figure 10 - The components of a TKR (Smith and Nephew 2014, Stryker Orthopaedics 2015)

A total knee replacement system typically consists of the components illustrated in Figure 10, including the optional polyethylene patella button shown. The femoral component replaces the femoral condyles and incorporates a central patella trochlea groove. The patella button is a dome-shaped element that can replace the surface of the patella and tracks along the trochlea groove within the femoral component. The tibial component includes a tray which replaces the proximal tibial plateau into which the polyethylene bearing insert is located.

There are currently 60 different designs of TKR used each year in the UK (National Joint Registry 2014b). The design of a TKR prosthesis can fall within one of three categories depending on the degree of mechanical stability provided; fully constrained (hinged), semi constrained or unconstrained (Figure 11). Hinged prostheses were the first TKR components designed and were first implanted by Shiers in 1953 (Shiers 1954). With the development of alternative designs with less constraint, they are now usually reserved for more complex procedures. The early hinged design had femoral and tibial components mechanically linked to allow movement in a single plane only, providing stability in cases with severe bone loss or ligament damage (Dorr 2002). Some of the more modern hinged knee replacement designs have a partially constrained degree of stability to allow for the removal of the cruciate ligaments, which usually takes the form of a post in the centre of the tibial plateau as shown in Figure 11. This post overcomes the removal of the cruciate ligaments by limiting anterior-posterior slide, particularly at high flexion angles, therefore stabilising the knee. The unconstrained prostheses allow movement in all three planes as there is no physical link or stability built in between the femoral and tibial components; they instead rely on soft tissue for stability. There has been a general trend in recent years embracing the modern kinematic theory discussed where implant companies have released TKR designs with a single radius of curvature around the femoral condyles to replace the earlier multi-radius designs. Reports from multi-radius designs such as the DePuy Sigma, refer to a mid-range instability caused by the transition of the axis of rotation between different radius profiles. The newer single radius knee designs, such as the Stryker Triathlon knee replacement, typically result in a reduced quadriceps force for the equivalent flexion movement. This is due to the more posterior axis of rotation leading to an increased patella femoral lever arm, similar to that of the normal knee (Ostermeier and Stukenborg-Colsman 2011). Thus, a range of differing knee designs exist which allow surgeons to meet the differing requirements and constraints for dealing with patient specific knee disorders.

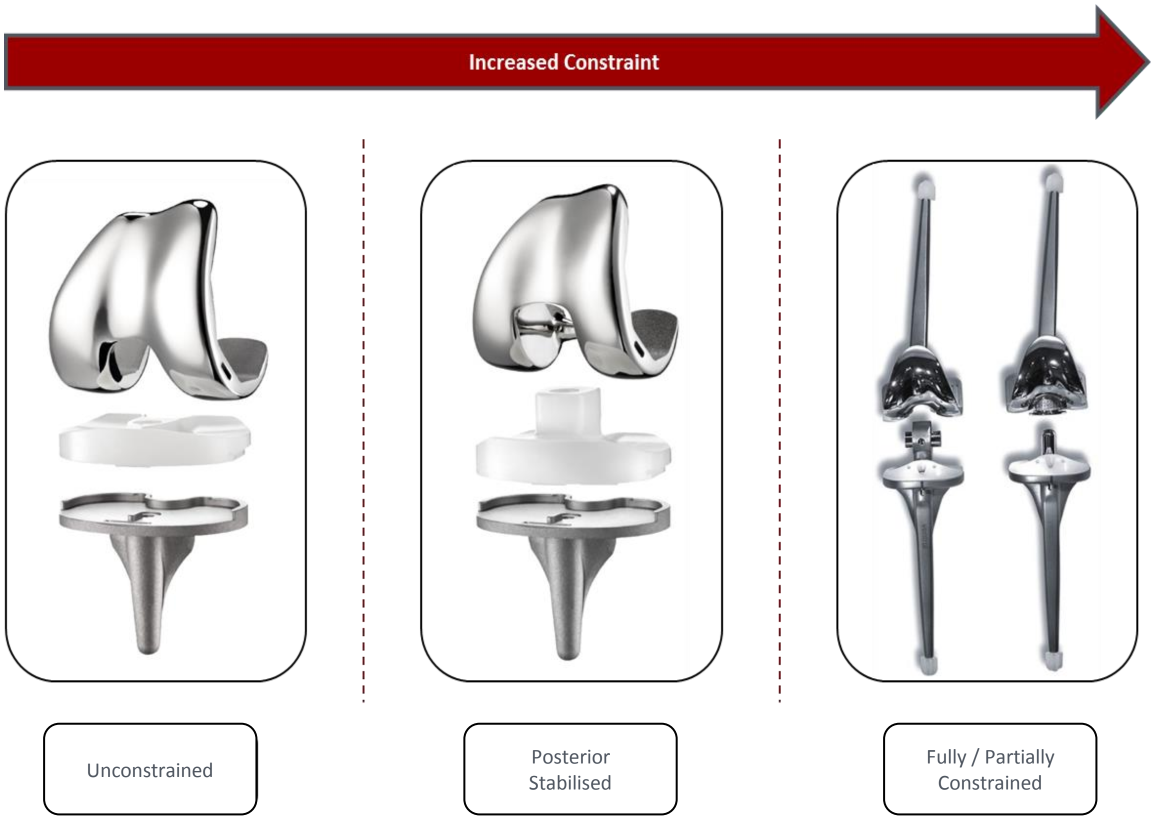

Figure 11 - The constraint categories of a TKR (aap Implantate 2011, Aquilant Orthopaedics 2015)

Despite significant developments in TKR design and improvements in surgical procedures over the past 60+ years, patient satisfaction after TKR still fails to achieve above 75% (Noble et al. 2006) and just 70.8% of patients in the UK report themselves as being 'much better compared to how they were before the operation' (National Joint Registry 2012). Extensive research has been carried out to establish the cause for patient dissatisfaction and primary implant failures. Post-operative issues associated with TKR include; instability, aseptic loosening, component malfunction, infection, wear and poor surgical technique (Labey et al. 2000, Manopoulos et al. 2012). An analysis combining worldwide arthroplasty registers found the most common causes reported for a revision operation to be loosening (44.6%), pain (9.5%) and wear (8.2%) (Sadoghi et al. 2013). Further down the list but still associated with a substantial number of patients from the large pool of data were implant breakage (4.7%) and periprosthetic fractures (3%). A summary of the main complications associated with TKR can be seen in Figure 12.

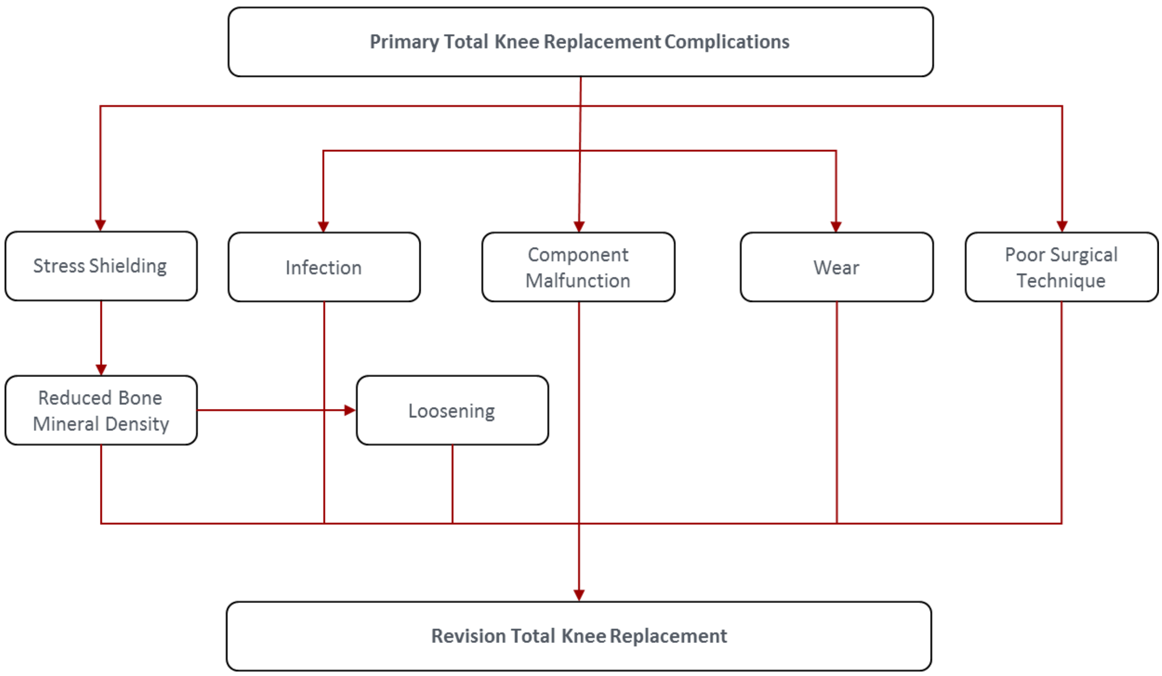

Figure 12 – A summary of the complications related to TKR, often leading to RTKR

A common complication thought to be associated with all joint replacements, which can contribute to post-operative difficulties, is the occurrence of stress shielding. After a TKR procedure, the natural remodelling process of the bone surrounding the knee joint is altered (Meireles et al. 2010) due to the change in stress patterns in the bone (Huiskes et al. 1987). The addition of an implant with a large difference in material stiffness compared to the host bone can cause the body weight reaction forces to transfer from the femur through the tibial implant into the tibia, bypassing the surrounding bone. As previously discussed, the strain levels in bone must be high enough for the adaptive remodelling process to continue, and if the bone is bypassed the levels are likely to be too low, leading to bone resorption. It is not just the addition of an implant with a disparity in stiffness that causes stress shielding. Other changes to the loading conditions after TKR such as the load placement, load pattern and the congruency of the condylar surfaces can also have an effect (Au et al. 2007). The level of stress shielding is also reliant on surgical technique, which determines where the implant is supported in terms of the proportion of cancellous bone and the cortical rim. Stress shielding can affect the bone mineral density (BMD) and trabecular structure of the surrounding tibial bone and hence contribute to implant loosening and poor fixation (Meireles et al. 2010). A study that measured long-term changes in BMD after TKR in 31 patients concluded that the density in the proximal tibia reduced by 36.4% over eight years post TKR (Levitz et al. 1995). As improvements to the design, materials and placement of primary knee replacement are implemented it remains to be seen if they produce positive effects on the surrounding bone.

The continued growth of TKRs, coupled with the increasing trend for surgery to be performed on younger and more active patients with longer life expectancies, is likely to lead to a parallel increase in the requirements for revision TKR. Higher functional demands and prolonged use may strain the primary components and surrounding soft tissue causing an increase in the requirement for a second operation to alleviate pain, improve function or avoid further damage.

3.2 Revision Total Knee Replacements (RTKR)

There has been a distinct rise in RTKR in recent years to deal with failures of primary TKR. This can largely be attributed to the growth in the number of primary knee replacements, greater life expectancy and the increasingly younger and more active patients requiring surgery (Bono and Scott 2005, Thongtrangan et al. 2003). RTKR has been the fastest growing segment of joint arthroplasty in recent years (Bugbee et al. 2001), with 5,783 revision procedures performed in the UK in 2013 (National Joint Registry 2014a) and 63,400 in the US in 2008 (Kurtz et al. 2011). Compared to primary procedures however, RTKR procedures are associated with inferior outcomes and the consumption of greater economic resources (Burns et al. 2006). Revision knee replacement procedures can range from revising a single component, such as the tibial component where failures occur more commonly (Toms et al. 2004), or a complete RTKR where all components are revised. The main purpose of any RTKR is to deal with the failure of a primary TKR by restoring knee function and addressing any associated bone stock loss. It also aims to relieve pain (Nazarian et al. 2002) and provide an adequate platform for optimal load transfer to the host bone (Whittaker et al. 2008). In order to achieve this, the key goals of surgery must include restoring alignment, ensuring a stable fixation between prosthesis and bone (Manopoulos et al. 2012, Tang et al. 2010) and enforcing the correct degree of constraint to allow ligament participation and stability (Nelson et al. 2003a). Good clinical outcomes should be achieved through precise implant positioning, alignment and restoration of the joint line height and a suitable surgical procedure and prosthesis (Dennis 2007), the latter of which will be discussed in detail.

3.2.1 Component Design

There are a wide variety of current implants for RTKR worldwide, with 36 different brands of prosthesis used in the UK alone in 2013 (National Joint Registry 2014b). The design is similar to that used in primary surgery; however, it is routine to use components that have been designed specifically for revision cases. This is due to the common view that primary components used in revision surgery do not provide adequate results due to the bone stock loss and joint instability (Dorr 2002) and it has been shown to be more cost effective in the long term to use revision specific components (Bugbee et al. 2001). One study specifically compared the outcome of RTKR with the use of revision components to using those designed for primary procedures but used for revisions, also investigating modified primary components used for revisions. The results of the study displayed the superiority of revision specific implants with only a 6% implant-related failure rate compared to 14% for modified primary components and 26% for standard primary designs all when used in revision procedures (Bugbee et al. 2001). When assessing failure types, it was found that aseptic loosening was only associated with the operations that had used standard primary designs in the revision scenario. Like the primary implant, the revision TKR has three components which can be separated into three categories by their level of constraint. The revision component can allow optional attachments such as modular stem extensions and wedge or block augments which can be selected by the surgeon to aid joint reconstruction (Nelson et al. 2003a). Figure 13 illustrates a selection of the RTKR designs available, with some optional modular components attached. This research focused on the tibial side of RTKR and so further review of the literature was focused on the tibial component.

Figure 13 - Various examples of Revision Total Knee Replacement components including modular stems and augments (Biomet 2015, Stanmore Implants Worldwide 2015, Stryker Orthopaedics 2015, MicroPort 2015 and Zimmer 2014)

The variation in designs seen in Figure 13 is attributable to the broad scope of the design specification created for revision cases and the many challenges that the revision components must overcome. One of the most significant challenges of RTKR is the issue of surrounding bone loss and the need for bone stock restoration (Thongtrangan et al. 2003, Toms et al. 2004, Whittaker et al. 2008, Haas et al. 1995). As previously discussed, the problem of stress shielding in primary TKR causes resorption of the surrounding bone. This is compounded in the revision scenario due to the removal of the primary component causing further bone loss. After revision surgery, this bone loss is followed by further stress shielding in the bone due to the insertion of the revision component, exacerbating the problem of inadequate bone stock (Thongtrangan et al. 2003). In addition, further reduction in host bone can be caused by a combination of osteolysis, instability, implant failure and infection (Toms et al. 2004). The management of these bone deficiencies initially through careful component selection is essential to achieve a successful outcome after RTKR (Mabry and Hanssen 2007).

3.2.2 Component Selection

Bone Loss Classification

The selection of an appropriate tibial component assembly to adequately manage bone loss and restore function in patients is made following patient specific evaluation by an orthopaedic surgeon. The decision must be a balance between conformity and constraint in the knee joint (Bono and Scott 2005) and depends greatly on the extent and integrity of the remaining bone observed during preoperative planning. In addition, the patient demographics and state of the soft tissues should also be considered (Radnay and Scuderi 2006). The standardised classification of the extent of this bone loss in a patient is important in order to establish the most appropriate surgical approach and implant selection. Defects can be contained, where the deficiency is central and surrounded by intact cortical bone, or uncontained where a cortical defect exists. The most widely used categorisation is the Anderson Orthopaedic Research Institute (AORI) system which describes three defect groups, summarised in Table 1 and Figure 14 (Nelson et al. 2003b, Thongtrangan et al. 2003). Various options exist to attempt to deal with any degree of bone loss in the surrounding tibial bone, including the use of cement, bone grafting, modular augments and stems which will be discussed in detail (Whittaker et al. 2008).

Classification	Type 1	Type 2A (one condyle) Type 2B (both condyles)	Type 3
Defect Type	Contained. Intact metaphyseal bone with near normal joint line	Metaphyseal bone damaged, joint line restoration needed	A major portion of a condyle compromised by deficient metaphyseal bone
Treatment	Cement or bone graft	Any combination of cement, bone grafts and augments	Structural bone graft, hinged implant or custom component

Table 1 - AORI Defect Classification (adapted from Nelson et al. 2003b. and Thongtrangan et al. 2003)

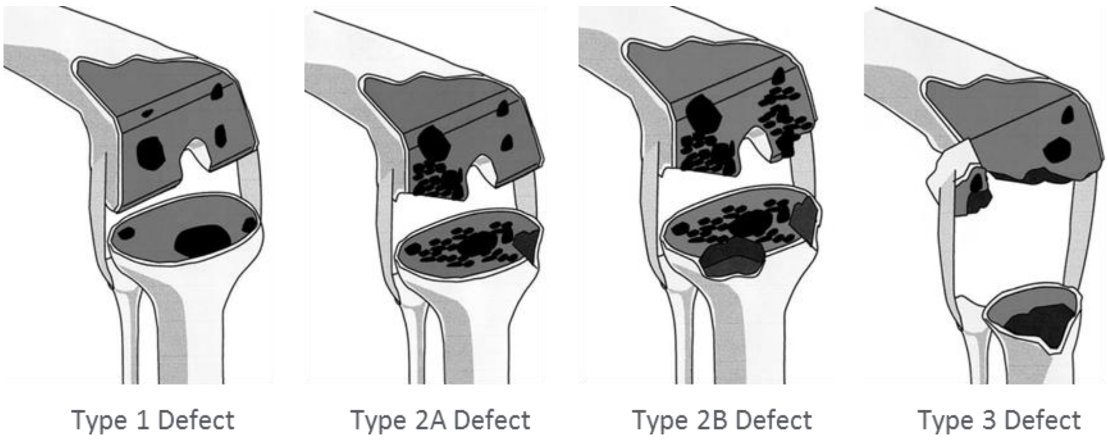

Figure 14 - AORI defect classification (adapted from Nelson et al. 2003b. and Thongtrangan et al. 2003)

Bone Loss Management

A variety of options are available at the time of the revision operation to manage any bone loss that has occurred and these will be discussed to describe which approaches are appropriate and their clinical success. The options range from bone grafting techniques to restore bone stock, to a synthetic solution using prosthetic augments and stem extensions. The effectiveness of these augments is closely linked to the method of fixation used; of which the options are also discussed.

Bone Grafting

To select the technique used to manage the degree of bone loss seen in a patient, many considerations are made by the surgeon to guide their decision. The preservation and restoration of bone stock with RTKR is important, particularly in younger patients. If the bone defects are beyond the size which can be filled with cement, then the use of a bone graft is often considered as indicated in Figure 14 (AORI). This can be performed using autograft or allograft bone to provide a scaffolding for bone regeneration. Although autograft is the preferred option, it is not readily available and so allograft is usually used. There are, however, many biological issues associated with using allograft bone. The form of bone graft used may either be structural or morsellised. A structural graft allows for the geometry to be matched to that of the defect and maintains a cancellous bone structure. Although this provides initial stability, a structural graft may not be available and the process can be time consuming. A morsellised graft fills the defect with many fragments of bone graft, which has the benefits of availability and use in defects with an unusual geometry. A progression of this graft type is the use of impaction grafting of morsellised bone (Thongtrangan et al. 2003), which can be used in contained or uncontained defects.

The technique of impaction grafting involves filling the defect with allograft chips before compacting them into the host bone, with the optional use of a wire mesh for support of uncontained defects. The aims are to achieve implant stability, induce bone ingrowth (Toms et al. 2004) and prevent subsidence (Putzer et al. 2011). Impaction bone grafting can improve bone stock restoration and manage a variety of bone loss situations however it is time consuming, technically demanding and has a major risk of associated biological issues (Toms et al. 2004). The use of impaction grafting in the tibia is debated in the literature, particularly its use for large uncontained defects. A study based on the short term results of 17 cases supported the use of impaction grafting with wire mesh on large uncontained bone defects (Lonner et al. 2002), as does a retrospective clinical analysis of using impaction grafting on contained defects (Steens et al. 2008). However, the latter study does tend to agree with other authors who discourage the technique for use on large uncontained defects in the tibia because they believe it may not provide sufficient initial stability (van Loon et al. 2000). Although the use of bone grafting in the tibia is still contested depending on the nature of the defect, there is a common acceptance that a tibial stem and augments are necessary to offload the graft during its incorporation in the tibia (Sculco and Choi 1998).

Prosthetic Augments

If the degree of bone loss is too great, or uncontained, then prosthetic augmentation or custom implants are often used to substitute the bone. Modular metal wedges and blocks allow for a custom implant to be assembled and fitted with the aim of improving the outcome of each procedure where there is compromised bone. The advantages of prosthetic augments include the mechanical support provided, availability of a variety of augments, removal of the biological issues associated with grafting, reduced technical demand, stability and the allowance of immediate weight bearing and range of motion. Despite these advantages, they are often preferred only in older patients as they do not restore bone stock (Thongtrangan et al. 2003) and if future complications occur, they are increasingly difficult to extract. A combined experimental and computational study was performed to assess the effect of different augments on the tibial strain. It highlighted that the use of augments does significantly change the biomechanical conditions in the proximal tibia compared to the intact bone, presenting a risk of bone resorption (Completo et al. 2013) and hence further work on implant and augment design was required to improve this.

Progressing from the standard metal augments discussed, a more recent development in bone loss management involves the use of trabecular metal cones and augments. These consist of a porous metal structure which is a particularly useful treatment option for severe bone loss, when classified as Type 2b or 3, as they allow bone ingrowth for biological fixation (see Radnay and Scuderi 2006). The commonly used design is a porous tantalum cone which is used in conjunction with the tibial component and stem extension. These can provide good mechanical stability by filling defects and tolerating physiological loads, they can aid fixation and allow early biological ingrowth to restore bone stock (Jensen et al. 2012). A study which assessed the short term outcomes of using these tantalum cones in ten knees (in conjunction with a tibial component, stem, bone graft and, in some cases, additional wedge augments and offsets) found them to be a successful technique to manage bone loss and reduce the extent of bone graft used (Radnay and Scuderi 2006). A selection of prosthetic augmentation components is illustrated in Figure 15, where a comparison between standard and trabecular models can be made.

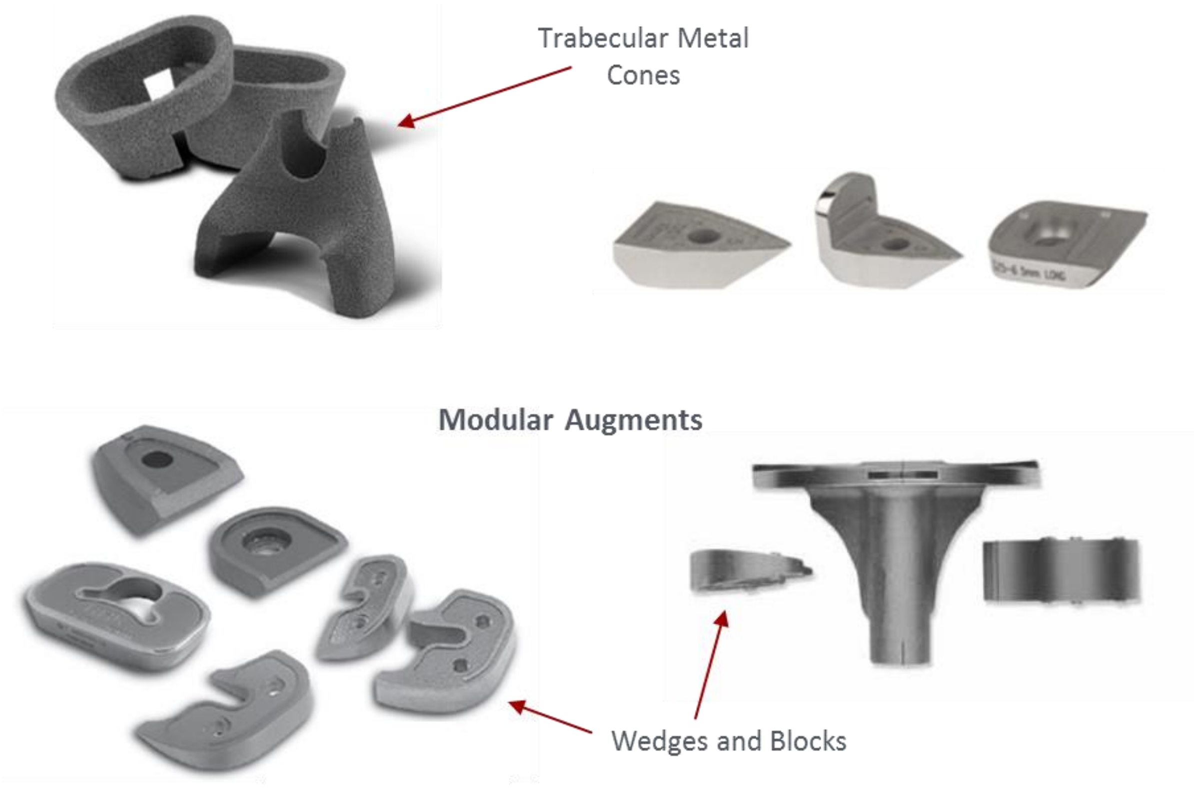

Figure 15 - Various examples of modular augments including standard and trabecular metal (MicroPort 2015 and Zimmer 2014)

Stem Extensions

A frequent method of managing the high levels of bone loss or poor quality bone seen at revision surgery is the inclusion of a stem extension, which is an important design feature of revision implants (Bugbee et al. 2001). It is usually optional to use a stem alone or coupled with any type of augment discussed, depending on the implant manufacturer. Stems are capable of extending through to the diaphysis, bypassing the damaged area of bone and transmitting the joint load through to the distal cortical bone to protect remaining proximal bone stock (Mabry and Hanssen 2007, Scott and Biant 2012). This is illustrated in Figure 16. One cadaveric study has shown that a 70 mm long stem was capable of decreasing the proximal tibial load by 23-38%, successfully relieving the deficient proximal bone (Brooks et al. 1984). There are further advantages to the use of a stem extension, in addition to it reducing proximal stress and protecting the remaining bone stock and graft used (Completo et al. 2008a) and these are discussed. The addition of a stem increases the stiffness of the tibial construct and provides resistance to bending and torsional forces found in the knee joint (Rawlinson et al. 2005, Reilly et al. 1982). They also reduce the occurrence of toggling by encouraging movement to be predominantly along the axis of the bone (Albrektsson et al. 1990). All studies historically agree that the long stem implantation aids positioning and alignment during surgery (Barrack et al. 2004) as well as enhancing fixation and stability in the long-term (Bertin et al. 1985, Completo et al. 2012). The quality of bone at the time of revision is regarded as the most important consideration in determining the use of stems (Nazarian et al. 2002) and can influence the type and geometry used.

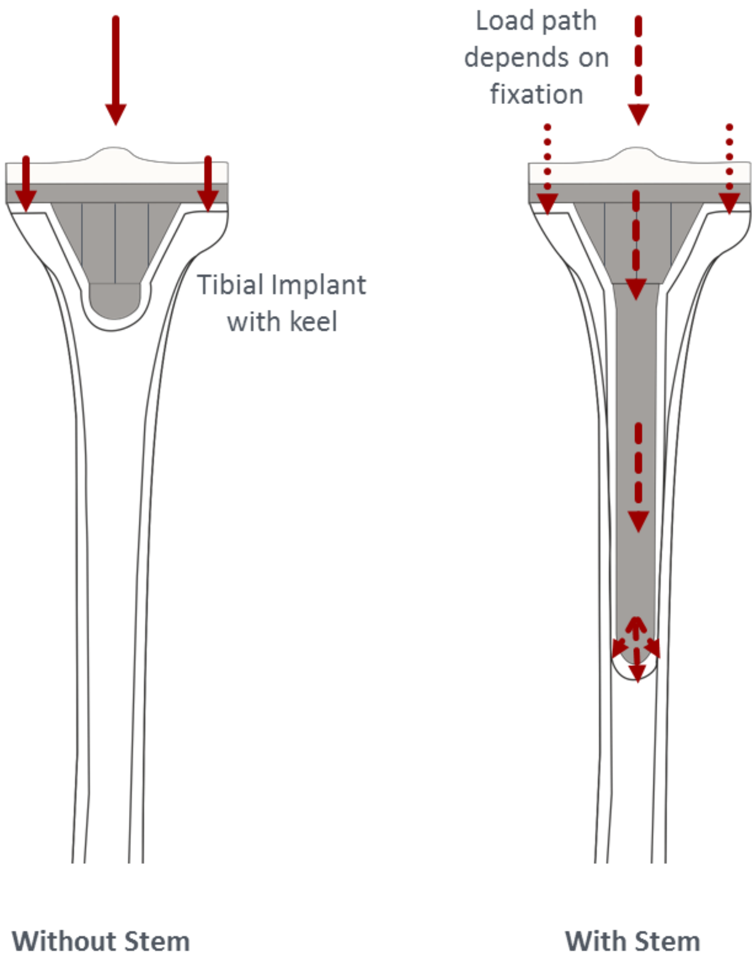

Figure 16 - The load transfer changes with inclusion of a stemmed tibial component

There is great variety in the design parameters of available stem extensions for RTKR, including options of length, diameter, surface finish, material and shape features as shown in Figure 17. Their geometry is designed to engage in the metaphysis or diaphysis (Fehring et al. 2003) depending on the bone stock and shape of each patient. Diaphyseal filling stems are useful to aid alignment, unless the canal geometry is particularly unusual (Mabry and Hanssen 2007). The orthopaedic surgeon will determine which options to use through a combination of preoperative planning and assessments during surgery. There are no existing evidence-based guidelines available, however, for surgeons to make informed decisions on the type of stem to use (Fuchs-Winkelmann et al. 2012). Throughout the literature there have been studies comparing lengths and other geometric parameters of tibial stems, with varying results and conclusions drawn. An experimental study on 12 cadaver knees highlighted a trend of increased stress shielding with stems which increased in length and diameter, although the difference was not found to be statistically significant (Jazrawi et al. 2001).

In conjunction with the length and diameter of the stem used in revision knee components, additional design features must be considered. In the tibia, the connection method of the tibial stem to the tibial baseplate can be a screw thread, Morse taper with or without a grub screw, or a snap lock mechanism. The design choice made in this case can affect the assembly process and the modularity of the device for later ease of removal. Another design element of the stem is the possible inclusion of fins or flutes around their circumference as shown in Figure 17, which have been found to ensure rotational alignment and stability (Gofton et al. 2002, Peters et al. 2005). The material used for the stem can also have an effect on success; however one computational analysis shows that it had less effect than the geometric design parameters (Completo et al. 2009). Further parameters, such as the surface finish of the stem extension, relate to the intended method of fixation of the tibial stemmed component.

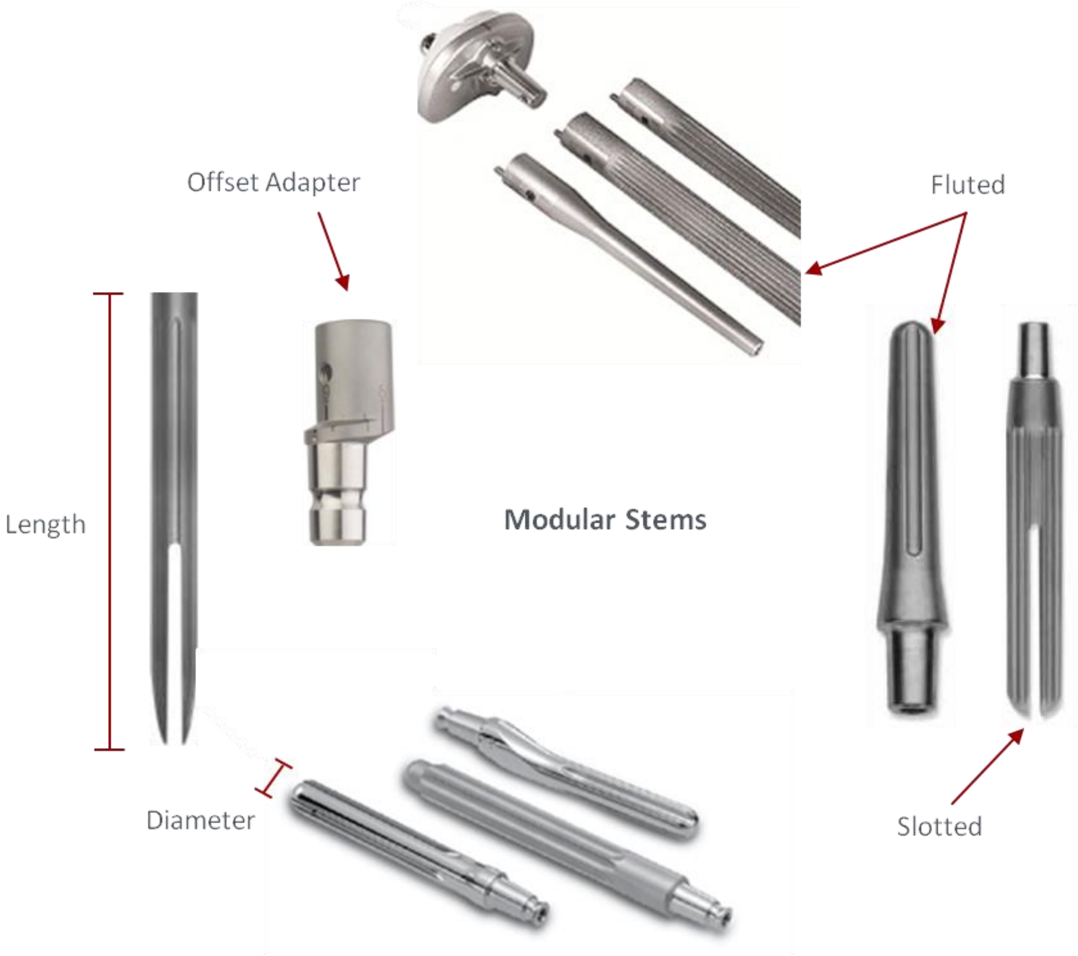

Figure 17 – Examples of available stem extensions including significant design features (Aquilant Orthopaedics 2015, MicroPort 2015, Smith and Nephew 2014 and Zimmer 2014)

Fixation

An important decision that the surgeon must make during RTKR is the method of fixation of the stemmed implant to the bone, as this has been found to be a key determinant of implant stability (Lee et al. 1991) and is debated widely in the literature. In the tibia there are three methods of fixation; the tray and stem can either be uncemented (press-fit), fully cemented, or cemented using a hybrid technique which includes a layer of cement underneath the tibial tray but no cement surrounding the stem (Mabry et al. 2007). The advantages and disadvantages of each technique have been widely discussed and investigated to aid the surgeon in the decision making process, although this is yet to lead to the publication of any fixed guidance. Many studies have specifically compared fixation techniques with their effect on clinical success and load transfer in the tibia. A combined experimental study and computer simulation to compare the strain in press-fit stems against those that are cemented found that the outcome was dependent on the extent of bone loss present (Completo et al. 2008b). A recent study that has carried out a comparative evaluation using a literature review of medical databases over 30 years was unable to draw a conclusion as to the optimal fixation technique for RTKR (Beckmann et al. 2011). To gain a full understanding of the options available, it is important to have an appreciation of the theoretical benefits and rationale for each technique.

The two main fixation techniques are the fully cemented method and the contrasting uncemented method, whereby the stem is press-fit into the tibia. By fully cementing the tibial component, the initial stability and fixation of the construct is improved in comparison to either of the alternative techniques (Mabry et al. 2007). Other advantages to full cement fixation include the flexibility of implantation into different shaped bone, a proven record of good results and the possibility of local antibiotic delivery (Shannon et al. 2003, Whaley et al. 2003). The option of fixation where no cement is used is claimed to also provide adequate initial mechanical fixation whilst allowing the preservation of bone stock and easier removal upon re-revision (Nelson et al. 2003b, Shannon et al. 2003, Whaley et al. 2003). The cementless stemmed implant may also achieve joint alignment (Parsley et al. 2003) if it is canal filling as the stem is guided into place and no compliant cement layer exists. Contrastingly, there is a suggestion of the possibility of inferior fixation with cementless stems as they may not provide long-term biological fixation and some studies authors have expressed caution when using these in RTKR (Fehring et al. 2003). This will be discussed in detail when assessing the clinical performance of RTKR components used.

The intermediate fixation option is a hybrid cementing technique, often referred to as partial cementing. It is important to note that this method has often been described in published literature as a cemented or a cementless procedure, leading the reader to a false comparison (Fehring et al. 2003). In the context of this report the hybrid technique involves the partial cementing of the tibial component where cement is placed in the metaphysis (on the cut surface below the tibial tray and around the keel) and is combined with a cementless tibial stem (Sah et al. 2011, Peters et al. 2005). The advantage of this technique is the ease of insertion and alignment and the ability to allow easier removal if required as with the cementless technique, whilst providing adequate fixation similar to the fully cemented option (Sah et al. 2011). A combination of fixation methods, components and augments used and good management of bone loss should in theory lead to a successful RTKR operation, however to be able to assess this, the long-term clinical performance of the implants must be studied.

3.2.3 Clinical Performance

The challenges and complications associated with a revision TKR procedure result in inferior survivorship statistics compared to the primary operation (Burns et al. 2006); with a 79-83% 10-year survival rate compared to 93-95.5% for primary replacements (Sah et al. 2011). Patient satisfaction or outcomes after RTKR are not currently published in the National Joint Registry for England and Wales, or the Swedish Knee Arthroplasty Register. The Australian National Joint Replacement Registry does, however, report a 22.8% re-revision rate at 10 years (Australian Orthopaedic Association 2014). To increase the success of revision operations, it is important to assess the reported modes of failure.

There are a host of modes of failure reported for revision knee replacements, many of which are similar to those reported after primary operations. These documented failure modes include the breakdown of fixation, wear, subsidence, instability and loosening (Bono and Scott 2005). In addition to these, patient reported pain and limited motion should be considered as they can affect patient satisfaction levels. A recent study which assessed 81 knees after RTKR found a higher re-revision rate compared to an equivalent group of primary TKR (17%: 5%) and the main reasons for failure were infection and instability (Stambough et al. 2014). Figure 18 includes a selection of images of RTKR failure examples, including surrounding bone loss and loosening of the components. Both of these patients presented with increasing pain and the knees were re-revised. Fracture of the tibia or femur is a rare but catastrophic failure, more likely in an active and/or overweight and/or elderly patient as these factors will affect the transfer of load through the revised joint. To avoid the discussed failures in future procedures, it is necessary to assess what factors may have caused them to occur and where it may be possible to improve these.

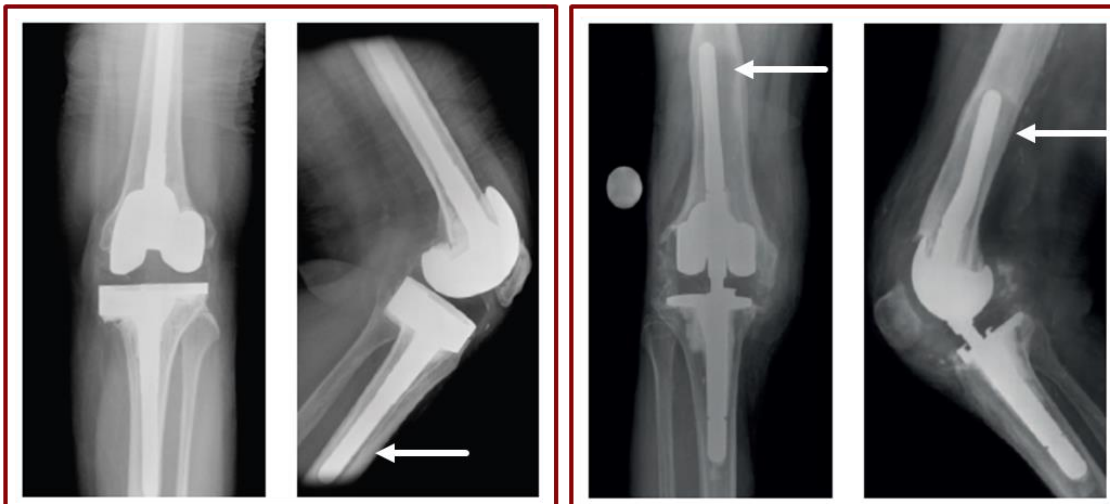

AP and Lateral x-rays showing a loose tibial component

AP and Lateral x-rays of right knee showing progressive bone loss and loosening

Figure 18 – Radiographs showing failure of RTKR due to bone loss and loosening (DePuy Synthes Institute 2014)

Failure of a RTKR is often due to a combination of stress shielding, bone loss, aseptic loosening, osteolysis, and infection (Bono and Scott 2005). Further factors can include malalignment, patient instability and loss of motion and it is usually a combination of these that contribute to failure, such as the occurrence of stress shielding leading to loosening and instability and ultimate failure. Many of these complications can be attributed to the implant design, method of fixation and surgical technique; the aspect of stem use and fixation will be discussed in detail. The use of stems is believed to cause both stress shielding proximally and stress concentrations distally at the stem tip (Bourne and Finlay 1986, Gofton et al. 2002) in addition to various other detrimental effects. Such problems associated with the use of stem extensions should be investigated and assessment made as to whether the advantages outweigh the limitations.

The use of long stems in the revision setting can cause complications that have an adverse effect on the success of the procedure. In some patients with deficient bone stock it is useful to avoid the proximal tibial bone defects and ensure the stress is transferred to the stronger distal bone (Scott and Biant 2012). However, the occurrence of stress shielding in the proximal metaphysis, as previously described, is often then compounded with the use of long revision components which contribute to further proximal bone loss as load is transferred distally. The use of stem extensions in RTKR has been found to consistently reduce strain in the proximal tibia by 30-50% (Rawlinson et al. 2005), although the authors of this study conclude that patients with poor quality bone would still benefit from this. A cadaveric study using 26 strain gauge rosettes demonstrated marked stress shielding with the use of stem extensions and discouraged their use. This method was limited as it used a simplified implant and re-used the same samples for various experiments which may have affected the results (Bourne and Finlay 1986). The effect of strain shielding with long stemmed implants is experienced with all fixation techniques; however, the extent of bone reduction has been found to be influenced by fixation. An early experimental investigation to assess the load transfer in a cadaveric tibia concluded that load bypassing occurred in the proximal tibia with cemented stemmed components which had the potential to lead to osteopenia (Reilly et al. 1982). The authors do highlight that this would be a useful occurrence in a revision scenario and so even early analysis revealed the fine balance that must be found with stem extensions. Another experimental study of cemented stemmed implants found stress shielding occurred around the implant over time, specifically in the proximal level, which can lead to bone resorption. This study to compare fixation techniques found that the prominent strain reduction in a cemented stem was three times that of a press-fit stem in the proximal synthetic tibia compared to an intact synthetic tibia (Completo et al. 2008a). A cadaveric investigation which assessed the effect of fixation technique on the stress distribution could not find a significant difference between cemented and press-fit stems, however the cemented stems did produce a 7-18% proximal tibial stress reduction (Jazrawi et al. 2001). Contrasting all of these findings, a computational study recently demonstrated that any fixation leading to firm anchorage between implant and bone experiences high levels of proximal bone resorption, and it is only the hybrid fixation that can help reserve bone stock (Chong et al. 2011).

Despite the abundance of published literature connecting stem use to stress shielding, numerous experimental and computational studies dispute this concept and the effect of stems remains a matter of debate. Many studies argue that stem use, or an increase in stem length, can cause little or no proximal stress shielding and no adverse effects on prosthetic fixation (Murray et al. 1994). Early studies found that extended stems do not cause significant stress shielding, just enough to aid the compromised proximal bone by transferring some force distally (Brooks et al. 1983). A retrospective clinical study found that there was no evidence of stress shielding after cemented RTKR (Murray et al. 1994). Another retrospective clinical study addresses the potential issues with the use of a stem as it showed that there was no difference in loosening rates between implants with or without a stem present. This allowed the conclusion that only revision procedures accompanied by significant bone loss necessitate the use of an intramedullary stem (Nazarian et al. 2002), however this does assume that the stem is only used to address implant loosening. The use of stems and their connection to stress shielding is clearly widely debated and there is still no consensus amongst experts as to what effect they have on the load transfer through the tibia.

In addition to the use of long stems leading to stress shielding in the proximal tibia, the transmission of force directly from the joint through the stem to the cortical bone can cause a stress concentration in the area of engagement (Chong et al. 2011). This often manifests as end of stem pain experienced by the patient and has been shown to affect 11-18% of cases (Barrack et al. 2004). Evaluation of whether there is a concentration of stress in the location of the stem end would help to identify if this is a likely contributory factor. This complication is clinically significant as it can reduce a patient's post RTKR quality of life, outcome scores and satisfaction (Barrack et al. 1999, Completo et al. 2012). Although the direct cause of shin pain is uncertain, the large stress transfer to the bone due to the difference in Young's modulus between stem and bone is a common theory (Kimpton et al. 2013). Another contributing factor may be the occurrence of stress shielding which as discussed may cause proximal bone resorption below the tibial tray, allowing movement of the stem and micromotion at the bone-prosthesis interface. The stress raising phenomenon has been highlighted by various studies, such as an early study assessing the cortical strain at various positions surrounding the tibia in vitro. The conclusions of this study discouraged the use of long stems due to the great increase in strain seen in the distal tibia (Bourne and Finlay 1986).

The high levels of strain and pain experienced at the stem tip has been discussed widely with regard to the method of stem fixation used. Barrack et al. (1999) found that the proportion of patients with end of stem pain was similar between cemented and cementless stems, however the link between end of stem pain and patient outcome was only found in the cementless group. This highlights the importance of clinical significance in any study and indicates that there may be more concern with cementless stem use than cemented. Many also argue that the press-fit technique has been found to cause end of stem pain as the stem engages the diaphysis (Completo et al. 2012, Haidukewych and Service 2012) and that pain is therefore more likely with cementless than cemented stems (Whaley et al. 2003). Despite this, other studies have shown that with cemented stems the majority of the load tends to transfer straight through to the stem tip, causing end of stem pain (Completo et al. 2008a). There are additional detriments of stem use in RTKR which may affect the clinical performance of tibial components. Modular stem extensions introduce another site which has the potential for junction failure, corrosion, fretting and debris generation, which could all lead to ultimate joint failure.

Many studies have chosen to provide alternatives to stem use in revision situations and test the effect that they have on the stability and load transfer through the tibia. For example, one investigation concludes that isolated bone defects can be dealt with using a block and tray instead of a stem (de Beer and Leone 2005). Alternatively, it has been suggested that short stemmed primary implants can be used in bone loss revision cases when using a standardised technique, specialised instrumentation and impaction grafting (Heyligers et al. 2001). The latter study only consisted of 9 patients however, with mainly T2a defects in the tibia, and the mean follow up time was less than 2 years (Heyligers et al. 2001). Regardless of the various arguments regarding bone reconstruction technique, stem use and design, it is important to evaluate in vitro the predicted load transfer characteristics of the approved long stems before surgical use.

As discussed, it is clear that sound revision total knee replacements are vital in the current climate of increasing primary surgery and patient demographics. The increasing demand places greater importance on ensuring that the component design is sufficient in allowing the surgeon to successfully replace the failed prosthetic joint and provide each patient with a pain free and functional knee. The surgeon is currently faced with many decisions regarding the type of implant and method of bone loss management used, with no clear guidelines or consensus on the best choice. The success of revision knee operations could be improved if there was a clear understanding of the effect of the implant design on the mechanics of the knee joint. Further improvements could address the remaining issues with stress shielding and end-of-stem pain if they are found to be an ongoing issue. Some studies have begun to address these topics, which will be discussed in detail in the following section.

4 Review of Load Assessment Techniques

Knowledge of the load transfer mechanism through the knee joint and specifically in the proximal tibia is essential to improving understanding and clinical outcomes in RTKR. The investigation of load distribution through the tibia was aided by a thorough evaluation of the literature with regard to the techniques that have been used in previous research. This provided information on the options available to make a quantitative assessment of the tibial load transfer under a physiological loading environment. Critical analysis of the literature allowed limitations to be identified which needed to be considered for the design and implementation of an appropriate test methodology and the equipment needed for this research. The measurement of load distribution through the tibia has been carried out using a variety of techniques which can be grouped into in vitro and in vivo methods. Historically, this has been performed through methods using gait analysis and mathematical modelling with video analysis and force plates to estimate joint forces (Kuster et al. 1997, Taylor et al. 2004). More recent approaches have included the use of strain gauges, digital techniques and instrumented implants. Research which has discussed the assessment of load transfer through the tibial condyles was also reviewed and presented as compartmental loading patterns. Finally, the past experimental testing facilities were analysed for their strengths and limitations.

4.1 In vitro

It is well accepted that the measurement of strain levels in the tibia can be used as an indication of the load transfer through the bone. Strain in the natural bone is the main stimulus for the bone remodelling process, so assessment of changes in strain compared to the natural strain levels can give an insight into potential changes to bone remodelling responses (Al Nazer et al. 2012). The biomechanical assessment of knee prostheses must include the load transfer characteristics of the different designs. The use of strain gauges is considered the gold standard for experimental strain analysis (Al Nazer et al. 2012) and various studies have been published describing their use for orthopaedic load transfer analysis. An early study by Finlay et al to develop a technique for measuring strains in the tibia highlighted the effect that the gauge angle at the point of measurement has on the strains measured. Based on this the authors concluded that it is vital to use strain gauge rosettes to obtain meaningful data when assessing strain distribution in the tibia (Finlay et al. 1982). A selection of studies that used strain gauge rosettes to assess load distribution have been analysed to provide a basis for their use and results produced. Investigations which have used alternative techniques to measure strain in the tibia were also reviewed to establish their potential use.

4.1.1 Strain Gauge Rosettes

Strain gauge rosettes, also known as tri-axial gauges, use three strain gauges to measure the strain in three axes so that the principal strains can be calculated. Although some experiments have attached gauges directly to the implant prior to implantation (Brooks et al. 1984), most have bonded them to the external tibia and measured the cortical surface strain instead (Bourne and Finlay 1986, Chang et al. 2011). This allowed measurements to be taken on the bone before and after implantation in order for a direct comparison to be made. Examples of such studies are contained in Figure 19. The extensive work by Completo et al also employs this method, where tri-axial strain gauges were attached to the cortical surface of a synthetic tibia (Completo et al. 2008a, Completo et al. 2010, Completo et al. 2012 and Completo et al. 2013). A similar approach was taken when assessing the load distribution after total hip replacement, using a synthetic femur model instead of the tibia (Politis et al. 2013). This study used a combination of triaxial and uniaxial strain gauges to assess the load distribution through the bone under physiological testing. Despite the promising methodology, the presentation of strain results in this study is unclear. The principal strains of the triaxial strain gauge rosettes were not calculated and the magnitude of strain recorded by the individual gauges was not discussed in any detail. The display of strain results in a series of bar graphs makes it difficult to determine the precise locations and circumstances that were being analysed. It does, however, point out that experiments of this kind may have the disadvantage that the location of the strain gauges may not reflect the locations of peak strains (Politis et al. 2013). Investigations of load distributions using strain gauges are not limited to synthetic bone models. However it is rare to find cadaveric studies that use strain gauge rosettes to present principal strain values. Jazrawi et al. performed biomechanical tests on 12 cadavers to assess the effect of fixation technique and stem geometry on stress shielding in the proximal tibia. The authors used 12 linear strain gauges bonded to the cortical bone of the tibia at three levels and tested at 0, 30 and 45° of flexion. Unfortunately, this study was limited as it is not possible to ascertain from the published paper how the stem and tray were secured together and the ability to remove cemented stems from a sample and re-insert alternative cemented stems without damaging the bone (and affecting the strain pattern) is questionable (Jazrawi et al. 2001).

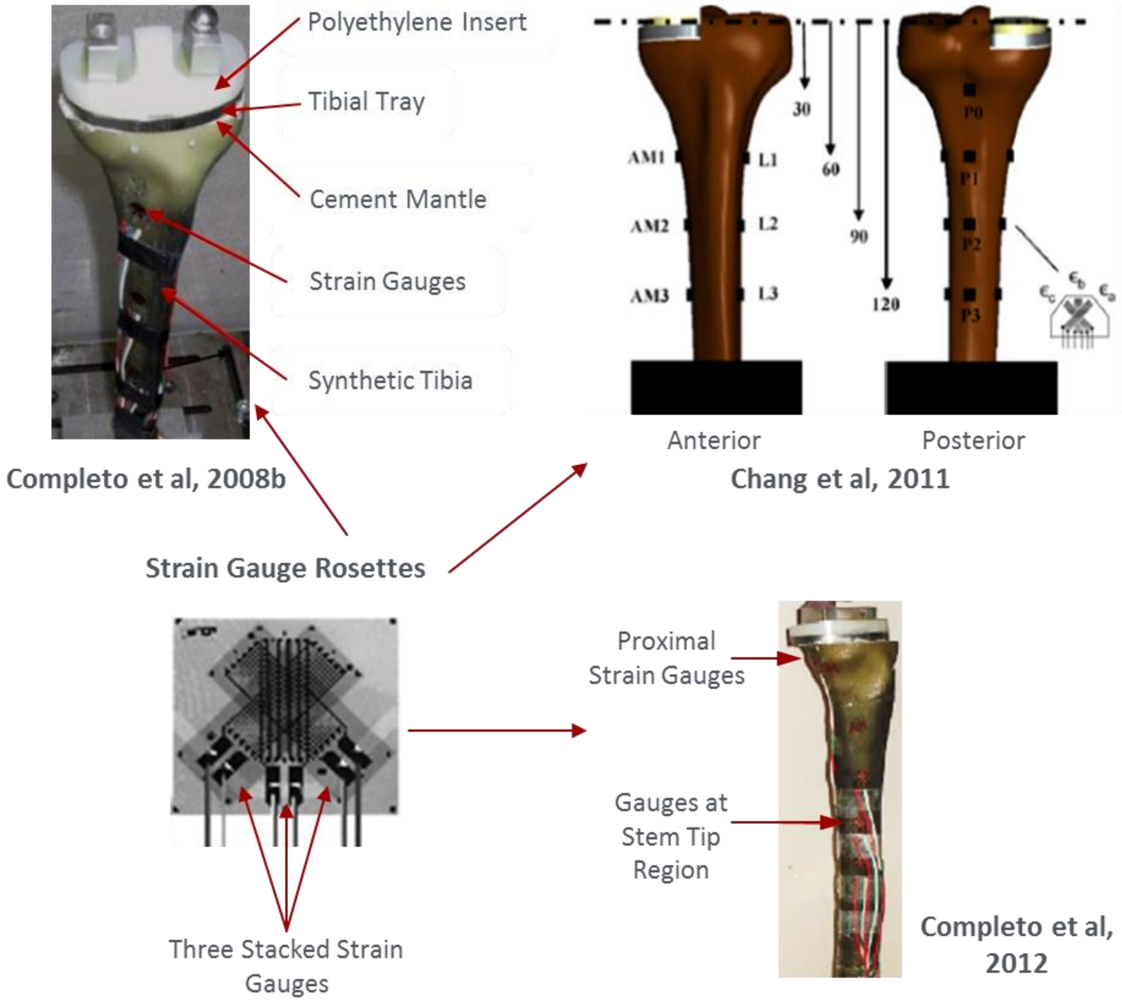

Figure 19 – Examples of published studies that have employed strain gauge rosettes to assess the load distribution through the tibia

As previously discussed, the position of the strain gauges on the bone is fundamental for the analysis of results as a small change in position can miss areas of significant change in strain, and strain gauge locations must be chosen specifically where the strain value is significant. The location of strain gauges varies in previous studies, for example some chose the posterior, antero-medial and lateral sides of the cortex at different levels (Completo et al. 2008b). Typical strain values published from experiments measuring cortical strain are in the range of 200-400 µstrain when the tibia was loaded to three times body weight (Reilly et al. 1982). Although such values will vary depending on the test set up and parameters used, they are still useful to have an understanding of the order of magnitude of expected strains.

4.1.2 Combined Experimental and Finite Element Analysis (FEA)

The experimental analysis of strain through the tibia has been accompanied by a finite element analysis, which has the advantage of allowing the internal strain and overall distribution to be analysed (Chang et al. 2011). An experimental and FEA study which investigated the load transfer pattern in the femur with total hip replacements is also a useful example as it combined techniques to determine both the cortical bone and cement strains using 10 strain gauge rosettes on the cortical bone and three embedded gauges on the implant (Waide et al. 2003). The methods used for this study unfortunately meant that there had to be new gauges attached to the bone for the implanted testing, producing the drawback of independent instead of paired samples for analysis. The work of Completo et al. using strain gauge rosettes on synthetic tibia was enhanced by combining experimental and finite element analyses. Six strain gauge rosettes were used to measure cortical strain in conjunction with a computational analysis to evaluate the proximal bone strains under different conditions (Completo et al. 2013). This allowed specific strain gauge values to be recorded whilst predicting the full strain field after different reconstructive techniques were used.

4.1.3 Digital Image Correlation

Alternative methods of investigating strain distribution exist which do not utilise strain gauges and are capable of assessing the full surface strain of the tibia. The technique of Digital Image Correlation (DIC) has been developed and used in orthopaedic applications as it is a non-contact, full surface method of measuring strain distribution in cortical bone. The DIC method overcomes the inherent limitation of strain gauges which measure localised surface strains. Localised measurement may miss locations of peak strain leading to misleading analysis of strain distribution. The DIC technique was successfully used by Mann et al. to take strain measurements from 21 retrieved human knees with cemented TKR (Mann et al. 2014). Another study used DIC to assess the full-field strain response of the proximal tibia with varying tibial implants and presented results of strain maps and magnitudes across the tibial surface (Malinzak et al. 2014). An example of their strain map results can be seen in Figure 20. Further investigation highlighted that this system of measurement does have its limitations which were discussed in these studies. The surface profile of the object of interest must be flat enough to allow accurate DIC results and so the application to long bones may be challenging. There is also a lack of validation studies to show that the quantitative strain results produced are reliable and accurate. Despite these limitations, the DIC technique seems to have a use in at least highlighting the areas of peak strain so long as it is possible to work within its limitations with the geometry of a tibia.

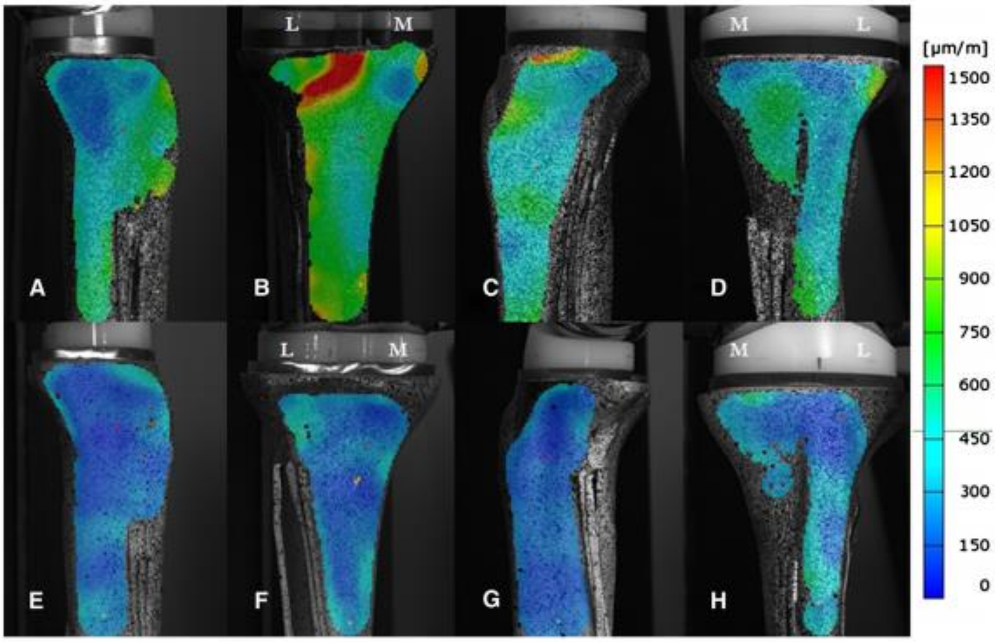

Figure 20 - An example of the strain response produced using the DIC technique on the loaded proximal tibia following RTKR. The top row illustrates the strain response after insertion of an implant with a fixed PE component, whereas the bottom row shows the strain with a mobile-bearing implant (Malinzak et al. 2014)

4.1.4 Laser

Another approach to measuring strain distribution is using the Electronic Speckle Pattern Interferometry (ESPI) laser-based technique. This is also a non-contact strain measurement system which has been used to assess the effect of malrotation on cortical strain distribution in the proximal cadaveric tibia after TKR (Kessler et al. 2006). This technique allows for non-contact full field strain measurement in contrast to the local strain that the authors measured using a strain gauge rosette, which demonstrated less than 7% deviation from the strain gauge results.

4.2 In vivo

The most accurate way to assess the load distribution through the tibial component is to use in vivo methods under physiological biomechanical conditions. Although it is possible to measure strain with strain gauges in vivo (Al Nazer et al. 2012), an invasive procedure is required which is considered unethical and does not allow for any level of repeatability. Instead the most accurate and suitable method of strain measurement in vivo is through the use of instrumented knee implants which have been used in recent years to measure the joint forces through sensors incorporated into the components (D'Lima et al. 2006, Mündermann et al. 2008). The advantages of using instrumented implants relate to the direct method of measurement they use, which produces readings of strain or force directly in the joint rather than the use of sensors on the surrounding bone. This also allows measurements to be taken during different patient activities in real in vivo conditions accounting for joint angles, weight and soft tissue forces. There are limitations of in vivo testing in this way, however, as each individual patient provides different results due to their different anatomy and function. The cost, time and ethical approvals required means that most studies only look at a very small sample size meaning that an outlier patient could have a bias on the results. The instrumented implant will measure forces experienced by the implant and not necessarily by the bone, which will be very specific to the type of implant used and the individual patient. If an average is taken across a number of patients and a number of studies are compared which use different implants, then a good understanding of the knee joint loads can still be found so further analysis of the literature was warranted. The first instrumented tibial implant was developed by Kaufman et al with a technical note published in 1996. This implant used four load cells below the tibial tray to directly measure the knee joint forces, however it was not capable of measuring shear forces and the original tibial tray had to be removed and replaced by a custom made one to accommodate the sensors (Kaufman et al. 1996).

The use of instrumented total knee replacements such as the tibial component seen in Figure 21 has allowed for the direct measurement of knee joint forces under a range of activities (D'Lima et al. 2006, Mündermann et al. 2008). One such study utilised the developed instrumented prosthesis which used force transducers embedded in the tibial component in combination with motion capture technology. It investigated several activities of daily living to find the magnitude of knee joint loads at varying flexion angles. The results provide a useful insight into knee joint forces at the tibial tray, however no force was measured through the tibia and the data presented is of a single subject only (Mündermann et al. 2008). The use of instrumented implants on small patient samples is valuable because they have recently been used to validate numerical models so that further information can be found on knee joint forces (Lundberg et al. 2012). Based on the previous research of D'Lima et al, a subsequent investigation improved in vivo load measurements by testing five subjects rather than one or two. An instrumented knee prosthesis was used in the study which used six strain gauges to calculate the load components acting through the tibia and presented extensive results to reiterate that the measured loading is greatly different from calculations (Kutzner et al. 2010).

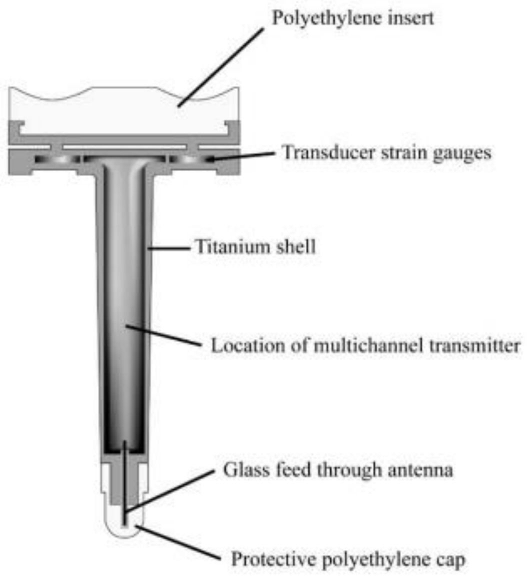

Figure 21 - Example of an instrumented tibial implant in cross section (D'Lima et al. 2005)

4.3 Compartmental Loading Patterns

The discussion regarding load assessment techniques so far has concentrated on establishing the load that is transferred through the tibia from the knee joint. It has looked mostly at the strain at the surface of the tibia either at local points or across the full shaft as shown in grey in Figure 22. These measurements allow for an understanding of how inserting a knee replacement component into the tibia affects the strain distribution through the tibia. It can be used to begin to understand the bone resorption and pain sometimes experienced by the patient's post-RTKR and the reasons for future failure. To have a thorough understanding of this load transfer, it is vital in experimental procedures that the loading through the knee joint mimics that in vivo. Studies have shown that the compartmental loading through the tibial plateau (shown in red in Figure 22) is not balanced between the medial and lateral condyles and so this WILL have an effect on the tibial load distribution which is not accounted for in any of the experimental studies discussed so far. This imbalance in load distribution is understood when the anatomy of the lower limb is considered. The average mechanical axial alignment of the natural knee is 1.1 - 1.5° of varus (Moreland et al. 1987), which causes the medial tibial condyle to be subjected to a higher proportion of the load (Scott and Biant 2012). Au et al. (2007) used a developed finite element model to assess the loading conditions in a tibia model with a TKR to establish their effect on the stress shielding. They concluded that there were many aspects of the loading conditions that influenced stress shielding post operation, which included the altered condylar surface geometry and the load pattern and placement on the condylar surface. This indicates that the proportion of load share across the tibial plateau will have an effect on the resulting strain in the tibia. The difference between the medial and lateral side was discussed as early as 1982 by Reilly et al. but no attempt to quantify it was made and so instead an unknown difference in force was applied across the condyles during the experimental work (Reilly et al. 1982). Since then, some studies have tried to estimate what the compartmental load share is although very few take it into account when designing their experimental procedure despite its potential effect on their results.

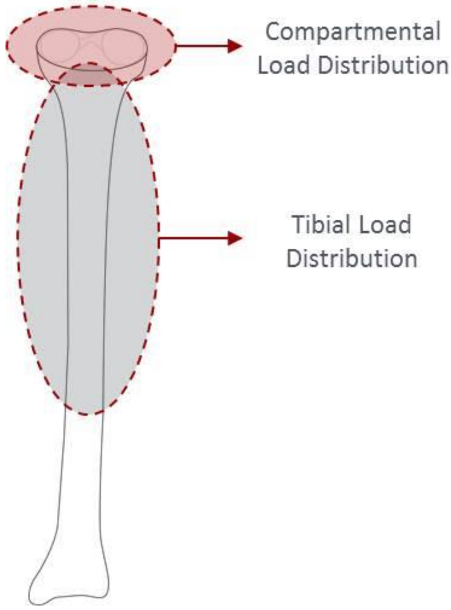

Figure 22 – A diagram illustrating the different areas of load distribution in the tibia. The grey area encircles the bone that is commonly assessed during testing. The red area shows the compartmental load distribution that is rarely accounted for.

Some research has focussed on the effects of misalignment of TKR components on the load distribution through the tibia. An early study by Bartel et al. highlighted the importance of aligning the components to produce the best load share across the tibial plateau (Bartel et al. 1982). The only study found to have in some way assessed the effect of a changing medial: lateral loading was Green et al in 2002. They used a photoelastic coating on cadaveric tibias inserted with a cemented TKR to assess what effect proportions of 50:50, 58:42 and 75:25 had on the tibial surface strain (Green et al. 2002). However, the main part of the study compares the difference between varus and neutral implanted tibia, leading to most of the analysis being centred on this. The study did find that the effect of medial loading was greater with varus aligned tibial components, but it is uncertain if this effect would be reflected with the use of RTKR components.

From the published studies that have applied the use of instrumented implants, experimental procedures, mathematical modelling or finite element analysis, the compartmental load share under different activities of daily living can be estimated. As early as 1970, Morrison published a paper that had analysed the forces transmitted in the knee joint in 12 subjects. He found that a greater proportion of the force was transmitted through the medial condyle than the lateral in the stance phase of walking (Morrison 1970). Morrison's results were often referred to in further research such as Reilly et al, who aimed to replicate a 1.4:1 medial to lateral force across the condyles. The authors used air cylinders to supply varying compressive force through medial and lateral loading arms, but with no validation of what force was transferred through the compartments (Reilly et al. 1982). A study which analysed joint loads in TKR did not discuss the variation in compartmental loading but did provide useful information on the typical tibiofemoral contact area that is loaded, 100-300 mm^2. It also laid out the typical joint forces reported for tibiofemoral and patellofemoral joints under different activities (Kuster et al. 1997). In more recent studies, instrumented implants such as that used by Kutzner et al have provided detailed information of the joint loads experienced by the individuals tested with the specific components implanted. The study in 2010 measured five subjects in vivo and reported the abduction-adduction moments experience by the instrumented tibial component varied across all eight activities tested (Kutzner et al. 2010). The medial to lateral load distribution was specifically measured by Mundermann et al with an instrumented total knee replacement in a single subject. It found a 1.7:1 peak medial to lateral load ratio during walking, rising as high as 2.7:1 in squatting (Mundermann et al. 2008). This loading was also measured directly in vivo in an earlier study with a single patient, and concluded that a load share of 55:45 % medial to lateral would be appropriate for testing conditions. These results are particularly limited due to the single subject and the understanding that the subject had his hands on the handrail of the treadmill during the testing which inevitably would have greatly affected the results (Zhao et al. 2007).

A selection of research has been published where the experimental set-up has partially accounted for the compartmental load share; however none have directly measured the loads. The early study of Finlay et al. (1982) used a simple and sophisticated method to allow the adjustment of varus – valgus loading through the knee joint, as illustrated in Figure 21. They did not, however, have any means of measuring the relative forces being transmitted through the condyles to verify their method (Finlay et al. 1982). A series of experiments by Completo et al. have included a 60:40 load share between the medial and lateral condyles using a development of techniques as shown in Figure 23 (Completo et al. 2008a, 2013). Both studies used the same basis of a ball bearing as a fulcrum which was offset from the centre to shift the load share towards the medial condyle. None of their testing actually measured the proportion of load transferred through the condyles and it is questionable given the complexity of the surface geometry and loading that force calculations will accurately produce the desired load share. Jazrawi et al. also considered eccentric loading as part of their loading conditions. They simulated varus-valgus loading by inserting a 5° wedge under the baseplate on each medial and lateral side in turn, however no further measurement was carried out to determine what compartmental force this produced and the effect of these loading conditions were not reported in the results (Jazrawi et al. 2001). A retrieval study by Mann et al. claimed to replicate the 60:40 compartmental load share whilst functionally testing strain in human knees. It is unclear how they applied the relative axial loads through the polyethylene (PE) insert at the wear contact points identified however and there is no indication that this was measured in any way (Mann et al. 2014).

Finally, the laser-based strain acquisition study used a pivot hinge and slider to alter the varus-valgus loading and compartmental loading patterns to be 60:40 medial: lateral. Like in all previous studies described here, there was no measurement made of this force and no mention of how the rig was validated to ensure the 60:40 loading (Kessler et al. 2006).

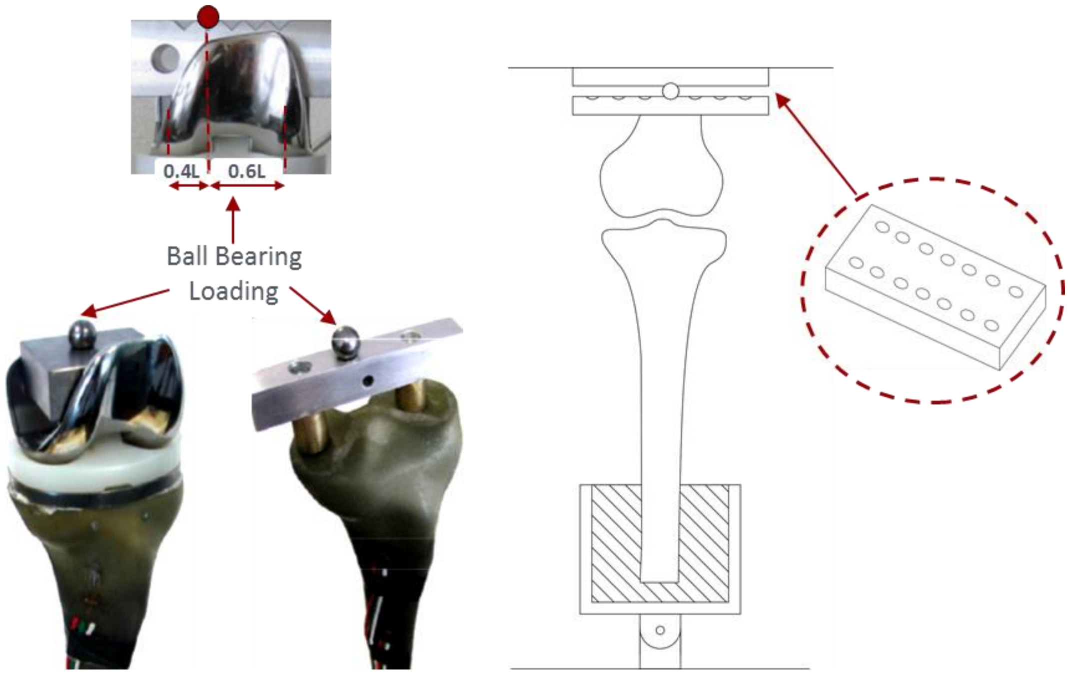

Figure 23 – A collection of published methods which have attempted to replicate the compartmental load share through the tibial condyles (Completo 2008a, 2013 and reproduced from Finlay et al. 1982)

From this literature evaluation, it was clear that compartmental load share is rarely measured directly in experimental studies that assess load transfer through the tibia. No reported experimental studies have assessed how the compartmental load share may affect the load distribution through the tibia after RTKR. To truly assess the load distribution in the tibia, the loading at the tibial plateau should be measured and controlled to ensure that the experiment accurately replicates the physiological conditions as much as possible. This would also allow an investigation into what effect altering this compartmental loading may have on the load transfer through the tibia.

4.4 Experimental Rigs

In the previous sections, the analysis of publications regarding the load distribution in the tibia has concentrated on the load distribution measurement and the inclusion of the compartmental load share at the knee joint. A final review was based on the design of the experimental loading rig and testing protocol used in each investigation. The considerations that need to be made when designing a test procedure of this kind relate to replicating physiological conditions as closely as possible with the resources available.

Most studies focus on the tibiofemoral joint and simulate single leg stance and stair climb in their investigations by altering the load and flexion angles. Some include other activities in addition to these such as deep bending. An example of this can be found in the study by Meireles et al, which is also the only one to include the patellofemoral joint forces because it investigates a patellofemoral arthroplasty (Meireles et al. 2010). Other studies do not attempt to replicate physiological conditions and instead simply apply a vertical load at 0° of flexion (Completo et al. 2008a) the results of which, although interesting, are not clinically relevant. The inclusion of muscle forces is often recommended to improve the understanding of the stability of tibial components, however no work has been published that does this using composite bone models. The range of loading scenarios used in past investigations is considerable with variable parameters such as the magnitude and direction of load, loading cycle, frequency and the degree of movement allowed for the tibia. All of the past studies are useful to consider during the rig and test protocol designs required to reach the objectives of this research.

5 Objectives

5.1 Literature Summary

A detailed review of the literature provided greater understanding of the mechanics of the natural knee and a full appreciation of the process of Primary and Revision Total Knee Replacements. It focussed on the tibial component of RTKR, establishing why they are needed, the variety of design options available and their strengths and limitations. The published studies and further research were also used to evaluate the various methods employed to assess the load distribution through the tibia including the issue of compartmental loading at the tibial plateau.

Following the literature evaluation it was possible to develop key objectives to explore further during this research into strain distribution in the proximal tibia when inserted with a revision tibial component. From this review it was deemed appropriate for the research to follow its original path, whilst the gaps in the published literature generated the need for further investigations into the effect of the applied loading on the strain distribution to reach the outcomes of the study. It is hoped that the conclusions from this research will help guide the future design on the tibial components whilst also improving future implant testing with a robust experimental rig.

5.2 Objectives

The overall objective of this research was to develop a robust experimental test protocol for pre-clinical evaluation of RTKR tibial components. This was approached in two main sections detailed below.

The first stage of the study aimed to develop a robust tibiofemoral testing rig and protocol to experimentally analyse the variation in cortical bone strain in the tibia before and after implantation of a RTKR component. This would give an indication of the load transfer through the tibia and how it is altered with RTKR surgery. This stage consisted of three main phases including the development of the test rig, the intact bone testing and the implanted bone testing. Development of the experimental rig and protocol included the selection and preparation of suitable implant components, bone and meniscus substitutes and strain and force sensors. These coupled with the design of the test rig allowed a preliminary study to be completed on a single specimen to ensure a robust experimental set up. Following this, the testing was expanded to multiple specimens to assess the intact and implanted scenarios under various simulated physiological loading regimes. During both intact and implanted testing, the study planned to explore the effect of altering the compartmental load balance on the load transferred through the tibia.

The second stage of the research then intended to develop a combined loading testing rig utilising the same bone preparation that resulted from stage one. The influence on the implanted load distribution of physiologically loading through both the tibiofemoral and patellofemoral joints would then be explored. After the combined loading rig was developed, the research planned to perform tests under the same conditions and with the same specimens used in the tibiofemoral rig to directly compare the effect of the applied loading. It was hoped that the result of these investigations would help guide tibial implant design and future pre-clinical testing techniques.

6 Development of the Testing Rig

To enable analysis of the load transfer characteristics of an intact tibia and a tibia implanted with a revision tibial component, it was necessary to develop an experimental rig and associated test protocol. This was a progressive process which included stages of selecting and obtaining appropriate materials, bone preparation, investigating measurement techniques and test rig development. The chart in Figure 24 illustrates this process and gives an overview of the stages necessary to arrive at the final solution used in the main testing. This chapter will detail the key findings and justify the decisions made throughout the development process. The first main output of this development was the design of an initial rig that was capable of replicating the physiological loading from the tibiofemoral joint similar to those used in past research. The subsequent development was a secondary rig that was capable of representing the load from a combination of the tibiofemoral and patellofemoral joints. In addition to the development of the experimental loading rigs, further requirements included the selection of materials and sensors and the design of a series of jigs to ensure repeatable and consistent preparation of test samples.

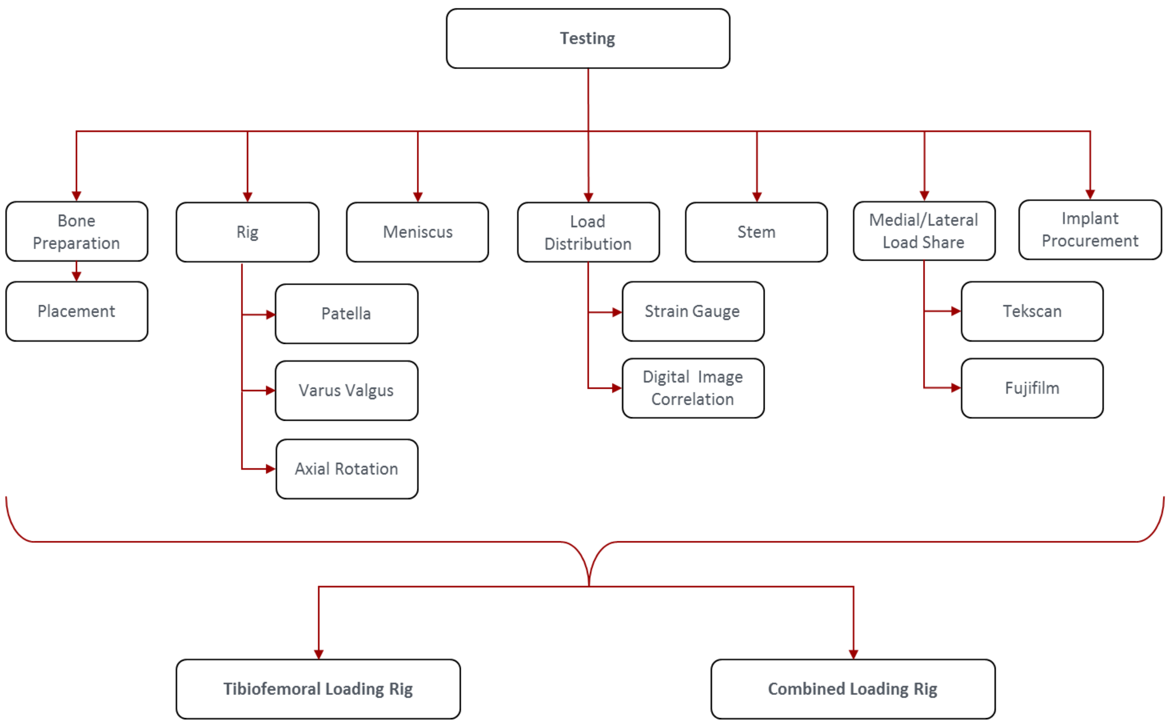

Figure 24 - A chart to summarise the main elements of the development of the testing rigs resulting in a 'Tibiofemoral Loading Rig' and a 'Combined Loading Rig' as detailed in this chapter

6.1 RTKR Component Selection

Of the 36 brands of revision total knee implants used in the UK in 2013, the three most widely used were the DePuy PFC Sigma, the Stryker Triathlon and the Zimmer Nexgen, accounting for 37%, 12% and 11% of the total procedures respectively (National Joint Registry 2014b). Over the past six years that the NJR have been publishing the data on specific prostheses used, the number of procedures using the Stryker Triathlon has been increasing steadily (National Joint Registry 2009, 2010, 2011, 2012, 2013b, 2014b). The Triathlon Total Knee Replacement Components (Stryker, Michigan, USA) were selected to be used in this study based on their use in current UK revision operations and their availability for testing. The selection of each component size was based a Sawbones medium left composite femur and tibia (models #3401 and #3403, Sawbones Europe AB, Sweden) using the manufacturers recommended surgical instrumentation and operating procedure. The components are shown in Figure 25 and consist of; Triathlon Total Knee Universal Tibial Baseplate, Triathlon Total Knee Cemented Stem – Diameter 12 mm and Length 100 mm, Triathlon Total Knee Posterior Stabilised (PS) Femur and Triathlon Posterior Stabilised Tibial Insert (all size 4). The Posterior Stabilised components were used due to the lack of cruciate ligaments on the composite model.

Figure 25 – The details of the revision total knee replacement components used throughout development and testing

Based on the desired minimum sample size of five specimens, six tibial trays were sourced to allow one to be used for the preliminary testing and five for the final testing. It was not possible to source the six tibial stems for the trays, so a single stem was obtained which was used for the preliminary testing and to aid the manufacture of five tibial stems to be used for the final testing. As manufactured stems were being used, it was important to ensure that they would have similar mechanical properties to the original stem to minimise any effect on the strain results. The manufacturing process of the five tibial stems involved accurately replicating the geometry of the Stryker stem, although due to manufacturing limitations four flutes were added instead of the original five causing them to be symmetric. This should not have any effect on the strain distribution results. The material chosen was stainless steel 316 which has a similar Young's modulus to the cobalt chrome Stryker stem (approx. 200 vs 220 GPa). This means that the stiffness of the two stems should be similar due to their similar geometry and any small change in stiffness is expected to have no effect on the final cortical strain results. A recent FEA study concluded that there is no significant difference in stress shielding between long stems made of titanium or cobalt chrome where there was a greater difference in Young's modulus than there was in this research and so a minimal difference in Young's modulus was considered acceptable for this study (Completo et al. 2009). The same study highlighted that the geometry of the stem produced greater effect than the material and so this was concentrated on during manufacture. Further tests were also performed to ensure that the manufactured stems were adequate replicas of the Stryker stem and are detailed in Appendix A – Stem Manufacture. The overall results of all investigations regarding the geometry, mass and material of the tibial stems confirmed that they were acceptable for use in this study and that they would not have a significant effect on the load transfer analysis. The final five stems used can be seen in Figure 26 alongside the Stryker stem to show the similarities. With the RTKR components selected and sourced it was possible to continue to develop the investigations by preparing the substitute bone specimens for testing.

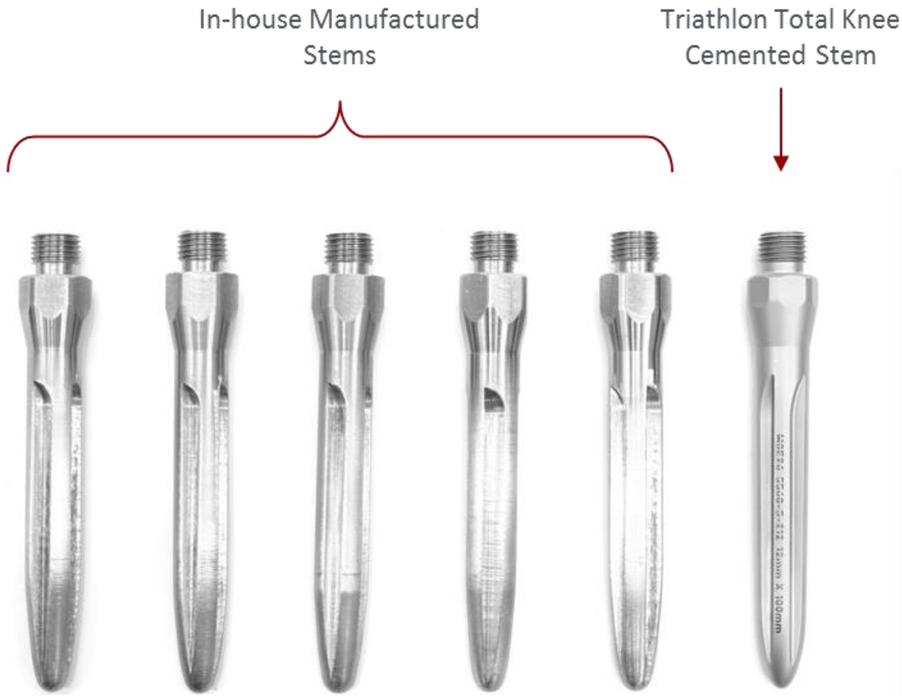

Figure 26 – The five manufactured stems used in the final testing alongside the original Stryker Triathlon stem that they were based on

6.2 Bone Substitute Preparation

This research required in vitro laboratory testing in order to be able to assess the load transfer through the tibia. The in vitro testing could either utilise cadaveric specimens or Sawbones synthetic bone substitute specimens. The mechanical properties of composite Sawbones have been found to be within the range of cadaveric specimens in terms of their geometry and mechanical properties (Cristofolini and Viceconti 2000, Heiner 2008). These biomechanical bone models also provide advantages such as consistent geometry and mechanical properties for repeated experimentation. They are also readily available and do not degrade with time. Sawbones specimens were therefore selected to be used for this study and are shown in Figure 27. Their design consists of an outer cortical shell of glass fibres and epoxy resin with an inner cancellous bone of rigid polyurethane foam.

Figure 27 - Tibia and Femur 4th Generation Composite Bones – Medium Left Sawbones #3401 and #3403

Every tibia used in the experimental study had to be prepared identically to ensure accurate comparison of results. A fixture to allow accurate and reproducible preparation of the Sawbones tibias was designed which could be converted to allow for preparation of each tibia before and after they were permanently fixed into their pots for testing. A CT scan of a Sawbones tibia was performed (Siemens SOMATOM Sensation 64 CT scanner, 1 mm slice thickness) and the DICOM files were then segmented and meshed to generate a 3D model using specialist image processing software (Simpleware ScanIP, Exeter UK). Using this 3D CAD model of the tibia specimen, it was possible to develop a series of Boolean moulds to surround the surface of the tibia. These moulds were designed to assemble in an alignment jig which could align the tibia along its mechanical axis and be placed in the same position consistently. Figure 28 shows the development of the alignment jig with the final seven moulds used to hold the tibia in place with and without positioning in the tibial pot.

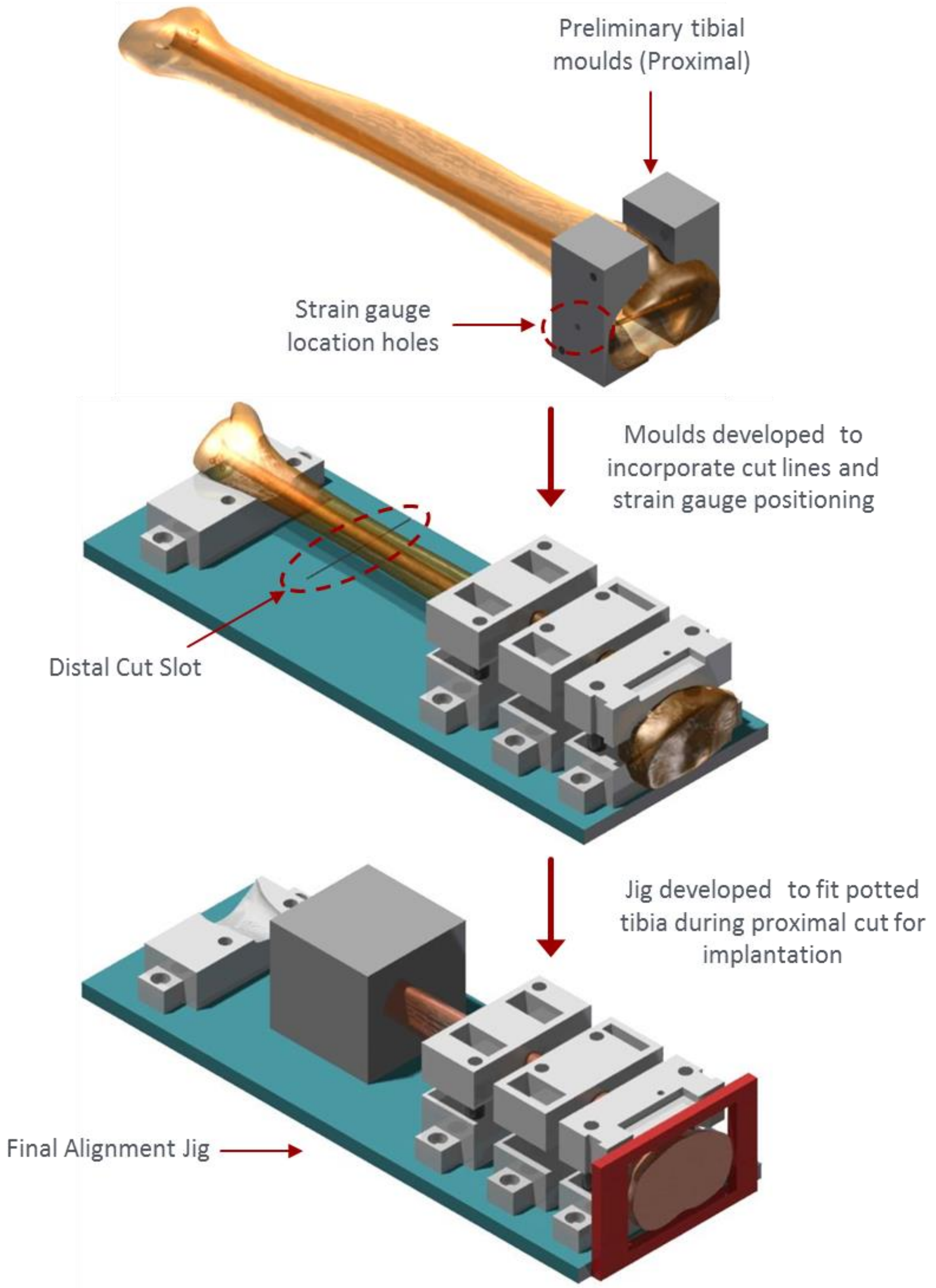

Figure 28 - Development of the Tibial Alignment Jig using 3D printed moulds to locate the tibia consistently in the jig

The tibial moulds were also developed to consistently locate and guide the distal cut of the tibia so that it could be potted ready for testing as shown in Figure 28. The distal cut was made at 278 mm from the most distal part of the medial tibial condyle based on the Saint Venant's Principle. This principle describes an allowable distance from the stem tip to the fixation point to be approximately twice the diameter of the diaphysis to ensure that the boundary effects did not influence the load distribution (Stolk et al. 2001, Jonkers et al. 2008). Once the distal cut had been made, each specimen had to be potted identically and at the correct angle to allow it to be mounted correctly in the test rig. The custom made tibial holder shown in Figure 29 was designed to utilise the hollow shaft of the tibia and a rotation puck was used to set the axial rotation of the tibia in the pot. The specimens could then be potted by surrounding them with a low melting point metal alloy known as 'Wood's metal' (MCP75; Mining & Chemical Products Ltd., Northamptonshire, UK) in a custom made specimen holder to ensure consistent tibial rotation. Once the tibias were potted and the intact testing completed, it was necessary to incorporate a method of consistently making the proximal cut and implanting the tibial components into the alignment jig. The position of proximal cut was taken from a 'gold standard' bone preparation performed by an experienced Stryker representative using the correct instrumentation. This coincided with the use of the tibial moulds in the alignment jig shown in Figure 28 to allow a repeatable proximal cut to be made and the remainder of the implantation process was completed using the correct instrumentation.

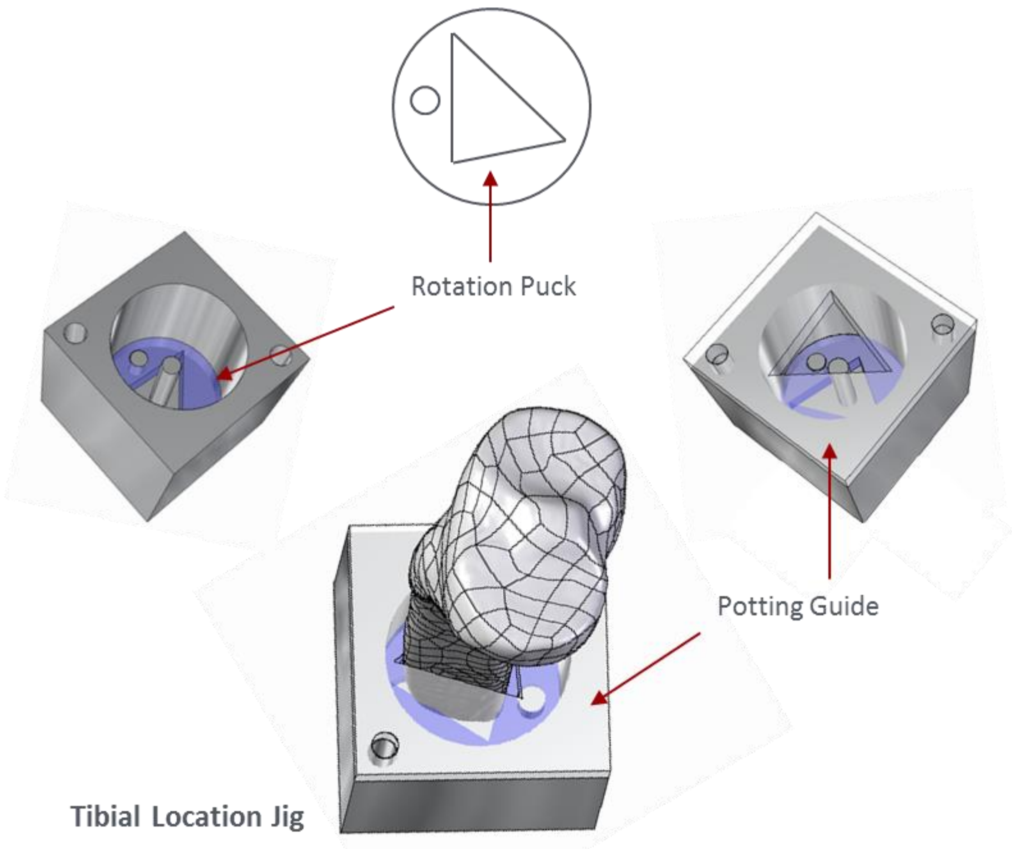

Figure 29 - Tibial Location Jig developed to fix the tibial shaft rotation angle and tibial axial alignment during the potting process

It was important that the locations of the strain gauge rosettes were repeatable across all specimens and ideally would be placed at the areas of peak strain. A method used in previous experiments marked the locations using a Coordinate Measuring Machine (CMM) (Completo et al. 2012); however this was not feasible in this study. After further review of past studies in the literature and a series of preliminary testing that will be discussed further, the strain gauge locations were set and a method created for consistent placement. The tibial alignment jig was designed so that it located the three posterior strain gauges using holes in the mould and baseplate. An additional jig to allow the location of the remaining two strain gauges on the medial and lateral tibial surfaces, the Sagittal Placement Guide, was also developed and is illustrated in Figure 30 with the final tibial alignment jig. The details of the strain gauge positioning can be found in a later section which details the use of past studies and DIC to select suitable gauge locations.

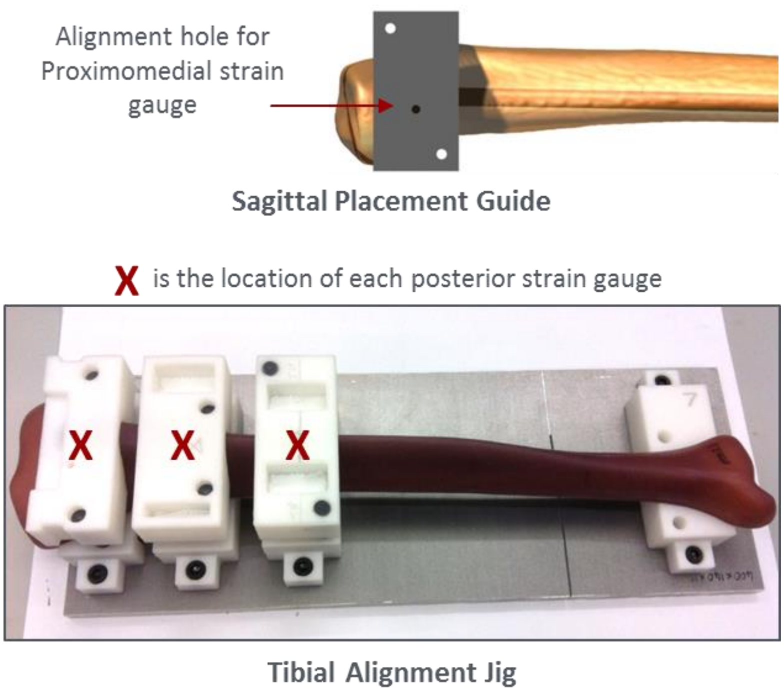

Figure 30 – The two sets of guides used to locate all five strain gauge rosettes on each tibia specimen. The sagittal placement guide was used to locate the proximomedial gauge on the medial side (shown) and the proximolateral gauge on the proximal side (not shown).

A composite Sawbones femur that was either intact or implanted with a Triathlon femoral component was prepared to apply the loading to the tibia in all experiments. This implantation was performed by a Stryker representative with experience in revision knee surgery and Sawbones implantations. The femur had to be correctly aligned to ensure accurate and repeated tibial loading. The flexion axis in the sagittal plane was fixed to match the axis of the single radius Triathlon knee. Rotation about the long axis of the femur was planned as part of the test set up and the shaft of the Sawbones femur was found to align well in the sagittal plane. This meant that only the coronal plane alignment had to be set to mechanical alignment during potting to correctly load the tibia. Using the CAD model of the Sawbones femur, the angle between the mechanical and anatomical axis was measured by aligning the bone along the anatomical axis and drawing a line between the centre of the femoral head and the intercondylar notch. The angle between these lines was then measured to be 6° and the femoral post was set accordingly as shown in Figure 31. To ensure the load was centred about the knee, the femur was then offset by 11 mm using an offset plate, completing the bone substitute preparation.

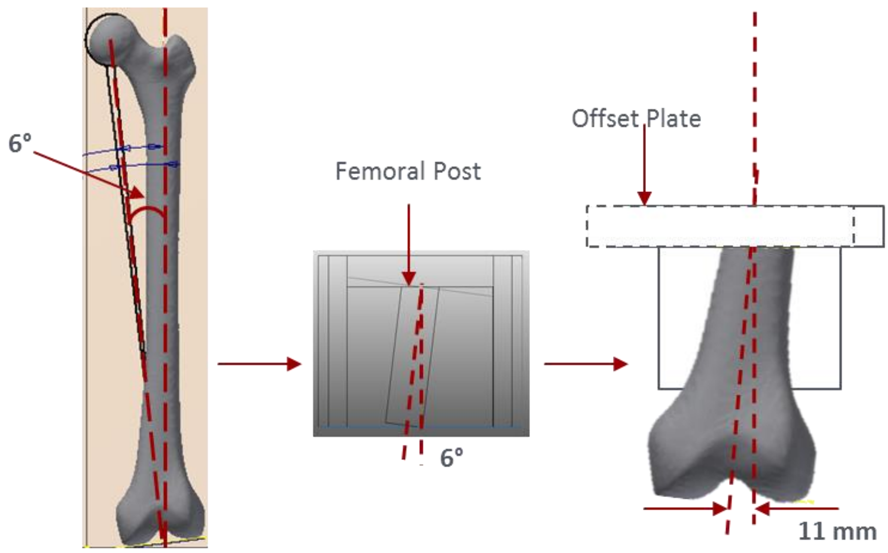

Figure 31 – The process of determining the necessary adjustment angle using a CAD model of the Sawbones femur and then setting it to its mechanical alignment in the test rig

6.3 Meniscus Substitute

To perform in vitro tests on the intact knee joint using synthetic bone specimens, it was necessary to obtain a suitable substitute for the meniscus cartilage that exists in the natural knee. As discussed in the background section of the report, the menisci are semi-circular structures which aid the load distribution through the TFJ. A full investigation of the material options available to act as a meniscus substitute was carried out which yielded four potential solutions, summarised in Table 2. As the bone substitutes had been sourced from a specialist company (Sawbones) attempts were made to establish if a meniscus substitute was also available. This provided Option 1 for consideration, Sawbones Meniscal Pads (#1457), which was geometrically similar to match the Medium Left Sawbones, however did not exhibit the correct mechanical properties. After further investigation into alternative materials, Option 2 and Option 3 were discovered and sourced. Through a review of the literature, a final material option, Sorbothane polyurethane (Sorbothane Inc, Ohio, USA), was found which claimed to have similar properties to the natural meniscus and had been used in previous biomechanical testing (Scott et al. 2013).

Option 1	**Option 2**	**Option 3**	**Option 4**
			
Sawbones Meniscal Pads # 1457	Fibrous Cloth	Sugru (Formerol Silicon) (Sugru 2015)	Sorbothane 70 & 80 Durometer

Table 2 – The four potential meniscus replacement materials that could be used during the intact testing.

Initial investigations ruled out the use of the Options 1 and 2, the Sawbones meniscus and fibrous cloth, as they did not replicate the material properties and were also difficult to manipulate and place in position in the joint space. The ability to mould the Sugru was useful but once set, it was not compliant enough to be used in the final testing. A published study used Sorbothane 75 Durometer as a meniscus substitute; however the only samples that were available were 70 Durometer and 80 Durometer. Both samples were therefore tested to validate their mechanical properties and find which one was the most suitable substitute for the natural meniscus. Compression tests were carried out on the samples as detailed in Appendix B– Meniscus Compression Tests.

From the results of the compression testing, it was confirmed that the 70 Durometer Sorbothane would be a suitable material to use as a substitute for the natural meniscus. This was based on the experimental Young's modulus which was found to be 1.4 MPa which is in the range of a natural meniscus (Scott et al. 2013). The limitation of Sorbothane was that it was not easily manipulated into a suitable anatomical shape. For this reason Sugru was used in the preliminary testing performed to develop the testing rig as the material properties were not vital for this stage whereas the geometry was. Two Sorbothane pucks were then cut to be used for the final testing where the mechanical properties of the meniscus substitute was the priority.

6.4 Axial Rotation

To perform preliminary testing on a single specimen a test rig was required that could allow the substitute tibia and femur to be mounted into it and be placed under physiological load using the Zwick hydraulic test machine (HBT 25-200, Zwick Testing Machines Ltd., Leominster, England). Once the bone preparation and alignment jigs were complete, a single specimen was prepared for testing and used in combination with the selected substitute meniscus. To analyse the load distribution through the tibia, a static test rig was required which would initially simplify the knee joint to a single axial degree of freedom to assess how the load would be transferred. The effect of the PFJ and all of the degrees of freedom about the TFJ were absent, apart from the axial rotation of one bone relative to the other in the transverse plane. This original test assembly was designed so that the femur would rotate about the axis of the tibia to allow the tibia to be later set at various flexion angles. From research it was clear that the rotational alignment of the femoral component was important for the success of a TKR but difficult to effectively align (Nagamine et al. 1998) and therefore the most appropriate way to allow for this was to implement a rotational degree of freedom. The final design of the original femoral sub-assembly of the test rig with axial rotational freedom is illustrated in Figure 32. This initial set up was used to perform pilot studies to evaluate the bone preparation, the preliminary use of strain gauge rosettes and their data acquisition. These studies found that this approach had shortcomings as it does not account for the changes in compartmental loading as discussed in the literature review. The test rig therefore needed to be developed to incorporate this.

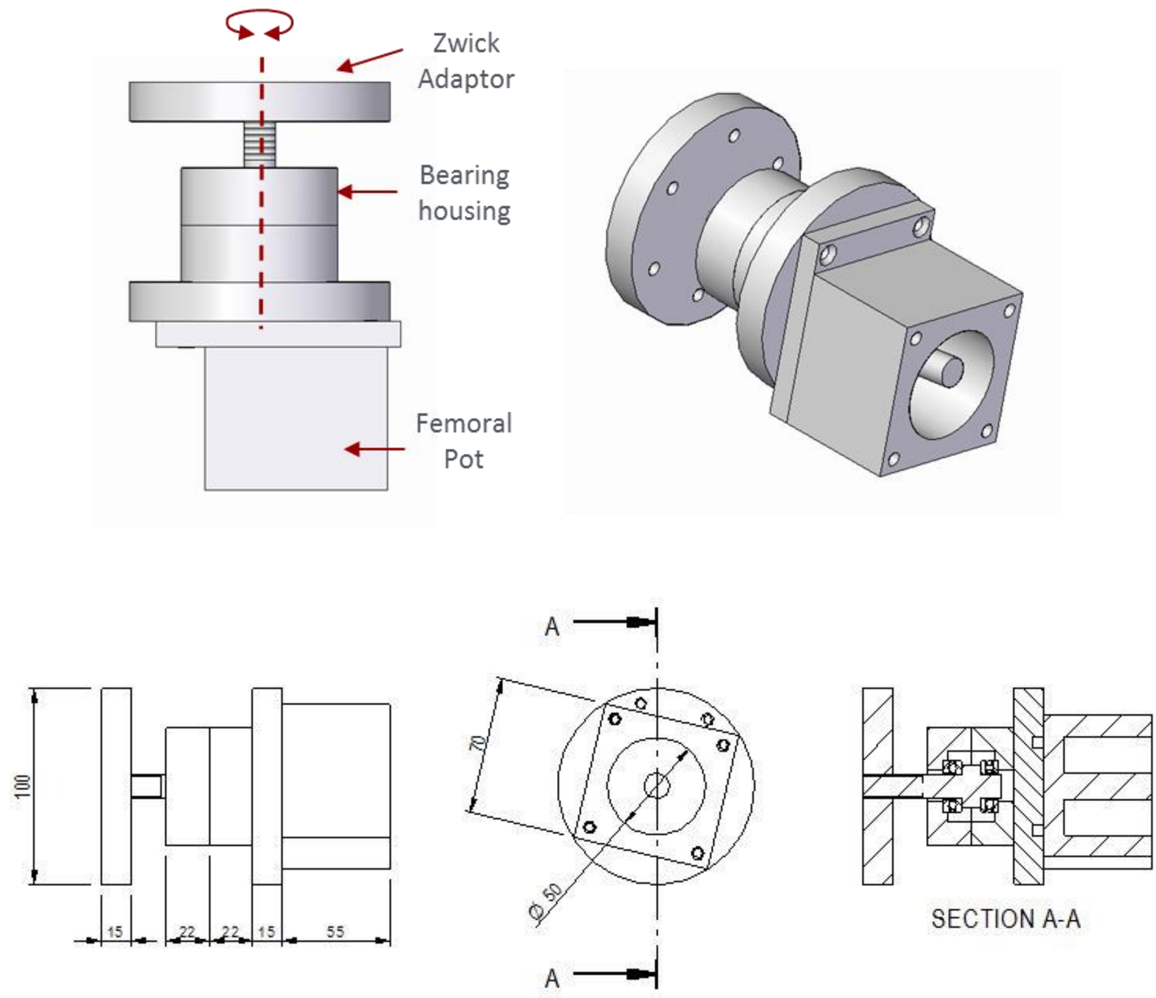

Figure 32 – Initial femoral sub-assembly of the test rig which produced one degree of freedom through axial rotation. A snapshot of the engineering drawing with overall dimensions is included with annotated illustrations.

6.5 Compartmental Loading

The review of the literature regarding the forces present in the knee joint during daily living activities illustrated that the load share across the tibial plateau (the compartmental loading) was not balanced and varied with activity (Morrison 1970, Mundermann et al. 2008). The investigation of previous studies that have measured the load transferred through the tibia without an instrumented implant highlighted that this compartmental loading is rarely accounted for during in vitro testing. The load share has also never been measured during in vitro testing to assess what effect it has on the load transferred through to the tibia. Using recent data published from instrumented knees, it was decided that it would be beneficial to develop the experimental rig to allow adjustment of the load share between the medial and lateral tibial condyles. A rig to allow this adjustment of force transmitted through each condyle, an assembly to allow rotation in the coronal plane, was designed as illustrated in Figure 33. If the preliminary tests indicated that there was a significant difference in the tibial strain with compartmental loading, then any future biomechanical testing of this type should have the ability to measure, and ideally adjust, the compartmental load share.

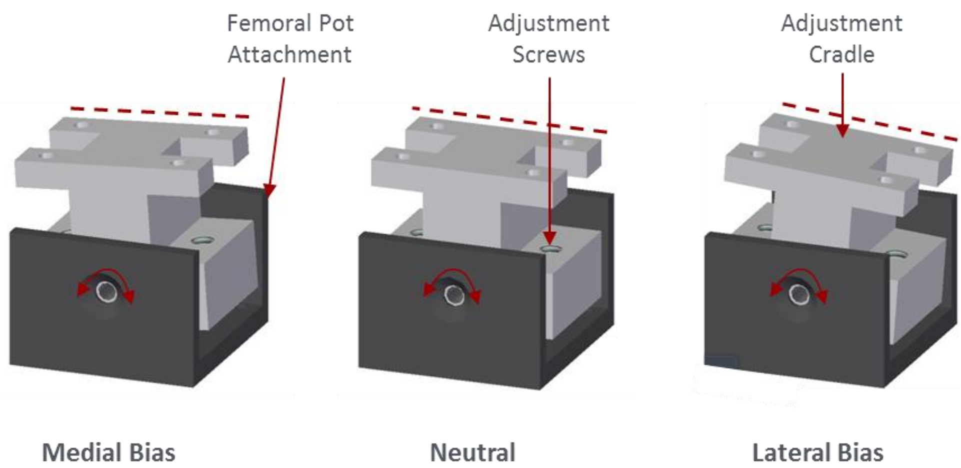

Figure 33 – The compartmental loading sub-assembly of the test rig that altered the varus – valgus alignment to allow fine adjustment of the medial: lateral load share experienced across the tibial condyles.

In theory, a change in the M:L loading will change the effective resultant axial load as illustrated in Figure 34 and subsequently effect the strain through the tibia. The effective of changing this load between 50:50, 70:30 and 90:10 on the strain is calculated below. This uses a simplified model of a tibia to a hollow cylinder with a central neutral axis and it was assumed that the distal end was fixed.

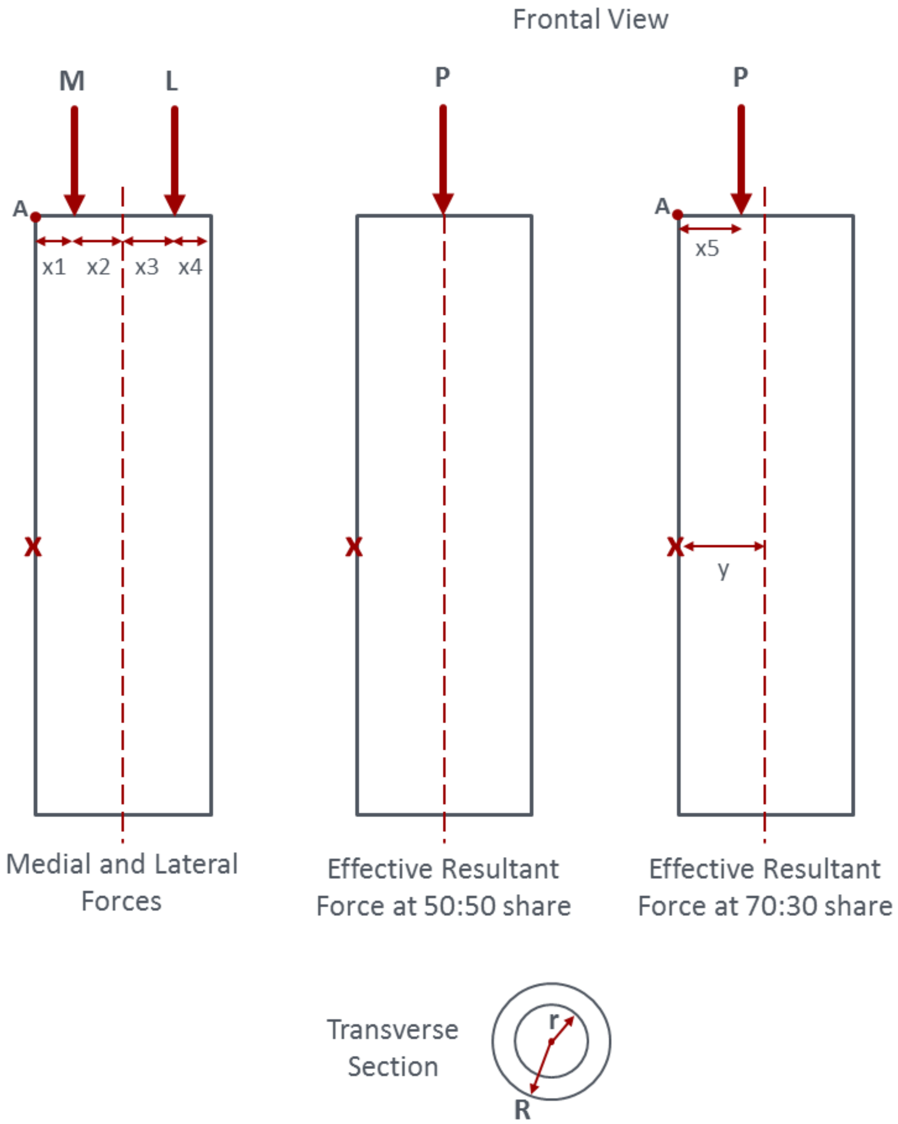

Figure 34 – Free body diagrams of a simplified tibia showing the compartmental loading and equivalent loads depending on what load share is analysed

Calculating the effective resultant axial load from a 50:50 compared to a 70:30 proportion M:L load share;

For 50:50, P = 500 N

For 70:30, x1 = 15 mm, x2 = 22 mm, x3 = 22 mm, x4 = 15 mm, taking moments about A;

$$M = (350 \times 15) + (150 \times 59) = 14{,}100\ Nmm$$

$$P \times x5 = 14{,}100$$

$$x5 = \frac{14100}{500} = 28.2\ mm\ from\ A$$

For 90:10;

$$M = (450 \times 15) + (50 \times 59) = 9{,}700\ Nmm$$

$$P \times x5 = 9{,}700$$

$$x5 = \frac{9700}{500} = 19.4\ mm\ from\ A$$

Also when R = 11 mm and r = 4.5 mm, the area can be calculated;

$$A = \pi R^2 - \pi r^2 = (\pi \times 0.011^2) - (\pi \times 0.0045^2) = 316.5 \times 10^{-6}\ m^2$$

At 50:50 there is no bending moment contribution;

$$\sigma = \frac{P}{A} = \frac{500}{316.5 \times 10^{-6}} = 1.58\ MPa$$

$$\epsilon = \frac{\sigma}{E} = \frac{1.58}{16700} = 94.6\ \mu\ strain$$

At 70:30 the stress at Point X, assuming the tibia as a hollow cylinder, can be calculated;

$$\sigma = \frac{My}{I} + \frac{P}{A}$$

$$M = P \times (y - x5) = 500 \times (0.037 - 0.0282) = 4.4\ Nm$$

$$I = \frac{\pi}{4}(R^4 - r^4) = \frac{\pi}{4}(0.011^4 - 0.0045^4) = 11.18 \times 10^{-9}$$

Giving;

$$\sigma = \frac{My}{I} + \frac{P}{A} = \frac{4.4 \times 0.022}{11.18 \times 10^{-9}} + \frac{500}{316.5 \times 10^{-6}} = 10.2\ MPa$$

Then the strain at Point X based on Sawbones cortical bone;

$$\epsilon = \frac{\sigma}{E} = \frac{10.2}{16700} = \boldsymbol{613\ \mu\ strain}$$

At 90:10 the stress at Point X, assuming the tibia as a hollow cylinder, can be calculated;

$$\sigma = \frac{My}{I} + \frac{P}{A}$$

$$M = P \times (y - x5) = 500 \times (0.037 - 0.0194) = 8.8\ Nm$$

Giving;

$$\sigma = \frac{My}{I} + \frac{P}{A} = \frac{8.8 \times 0.022}{11.18 \times 10^{-9}} + \frac{500}{316.5 \times 10^{-6}} = 18.9\, MPa$$

Then the strain at Point X based on Sawbones cortical bone;

$$\epsilon = \frac{\sigma}{E} = \frac{18.9}{16700} = \boldsymbol{1132\, \mu\, strain}$$

Modulus value E is based on simulated cortical bone (short fibre filled epoxy resin) = 16.7 GPa (Sawbones Biomechanical Test Materials 2015). This shows that increasing the medial portion of compartmental loading subsequently increases the strain on the medial side of the tibia.

A preliminary study was performed on a single tibia specimen to establish if the predictions on effect of changing the compartmental loading on strain in the cortical tibia were accurate. This research was presented at the British Orthopaedic Research Society meeting which can be seen in Appendix C and is detailed here. The study used two axial strain gauges mounted on the medial and lateral sides of the distal tibia to measure the cortical strain (Vishay: J2A-13-S109M-350. Using two force sensors (Flexiforce A201, Tekscan) as discussed in Section 6.9, the force through each tibial condyle could be measured when under a 400 N load applied by a hydraulic test machine as shown in Figure 35.

The results from the preliminary testing into the effect on tibial load transfer are summarised in Figure 36. When the load share measured by the force sensors was 40:60% (Medial:Lateral), the strain measured in the distal tibia was found to have similar proportions between the medial and lateral sides (70 and 100 µstrain).

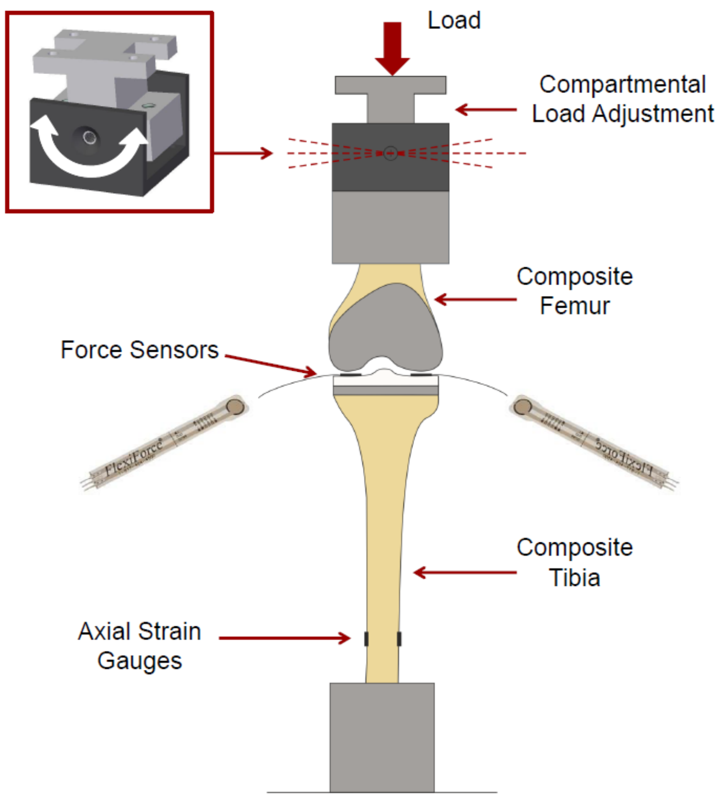

Figure 35 – Illustrating the experimental test set up used for the preliminary investigations into the effect of compartmental load transfer

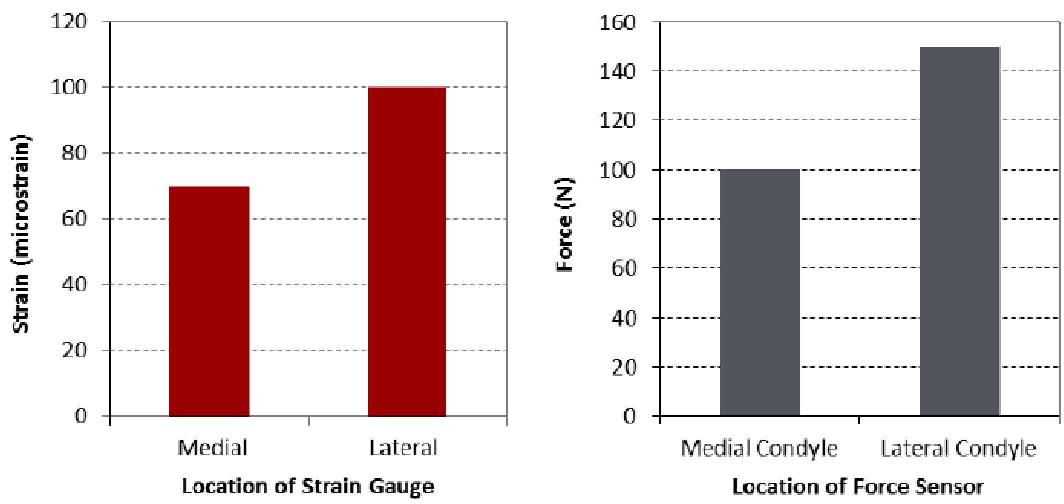

Figure 36 – The results of the preliminary investigations into the effect of compartmental load transfer showing the relationship between force applied and strain produced

This initial study to gauge what effect this share has on the load transferred distally through the tibia highlighted how closely related these factors are with the 40:60% compartmental load share transferring to the distal tibia. The study concluded that the proportion of load through the tibial plateau coincided with similar proportions of load transferring distally through to the tibia.

6.6 Placement Guide

A method to ensure consistent placement of the tibial assembly on the Zwick test machine with respect to the femoral assembly was required to remove any error from small inconsistencies between the specimens. Initially, once the trial specimen had been correctly positioned, the aim was to mark the Zwick table to ensure the base plate was put back in the same position each time. However, this did not overcome small inconsistencies with the specimens and so a placement guide was developed which could use the femur as a datum to ensure that the tibial assembly was always positioned identically in relation to the femur, the most important relationship when investigating the TFJ.

Two assemblies forming the placement guide were designed to sit over and be secured to the proximal tibia and distal femur respectively. The trial tibial assembly was positioned and clamped into place, and was this used to set the connecting holes forming the relationship between the two sections of the placement guide as shown in Figure 37. It was then possible to use this guide each time a new specimen was placed on the Zwick.

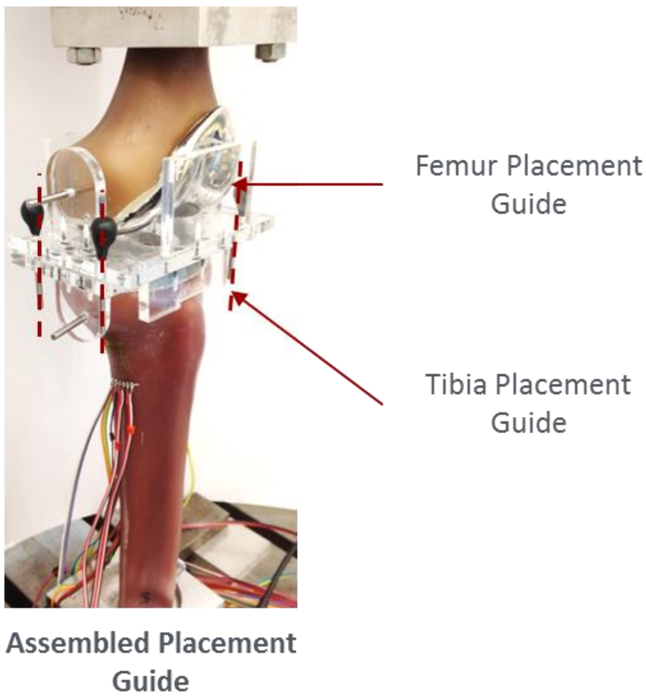

Figure 37 – The placement guide developed and used to ensure consistent placement of the tibial assembly on the Zwick testing machine with respect to the femoral assembly

6.7 Flexion Angle Adjustment

Following the developments in the design of the femoral side of the test rig to allow transverse and coronal plane adjustment, the tibial assembly was selected to allow adjustment of the sagittal plane or knee flexion angle. This was required to allow testing at various angles of flexion to replicate activities of daily living. From the literature it was clear a suitable range of angles would be 0°, 10° and 30° of flexion; however, the preliminary testing (Figure 38) showed that 30° was beyond the limit of the capability of the experimental rig due to its isolated reproduction of the TFJ without the inclusion of the PFJ. It was decided at this stage that the 0° and 10° flexion testing would provide useful results when comparing the intact and implanted states and when assessing the effect of the compartmental loading variations. This provided further weighting to the need to also develop a rig that was capable of replicating the combination of the TFJ and PFJ, allowing testing at greater flexion angles and a comparison between the loading scenarios.

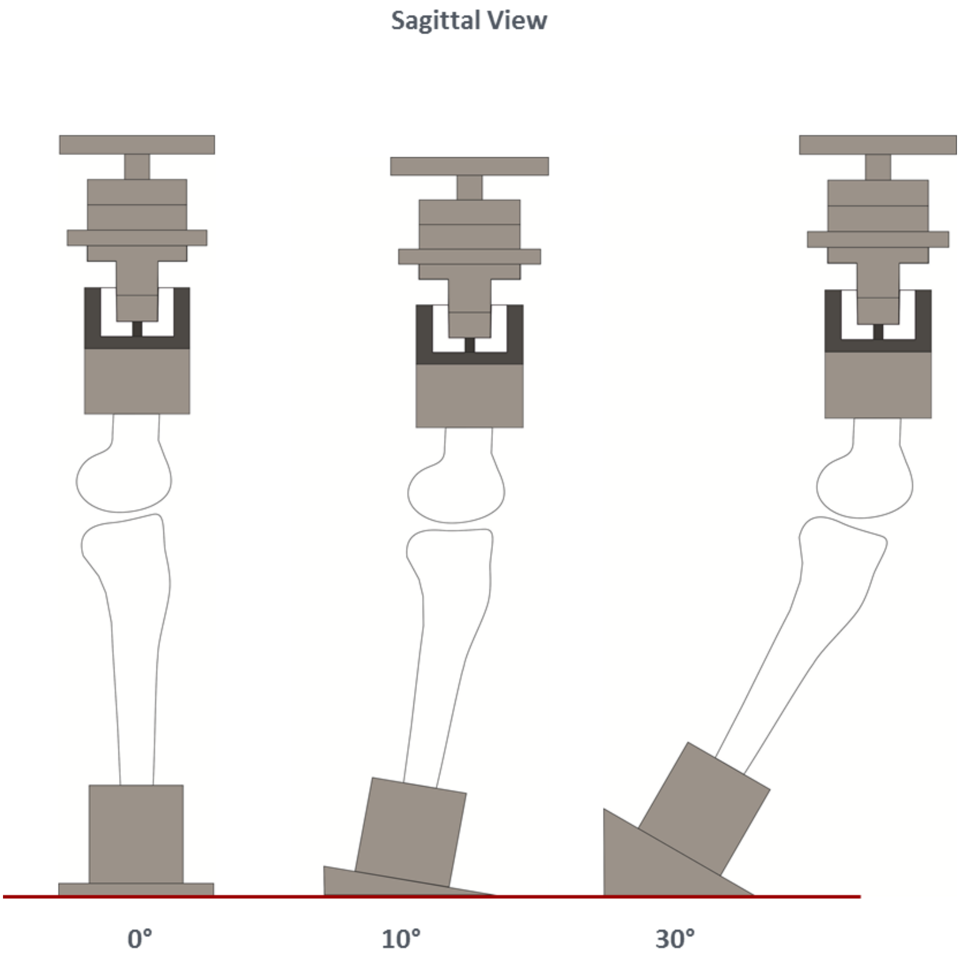

Figure 38 – Illustrating the method used to adjust the knee flexion angle through the tibial assembly between 0, 10 and 30° of flexion.

6.8 Load Distribution Assessment

Following the development of the experimental rig to produce a physiological load through the knee joint, it was essential that an accurate process of assessing the load distribution through the tibia was found. The review of the literature demonstrated that it was possible to measure the strain in the cortical bone and use these values as an indication of the load transfer through the tibia. Previous studies have also indicated that a variety of methods were capable of measuring this strain experimentally and computationally. For this study it was decided that strain gauge rosettes would be used to precisely measure the principal strains at five locations surrounding the tibia, with the assistance of a digital image correlation technique for optimum strain gauge placement and an appreciation of the full surface strains.

A prediction of the approximate strain values expected in the tibia was made to gauge an understanding of strain level measurement required and allow a comparison with the preliminary test results. A simplified free body diagram of the tibia and the forces acting on it is shown in Figure 39. The strain produced in the cortical bone is a product of the axial load applied and bending loads.

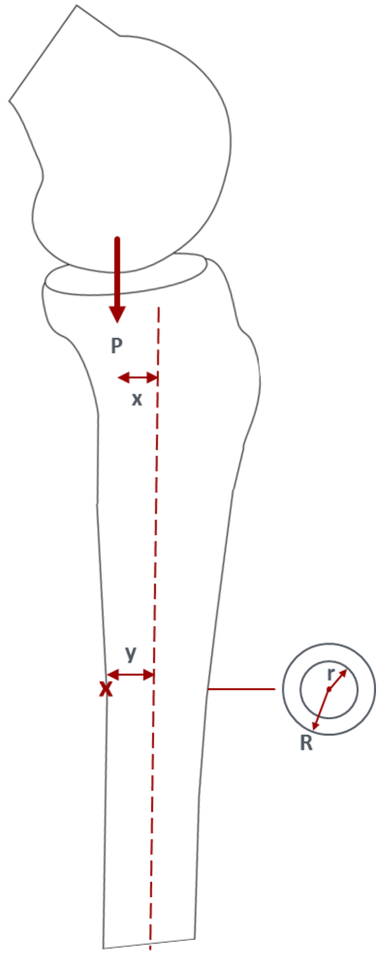

Figure 39 - Free body diagram of the simplified tibia under loading

$$\sigma = \frac{My}{I} + \frac{P}{A}$$

$$\epsilon = \frac{\sigma}{E}$$

So to calculate the stress at Point X, assuming the tibia is a hollow cylinder and the distal end is fixed;

$$M = P \times x = 500 \times 0.009 = 4.5\, Nm$$

$$I = \frac{\pi}{4}(R^4 - r^4) = \frac{\pi}{4}(0.011^4 - 0.0045^4) = 11.18 \times 10^{-9}$$

$$A = \pi R^2 - \pi r^2 = (\pi \times 0.011^2) - (\pi \times 0.0045^2) = 316.5 \times 10^{-6}\, m^2$$

Giving

$$\sigma = \frac{My}{I} + \frac{P}{A} = \frac{4.5 \times 0.011}{11.18 \times 10^{-9}} + \frac{500}{316.5 \times 10^{-6}} = 6.01\, MPa$$

Then the strain at Point X based on Sawbones cortical bone;

$$\epsilon = \frac{\sigma}{E} = \frac{6.01}{16700} = \mathbf{359.7}\ \mu\, strain$$

6.8.1 Strain Gauge Rosettes

The location of the strain gauge rosettes around the tibia was initially decided with the aid of the knowledge gained from the literature and the geometry of the bone and tibial implant. A summary of the literature used can be found in Table 3. From this a pilot study investigated if these locations were feasible and tested the strain gauge data acquisition protocol and LabVIEW (National Instruments Corporation, Texas, USA) data collection program. The locations were marked using the alignment jig which had been designed to allow consistent placement of each strain gauge. Five stacked strain gauge rosettes sourced specifically to suit this application (1-RY91-6/350, HBM, Germany) were bonded to a tibia specimen with the central gauge positioned parallel to the longitudinal axis at the locations shown in Figure 44. The rosettes were stacked due to the confined flat space available for mounting, as the profile tibia is complex curves. It would also allow for any high strain gradient as it was not known if this would exist at the time. The use of 350 ohm gauges was recommended due to their ability to reduce the heat generated compared to a 120 ohm gauge as heat dissipation may be an issue when using stacked rosettes.

Publication	Number of Gauges	Strain Gauge Locations
Chang et al. 2011	10	Anteromedial, Lateral and Posterior sides of the cortex at 4 levels
Reilly et al. 1982	16	Four levels 10-110mm from tibial plateau – four gauges at each level; Anterior, Posterior, Medial and Lateral
Completo et al. 2012	6	3 Proximomedial, Lateral and Posterior and 3 Periosteal cortex at stem tip Medial, Lateral and Posterior
Jazrawi et al. 2001	12	Tibial cortex; Anterior, Posterior, lateral and Medial at 10mm, 75mm and 150 mm

Table 3 – A selection of published literature that have used strain gauge rosettes to investigate tibial strain distribution including the locations of these gauges

Each strain gauge was connected to a custom written programme in LabVIEW which could record the gauge measurements of changing voltage, through the use of eight data acquisition cards. This data acquisition network is displayed in Figure 40.

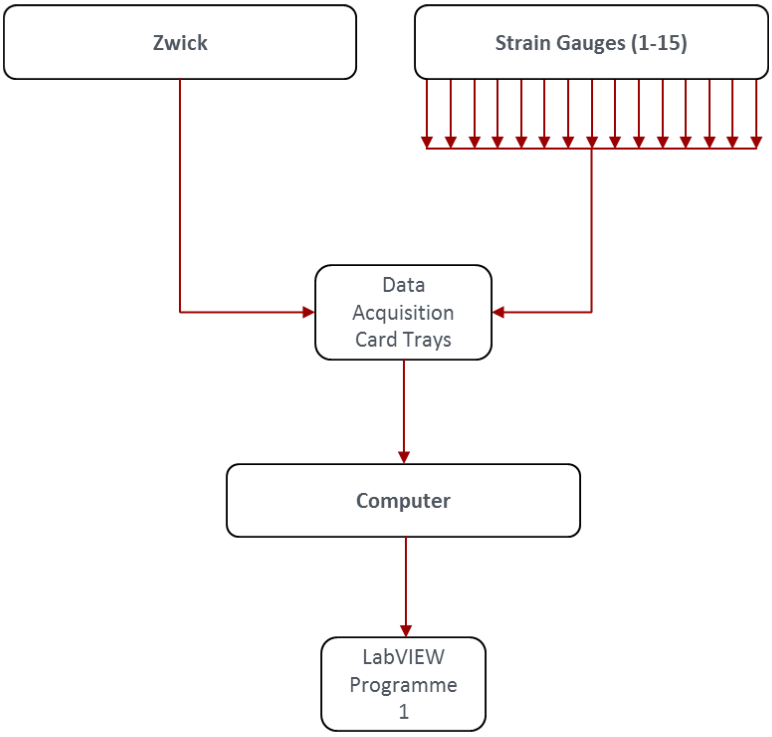

Figure 40 – A summary of the data acquisition network used in the preliminary testing

Once the strain gauges had been bonded in position and the data acquisition system prepared, the specimen was tested to ensure that the system was reliable. This was done by comparing with the results from the P3 strain indicator box and with the typical magnitudes of strain found in the literature using similar set-ups. Results from this preliminary study confirmed that this method was appropriate in assessing the strain at specific locations in on the tibia cortical bone. It was undetermined if the locations chosen to place the five strain gauges were appropriately measuring the peak strain in the bone and also it would be beneficial to see the strain across the full surface of the tibia. To establish the locations of peak strain and allow analysis of the full tibial surface, a preliminary study using the DIC technique was performed.

6.8.2 Digital Image Correlation

The use of digital image correlation techniques to assess the full surface strain across bones has been demonstrated in the literature as discussed previously. DIC provides non-contact, whole tibial surface strain measurements (Sztefek et al. 2010) by using two high speed cameras to track the relative movement of dark patterns on white bone. This technique was used at this stage of development to contribute to the understanding of the surface strain across the tibia, whilst also to compare the strain magnitudes measured at the strain gauges with those found from DIC analysis.

The study aimed to measure the tibial surface strain in a physiologically loaded intact and RTKR implanted tibia using digital image correlation for the reasons discussed to contribute to the development of an experimental procedure to assess the load transfer through the tibia. The tibia and femur specimens used for all preliminary testing were used again in this study. Both tibial surfaces were prepared for DIC analysis by applying a painted speckle pattern, as shown in Figure 41.

Figure 41 - The painted speckle applied to the tibia prior to DIC testing

The DIC cameras (Photron Fastcam SA3, USA) were positioned level with the tibia surface and calibrated according to a standardised procedure. The specimens were subjected to cyclic loading between 100-600 N for 50 cycles at 1 Hz (Zwick). Whilst under load, the cameras recorded data at 50 fps (Photron Fastcam Viewer, 2006) and upon completion all image processing was carried out on Vic-3D 2009 (Correlated Solutions Inc., SC, USA) to illustrate the corresponding strain pattern. Both the intact and implanted tibias were tested three times to view the three faces; anterolateral, posterior and anteromedial. The test set-up is shown in Figure 42, which was taken during the anterolateral test.

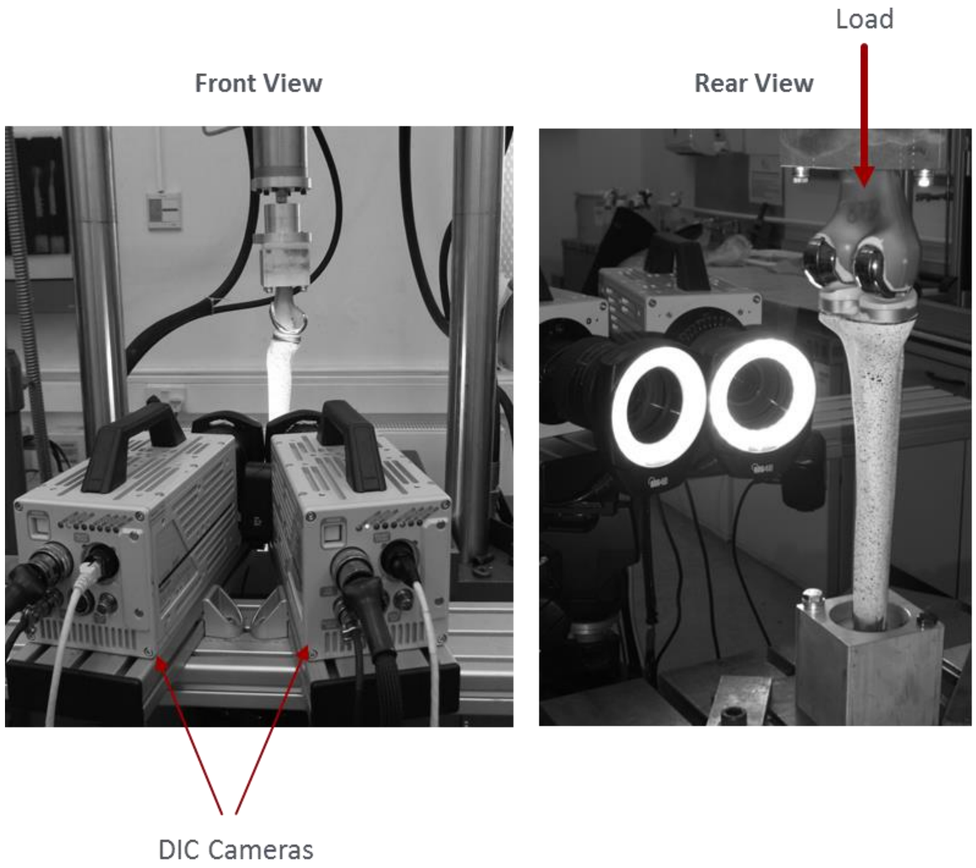

Figure 42 - The DIC test set up

An example of the DIC map results of this study shows Lagrangian strain fields on the three surfaces imaged and how the strain varied across the implanted bone surface (Figure 43). The implanted bone results ranged between 500 µstrain in tension to 600 µstrain in compression and indicate that the strain was concentrated distally post implantation in comparison to the more uniform strain across the surface of the intact bone. This distal stem concentration correlates with the gauge located at the stem tip level. The study allowed the DIC technique to provide an indication of differing strain patterns across the tibial surface with intact and implanted bone. This increased the understanding of the strain pattern across the tibia and verified that the location of the strain gauges was suitable and that there were no key areas of peak strain seen outside of the locations measured. The study did also highlight the inaccuracies involved in specific strain magnitude measurement, as it was found that this varied across tests more than would be expected. The results were at similar levels to that expected and the strain gauge results and it is predicted that the errors stem from the difficult surface profile measured rather than the technique itself.

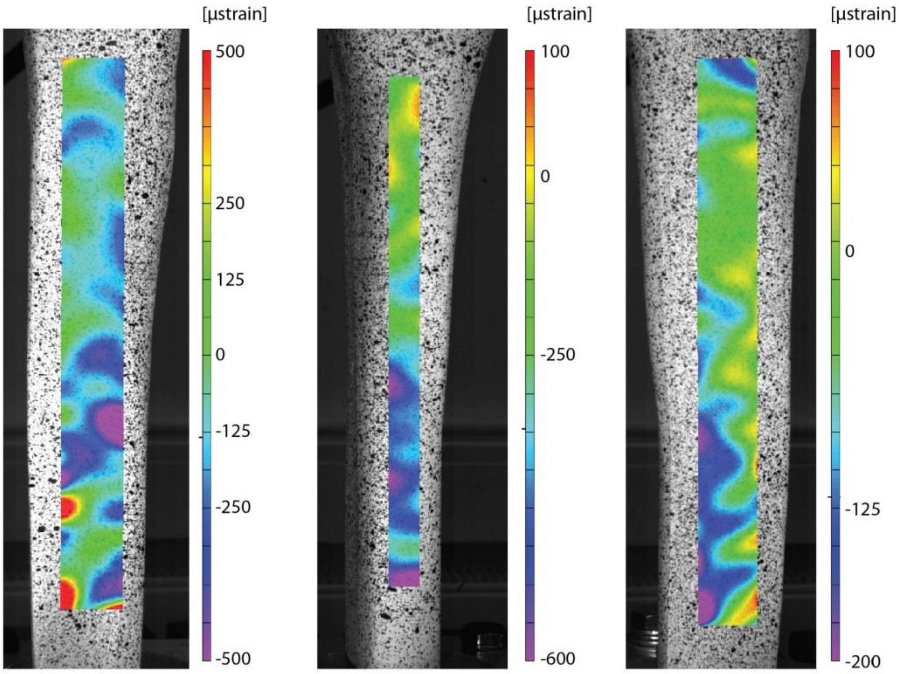

Figure 43 - Longitudinal surface strain results from axial compression at maximum loading of the implanted tibia, analysis the anteromedial (left), posterior (middle) and anterolateral (right) aspects.

From this series of investigations into the assessment of load distribution through strain gauge rosettes and DIC confirmation, the final decision was made on the location of the five strain gauge rosettes for all future testing. Figure 44 summarises these locations using the datum line of the proximal tibial cut as shown.

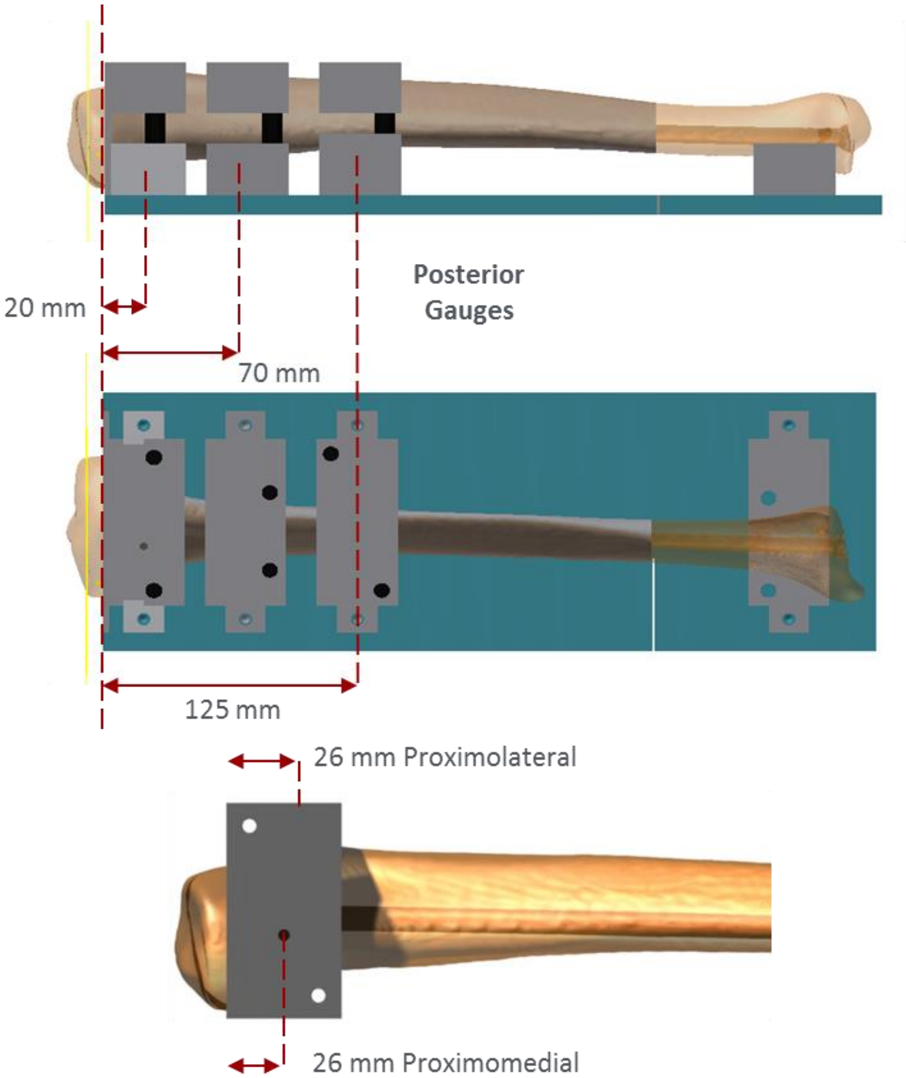

Figure 44 – The final locations of the five strain gauge rosettes used in the main stages of testing on all five Sawbones tibia specimen

6.9 Compartmental Load Measurement

The development of the experimental rig to allow for adjustment of the compartmental load share across the tibial plateau generated the need to be able to measure what this load share was during testing. Following the successful placement of the strain gauges which included a gauge on both the medial and lateral side of the tibia, there was further requirement to measure the compartmental loading. An investigation into the methods of measuring the proportion of load between two locations followed.

The most apparent solution to load share assessment was to use some form of load cell between the joint spaces. Various force sensing resistors were sourced which needed to be flexible, thin and have a diameter which allowed them to fit within the tibial condyles. Their specification had to allow a maximum load of no less than 300 N and ideally higher so that load magnitudes approaching physiological loads could be tested. These specifications meant that very few affordable sensors were available when a search was made of suitable solutions including alternative options such as pressure measurement sensors. An investigation into the most appropriate sensor to obtain an accurate understanding of the compartmental loading followed. The selection of options for measuring the compartmental load share were considered, which are included in Figure 45. This ranged from different types of forces sensors and load cells to pressure sensors. The concept of measuring pressure instead of force was studied as it would be across a known area of pressure. Following the investigation into potential methods of assessing the load transfer, the use of the pressure sensitive film was selected as an indicator with the need for an additional sensor to measure the force magnitudes. This was because the pressure film was found to successfully allow a visual assessment of location and area of the pressure, but was not a suitable indication of the magnitude of pressure. After experimenting with some of the options discussed, the Flexiforce (Tekscan) sensor selected as the most suitable sensor.

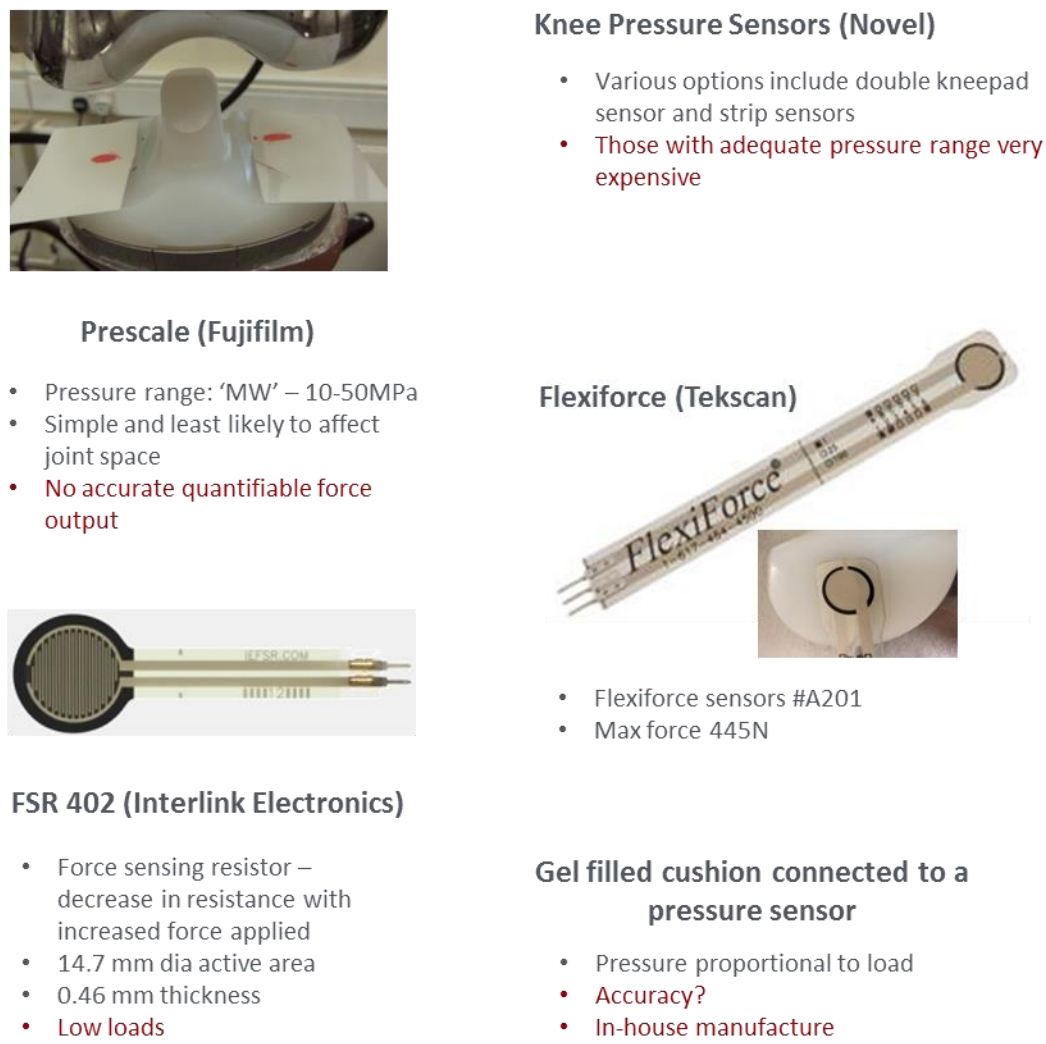

Figure 45 - Compartmental Load measurement options and their evaluation

A study to assess the superior method of use for the Flexiforce sensors was performed in addition to an investigation into their reliability and accuracy when used in the curved geometry of the knee joint. It was known from the sensor manufacturer that the most effective method of testing with the sensor involved the use of a 'standard' puck that covered the full sensing area. In order to use these sensors for the application in a knee joint it was important to understand if the results produced with alternate pucks and geometries were still accurate representations of force. After conditioning the sensors to 110% of their maximum load with five repetitions, the testing protocol to assess a variety of surface geometries was followed. Each puck geometry combination was tested on the Instron three times through a 0.1 mm / min compression to a maximum load of 400 N. This loading was applied in 50 N increments and a voltage reading from the sensor was recorded at each increment through a custom made LabVIEW programme. The sensors were positioned using pressure sensitive film to ensure they were located directly at the contact point between pucks. For Phase One of the testing, the 'standard' puck was re-tested in between each test to ensure consistency of the sensor readings across the testing period. This indicated a good repeatability across the sensor use, however it was clear from phase one that a curved surface would change the output from the sensor. Phase two of the testing therefore investigated this finding testing only the 'standard' puck at the beginning of the series as a reference point to compare; these phases of testing are summarised in Figure 46. A different sensor was also used for each phase to get an indication of the variability between sensors.

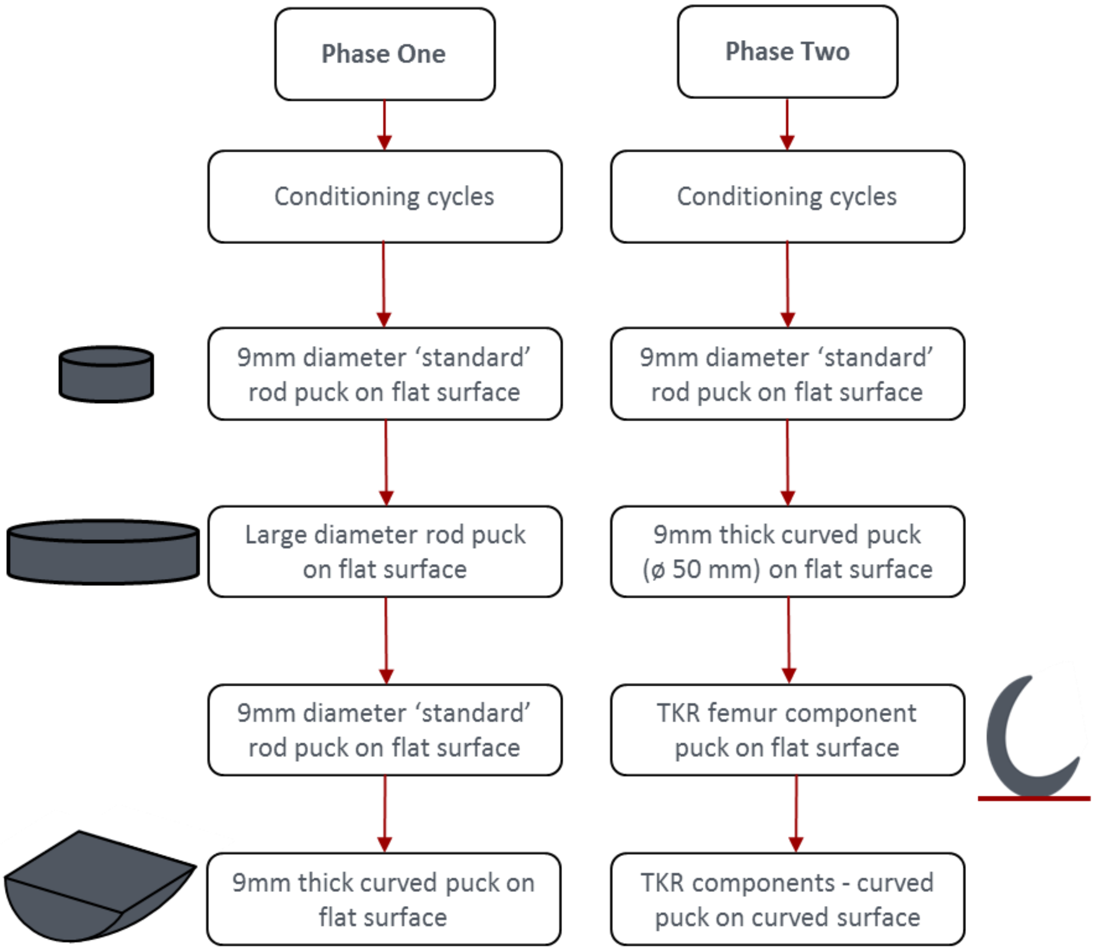

Figure 46 - The two phases of testing for the Flexiforce sensor validation

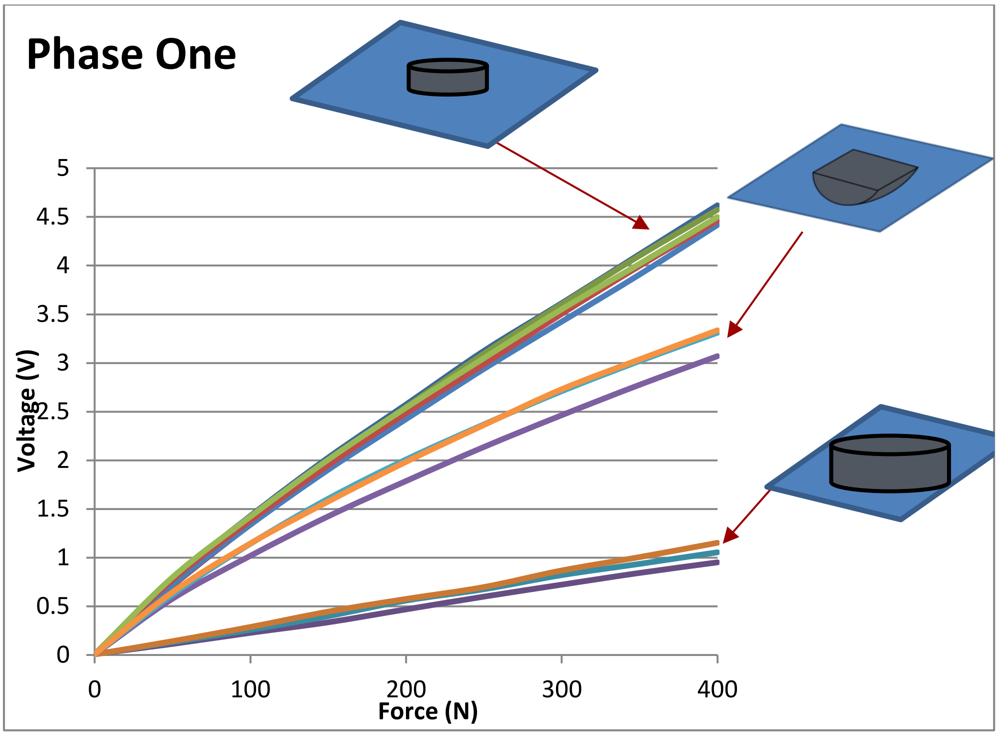

Figure 47 – The results from phase one flexiforce testing showing a repeatable and linear output with different geometries of puck

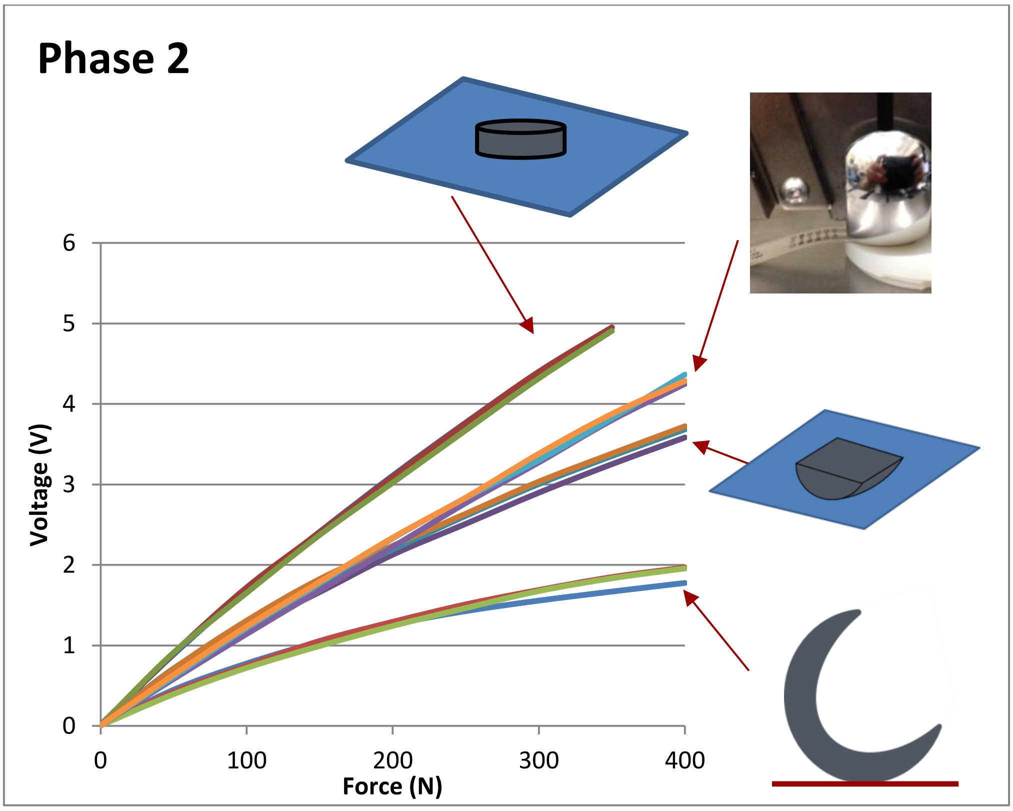

Figure 48 - The results from phase two flexiforce testing showing a repeatable and linear output with different geometries of puck and surface

The results of this testing displayed in Figure 47 and Figure 48 show that curved on curved or flat on flat produced the best results in terms of straight lines, but they do not produce the same results, so it is important that the calibration is carried out on the curved on curved RTKR component geometry that is present in the main testing. The force sensor performance testing recorded a mean combined load of 422.3 N with a standard deviation of 5.8 N (1.4%) when the applied load was 400 N. This average force equates to a 5.6% error from the sensor.

In summary, the outcome of the study indicated the use of a pressure sensitive film to identify the contact points and approximate pressures (Prescale, Fujifilm Corporation, Tokyo, Japan) with Flexiforce force sensors (#A201, Tekscan Inc, Massachusetts, USA) to record the force on each condyle throughout the testing as shown in Figure 49. Overall the tests showed that it was important that the contact area was not larger than the sensing area of the force sensors, otherwise the sensors would not be able to measure the full force transferred. For this reason pucks were used in the intact testing and the area was checked with the pressure sensitive film each time in the implanted testing. Testing also demonstrated that it was not an issue if the force transfer area was smaller than the sensing area, as indicated in the manufacturer's guidelines, allowing the implanted testing to continue as planned. Finally, the testing showed that there was a distinct difference in the voltage output under the same load when comparing a flat surface to a curved surface geometry. It was therefore important that the calibration was performed on curved geometry matching the knee set up rather than a flat surface to allow true force values to be calculated.

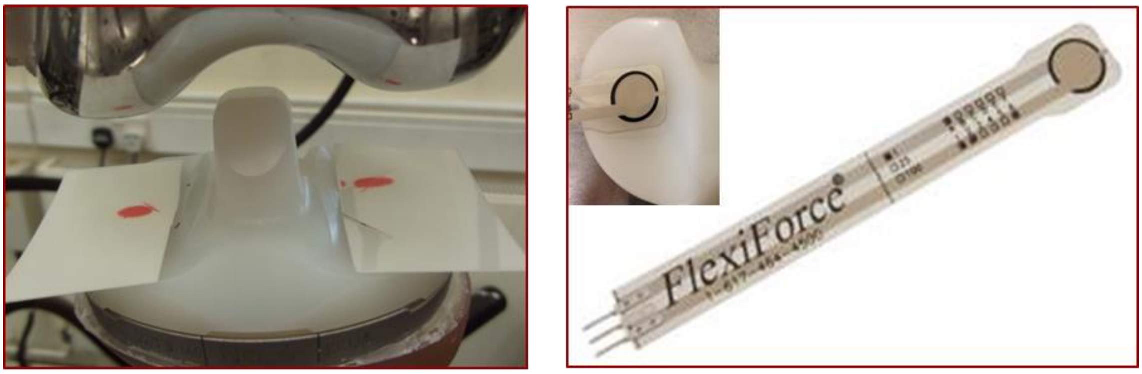

Fujifilm Prescale

Tekscan Flexiforce

Figure 49 – The two methods selected to be used to assess and measure the compartmental load share across the tibial plateau. The Fujifilm Prescale was used to identify the points and areas of contact during test set-up, followed by the Tekscan Flexiforce sensors to record the specific force through each condyle during testing.

6.10 Implantation Guides

To ensure that there was consistency of tibial component implantation between the five Sawbones tibias tested a series of implantation guides were developed to be used alongside the manufacturer's recommended surgical instrumentation. The proximal cut was performed whilst the tibia specimens were located in the alignment jig as shown in Figure 50. The proximal tibial cutting guide was then developed to fit over the cut proximal tibia and locate the central hole and tibial keel to prepare the bone for implantation. The remainder of the process could then be performed confidently with the surgical instrumentation.

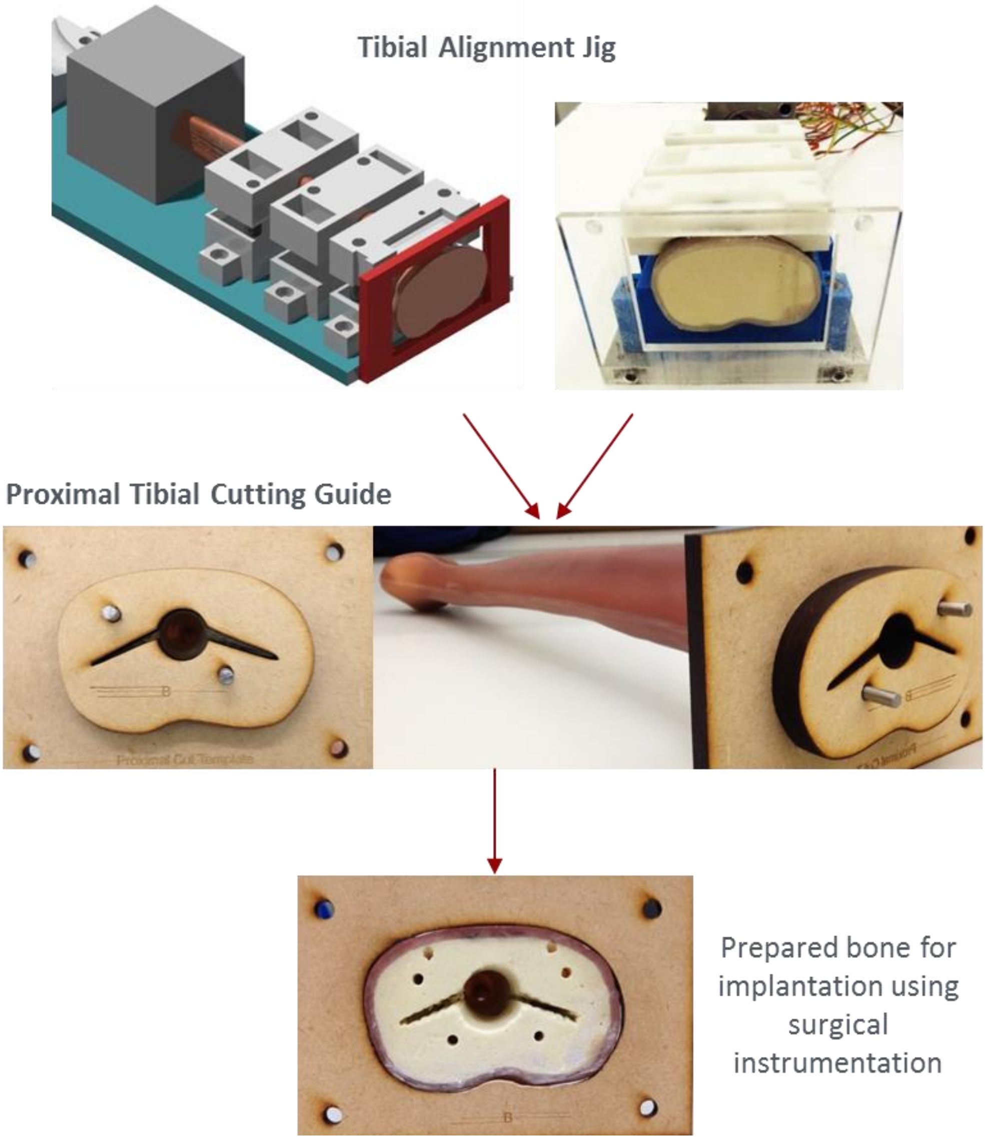

Figure 50 –The process of tibial specimen preparation for implanting a tibial revision total knee component using a Tibial Alignment Jig and Proximal Tibial Cutting Guide

6.11 Combined Loading Rig Development

As described in the literature review, to truly reflect the physiological conditions in the knee joint, the load distribution through the tibia should be a combination of loading of the tibiofemoral and patellofemoral joints. The tibiofemoral rig has many advantages such as the adjustment of the compartmental load share; however it only replicates the tibiofemoral joint loading. A study was therefore needed to compare the tibial loading in the implanted bones for the tibiofemoral and the full combined joint loading scenarios, to establish if the loading significantly affected the strain results. A preliminary test rig was designed in collaboration with another research project, supervised by the author, which was then developed for this research into the functioning combined loading rig used for the testing described. It was possible to use the knowledge gained in developing the tibiofemoral rig to aid the development of the combined loading rig.

The theory behind the combined loading rig stemmed from the literature where studies loading the hip joint typically included an abductor strap for loading instead of purely loading through the femoral head (Britton and Prendergast 2005). This analogy led the development of the combined loading rig and further progression is shown in Figure 51. Important features of this design included the need for axial rotation of the tibia or femur, which was assigned to the tibia through a nylon bearing. Additionally, to ensure correct compartmental loading it was necessary to allow adjustment of the femur within its cradle in the coronal plane. It was also important that the femoral flexion axis passed through the centre of the single radius implant, also termed the transcylindrical axis. A difficult aspect of the design was the attachment point of the quadriceps tendon as due to the assessment of cortical strain in surrounding local areas it was important that it was attached to the tibia in the most anatomical means possible. The quadriceps tendon needed to be removed and swopped between bone specimens, yet methods of screwing it into the bone may affect the proximal strain gauge results. The use of Velcro which was supported by a guide plate was therefore the best compromise of function over effect on strain results. The quadriceps and patella tendon was replicated with the use of wire rope connected with swageless eyes. Following this and the other developments presented, the combined loading rig was formed and prepared for use in the research to compare the effect of applied loading on strain distribution in the tibia. The final detailed assembly drawings can be found in Appendix D – Combined Loading Rig.

Based on the novel design of this combined loading rig, it was important to calculate the equivalent loads that were transferred through the femur when placing a load through the

Zwick adapter seen in Figure 51. The free body diagram of the lever arm component can be seen in Figure 52, illustrating the force transmitted from the Zwick test machine (L), the force transmitted to the femur (F) and the tensile force produced by the quadriceps tendon (T). From the test rig, the distances X_1 and X_2 were known, the angle α was set to 10° or 25° for testing and the corresponding angle β was measured. The details of the calculations used to find the magnitude of T and F are described below, concluding with a table showing what forces were being exerted at 10° and 25° of flexion when 200 N, 300 N and 400 N loads were applied (Table 4). It is clear from the table that when comparing the combined loading rig strain values with those of the tibiofemoral rig, 200 N of load should be applied by the test machine to the combined rig to produce approximately the equivalent 550 N of load through the femur in the tibiofemoral rig.

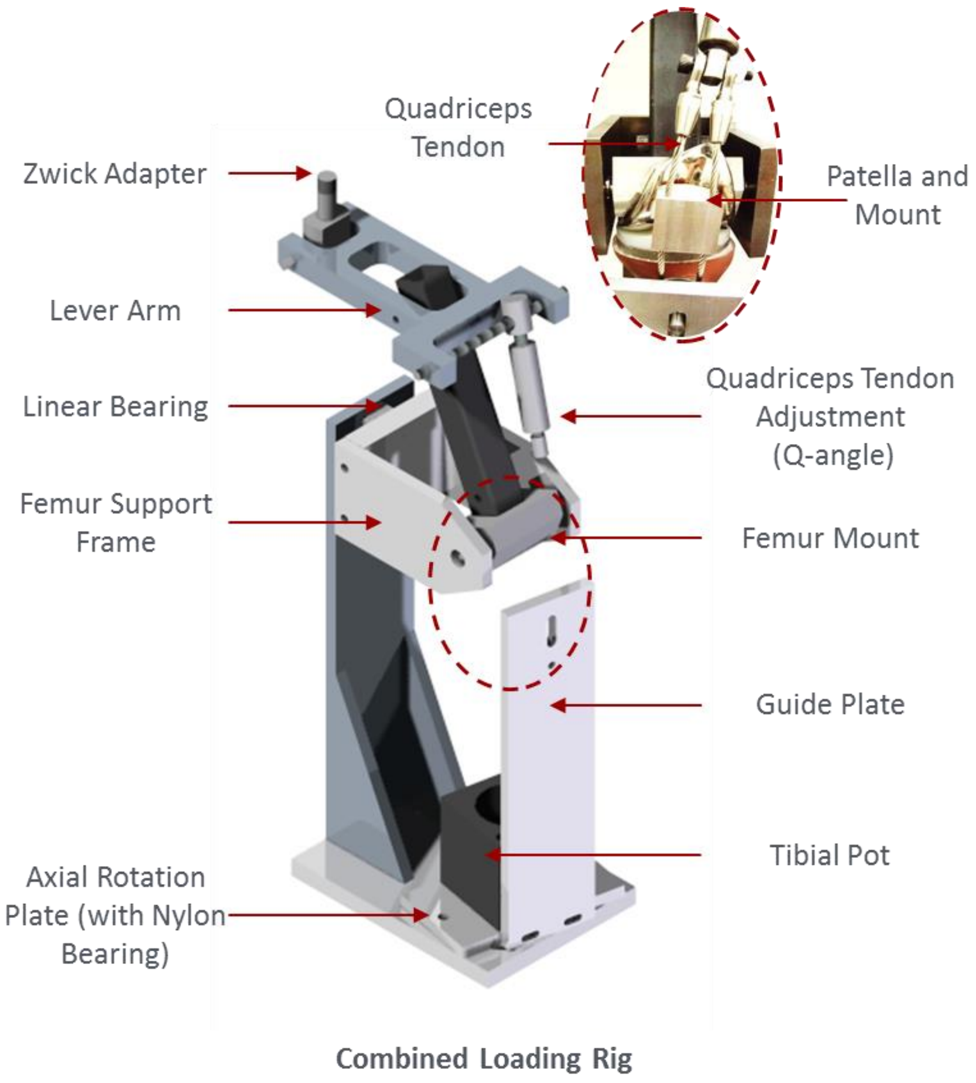

Figure 51 – The main features of the Combined Loading Rig following its development. The rig combines the forces from the TFJ and the PFJ to provide physiological loading through to the Sawbones tibia (not shown in diagram).

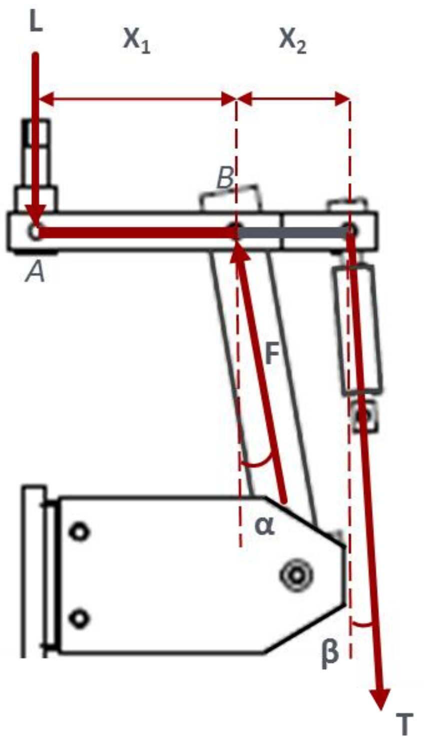

Figure 52 - Free body diagram of the lever arm component on the combined loading rig that applies a force from the Zwick test machine through to the knee joint

By taking moments about point B;

$$L \times X_1 = T \cos\beta \times X_2$$

$$T = \frac{L \times X_1}{\cos\beta \times X_2}$$

By taking moments about point A;

$$X_2 \times F \cos\alpha = (X_1 + X_2) \times L$$

$$F = \frac{(X_1 + X_2) \times L}{X_2 \times \cos\alpha}$$

X_1 (m)	0.107		X_2 (m)		0.058	
From the free body diagram (Figure 40)						
Load (N)	200	200	300	300	400	400
Flexion Angle (Deg)	10	25	10	25	10	25
Flexion Angle (Rads)	0.17	0.44	0.17	0.44	0.17	0.44
Tendon Angle (Deg)	7	23	7	23	7	23
Tendon Angle (Rads)	0.12	0.40	0.12	0.40	0.12	0.40
T (N)	372	401	558	601	743	802
F (N)	**578**	**628**	**867**	**942**	**1155**	**1256**

Table 4 – To summarise the results of the moment calculations, indicating an equivalent load to approximately 550 N is close to 200 N loading through the Zwick adapter on the combined loading rig

6.12 Final Test Rigs

From the development stage of the research two tests rigs were produced to allow investigation of the strain distribution in the tibia under two forms of physiological loading. These experimental rigs are summarised in Figure 53 and were used to meet the objectives of the research. They formed a method to locate and load the experimental construct to establish the effect of implanting a RTKR on the strain through the tibia. The tibiofemoral rig also allowed the exploration of the effect of compartmental load share at 0° and 10° of flexion on surface strain measurements. The combined loading rig can be used to investigate the difference in surface strain measurements under a change in flexion angle of 10° to 25°. Finally the rigs can be employed to determine the effect of varying the loading conditions on the load transfer results, as this may need to be considered for any further pre-clinical testing of RTKR designs.

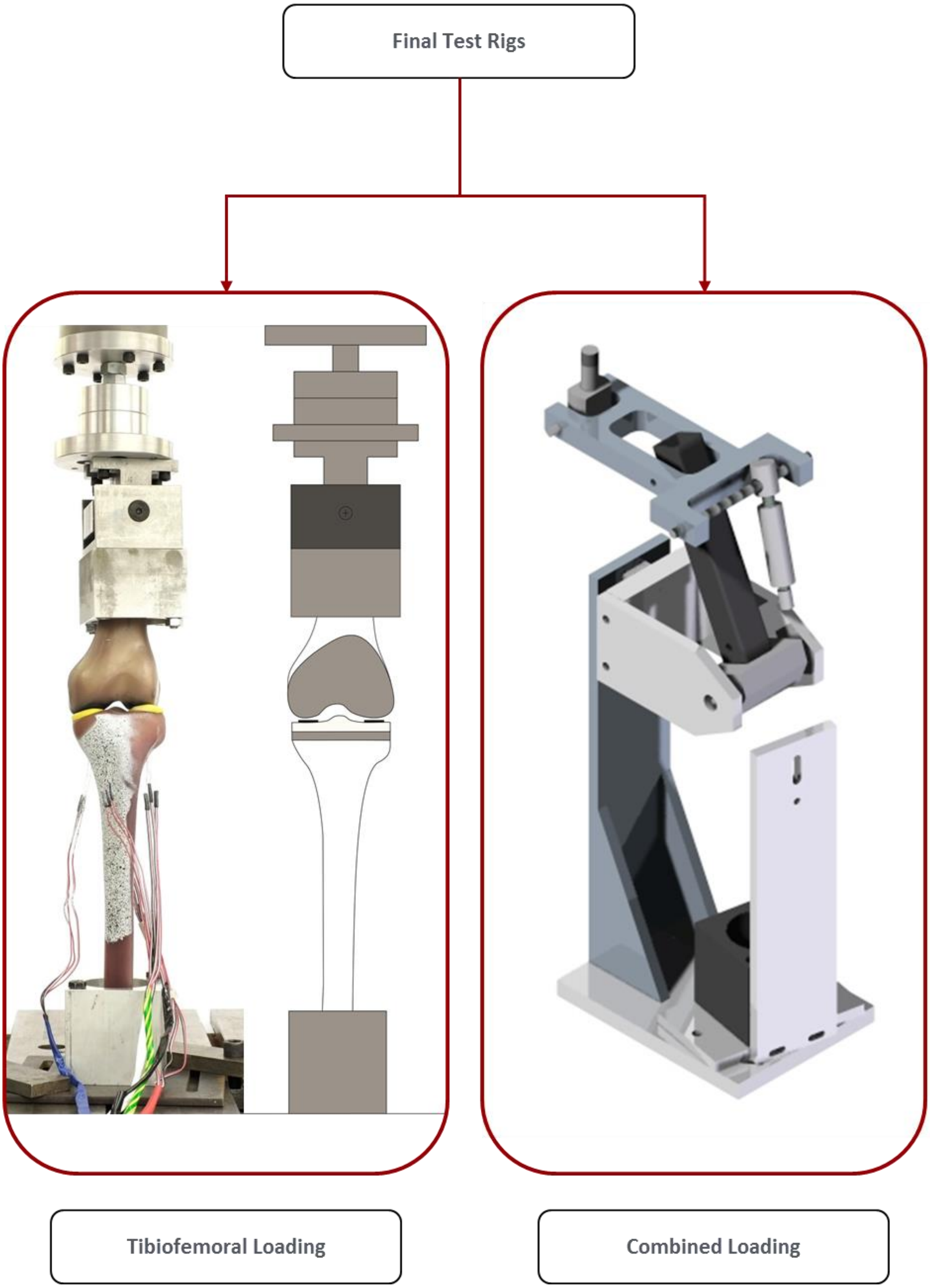

Figure 53 – An overview of the two experimental test rigs developed during this reaserch to investigate the strain distribution in the tibia as a function of the applied loading.

7 Materials and Methods – Tibiofemoral Loading

Following the development of the experimental rig and methodology from the preliminary testing, a reliable and repeatable series of tests were established capable of assessing the load transfer through composite tibia bones under physiological loading. This chapter outlines the testing protocol observed for the preparation, testing of intact tibias, implantation of tibial components and testing of implanted tibias in five Sawbones tibia specimens using the tibiofemoral experimental rig.

7.1 Sample Preparation

7.1.1 Tibial Alignment

Each tibia specimen was prepared using the series of preparation jigs that had been developed for this purpose and described in the previous chapter. Initially, the sagittal placement guide was used to mark the position of the proximomedial and proximolateral strain gauges using an ink marker guided by placement holes in the tibial moulds. The specimen was then placed in the alignment jig and secured to allow the location of the remaining three gauges to be marked. Whilst the specimen was in situ in the alignment jig, the distal tibial cut was made by using a band saw to follow the slot in the alignment jig. The specimen was then removed from the alignment jig and secured into the tibial pot using the tibial location jig and rotation puck described as shown in Figure 54. Wood's metal was poured into the pot to rigidly fix the specimen in place. This process was repeated for each specimen and then the femoral loading component was prepared for testing.

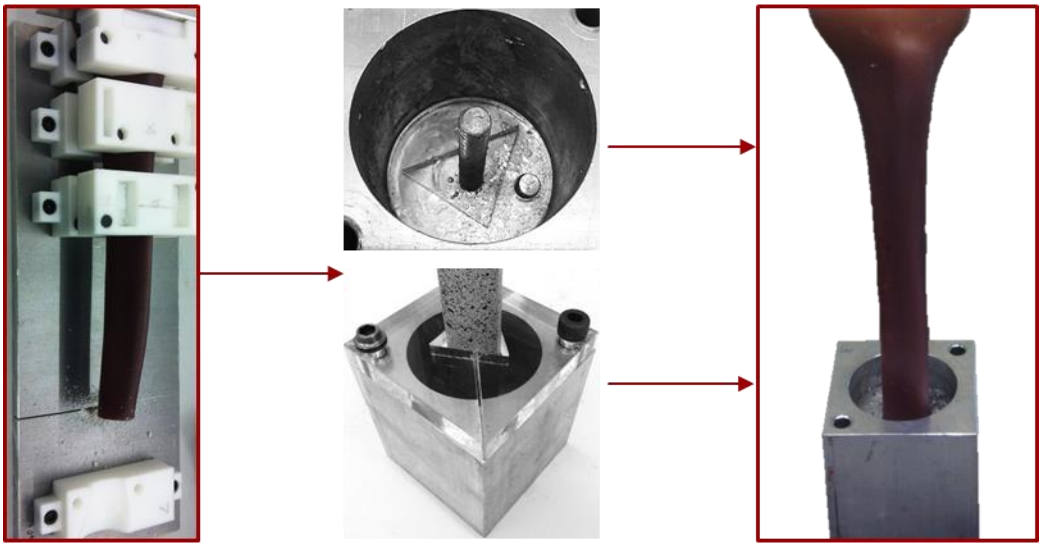

Figure 54 – The process of preparing and aligning each Sawbone tibia for physiological testing in the experimental rigs. This includes marking the strain gauge locations, making the distal cut and setting in the tibial pot.

7.1.2 Femoral Alignment

The femoral loading device was prepared for use with all intact and implanted tibia testing. With the condyles supported on a level surface, a height gauge was used to measure the required working length of femur necessary for the experimental rig. With the truncated femur prepared it was possible to secure it into the femoral pot using Wood's metal as described in the tibia preparation. As the femoral pot ensured the correct sagittal and coronal plane alignment of the femur, no further guides were used. The most posterior aspects of the femoral condyles were positioned so that they were parallel to the side of the pot, however this was not crucial as the rig allowed the femur to rotate about its axis with respect to the tibia. The assembly was then secured to the tibiofemoral experimental rig ready for testing.

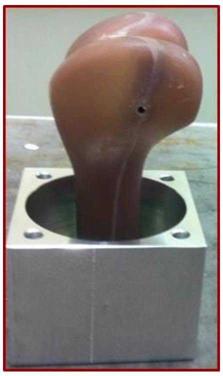

Figure 55 – The prepared Sawbones femur to be used in the tibiofemoral experimental rig as the femoral loading device.

7.1.3 Strain Gauge Bonding

Five strain gauge rosettes selected during development (1-RY91-6/350, HBM, Germany) were bonded to each specimen in the precise locations marked out during the tibial preparation. The process followed for every gauge bonded is summarised in Appendix E – Strain Gauge Bonding. After bonding, the resistance of each gauge was checked by ensuring that 350 ohms was measured across each one.

7.1.4 Force Sensor Calibration

Following the validation of the Flexiforce force sensors (Tekscan) during the development stage, both sensors had to be calibrated before each set of testing. The manufacturer's guidance then required that they were regularly conditioned directly before testing so this was performed every day when testing was taking place. The process of conditioning and calibrating each force sensor is summarised in Figure 56. The force sensors were calibrated at the start and end of the intact and implanted testing to ensure that the calibration factor had not altered during testing.

Force Sensor Conditioning

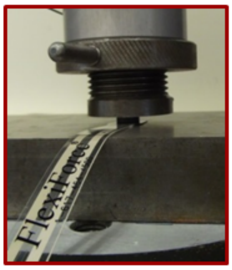

The simple loader was set up on the Instron Test Machine

Sensors were conditioned to 110% of their maximum load five times using the standard puck on a flat surface.
Test parameters; 5 x 480 N at 1 mm / min ramp compressive loading

Force Sensor Calibration

Knee replacement components were set up on the Instron (Unicondylar Knee and PE Tray)

Contact point between the components found using Fujifilm, marked on the PE component (applied a 500 N load) and used to position force sensor

Load applied in 100 N increments up to 400 N and the sensor voltage output recorded in a custom made LabVIEW programme

Repeated three times for each Force Sensor after removing and repositioning

Figure 56 – The process of conditioning each of the two force sensors that was performed at the start of every set of testing and on a daily basis

7.1.5 Rig Set-up

The next stage in the methodology was to set up the experimental rig following the specimen and sensor preparation discussed. For the 0° flexion testing, the tibial assembly was attached to the base plate and rigidly clamped to the bed of the Zwick. For the 10° flexion testing the tibial assembly was removed from the baseplate and the 10° flexion wedge inserted before assembling and clamping to the test bed (both options can be seen in Figure 57). The tibial assembly was clamped into position using the Placement Guide detailed in the development section. All strain gauges and force sensors were connected to the data acquisition system as indicated in Figure 58. Fujifilm was used to assess the centre of pressure through each condyle on the tibial plateau to determine the correct position for insertion of the force sensors.

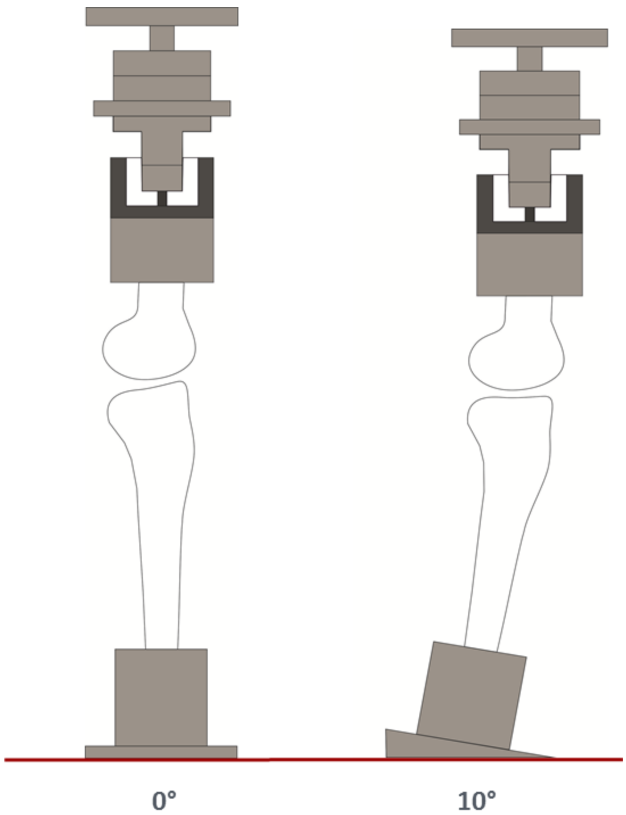

Figure 57 – A diagram to illustrate the two knee flexion states of the test set-up. All tests were performed at both 0 and 10° of flexion using the wedge shown.

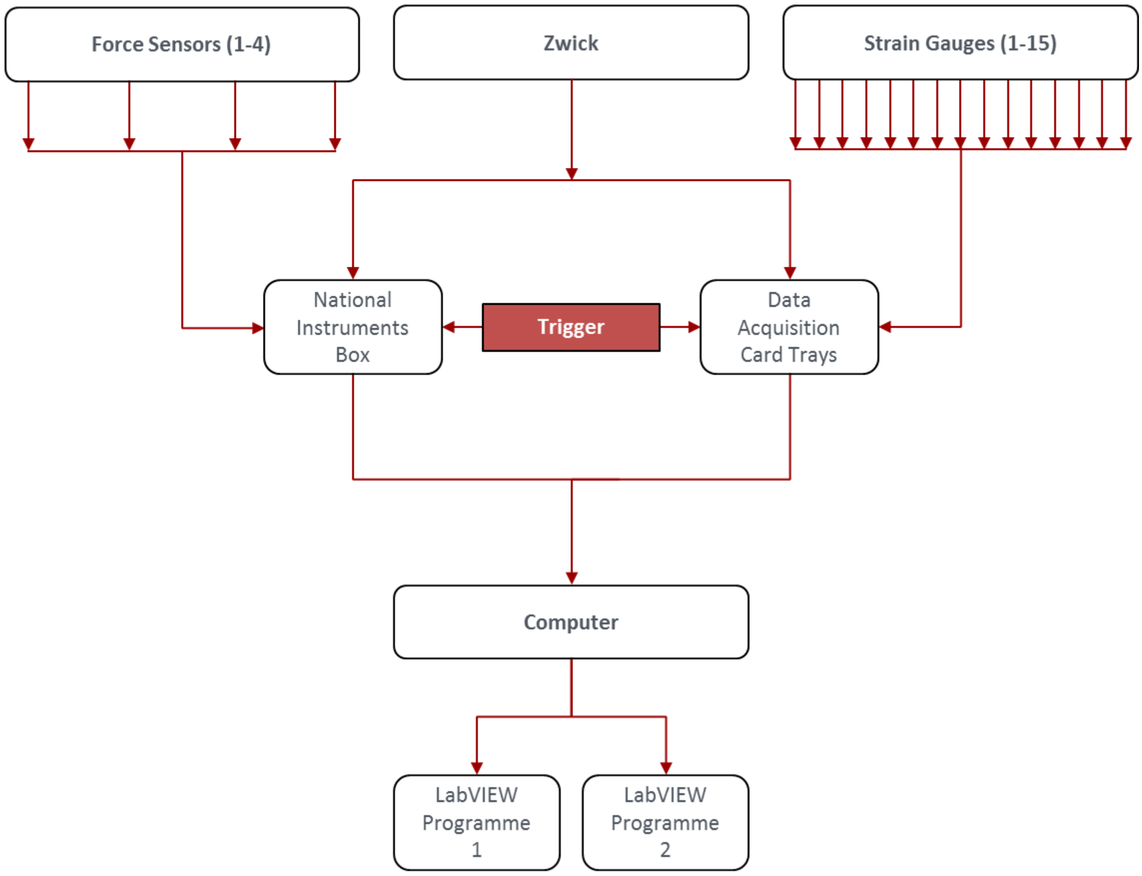

Figure 58 – The network of connections between the force and strain sensors and the loading machine through to the data collection computer

7.2 Intact Testing

The first of the two main testing stages assessed the surface strain under physiological loading in the intact tibia specimens prior to RTKR implantation. This was done at both 0° and 10° of flexion to enable analysis of the effect of a change in flexion on the strain measurements as illustrated in Figure 59. To ensure the later analysis of the strain measured through the data acquisition system was correct, a P3 strain indicator box (Vishay Precision Group Inc, Pennsylvania, USA) was used on various gauges and compared to the final results. Before applying the required load, each specimen was preloaded to a force of 50 N. A summary of the tests performed on each specimen can be found in Table 5. A cyclic load profile was used to assess the cortical strain in the tibia across 50 cycles. A ramp load profile was used to determine if the strain levels increased linearly with load. A total of 12 tests were performed for each specimen at each flexion angle using the testing protocol summarised in Figure 60.

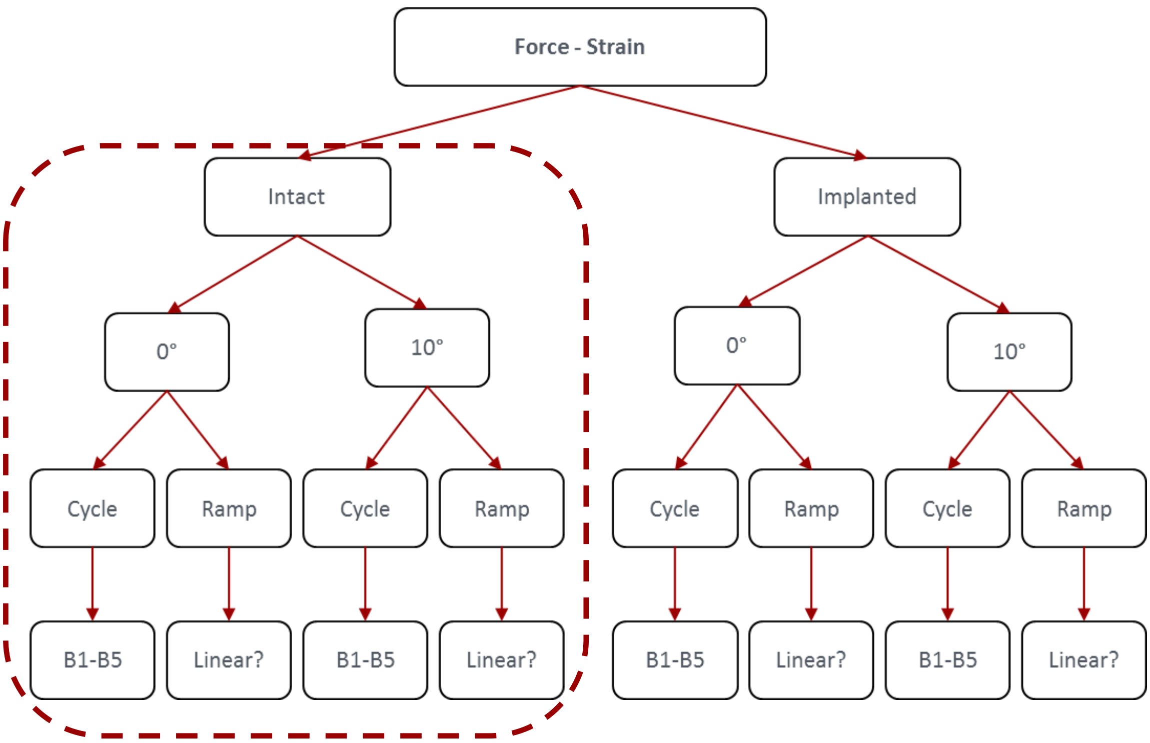

Figure 59 – An overview of the testing performed highlighting Stage 1: Intact testing

Intact Testing

↓

Force sensors calibrated and conditioned as described

↓

Substitute meniscus inserted into joint at the femur and tibia contact point confirmed by pressure film and force sensors

↓

The Zwick test machine and data acquisition system was prepared for testing

↓

A dummy test was run to ensure all of the strain gauges were producing an adequate output signal – connections checked and fixed if problem with output was found

↓

Preliminary tests performed to check the proportion of load through the medial and lateral compartments, and the adjustment screws used accordingly to set desired load share

↓

The tests described in Table 4 were run on each specimen in turn until all five specimens had been tested. The trigger was used to start both LabVIEW programmes simultaneously and collect all required data

↓

Rig set up changed to 10° using flexion wedge and placement guides as described

↓

All testing repeated at 10° of flexion

Figure 60 – A summary of the intact testing process used for each of the five tibia specimen analysed

<table>
<tr><th>Test</th><th>Load Profile</th><th>Load (N)</th><th>Sensors</th><th>Flexion Angle</th></tr>
<tr><td colspan="5">Cyclic Loading @ Frequency = 0.5 Hz, Cyclic Preload = 50 N
Ramp Loading @ Rate 0.01 kN/s, Ramp Preload = 10 N
3 x repeats for every test / row</td></tr>
<tr><td>1</td><td>Ramp</td><td>550</td><td>Strain and Force</td><td>0°</td></tr>
<tr><td>2</td><td>Cycle</td><td>500</td><td>Strain</td><td>0°</td></tr>
<tr><td>3</td><td colspan="4">For one of the five tibia bone specimen, full ramp testing was performed to assess linearity; additional tests at 300 N, 400 N, 500 N</td></tr>
<tr><td>4</td><td colspan="4">For one of the five tibia bone specimen, tests performed to measure strain with the P3 box (4 channels at a time)</td></tr>
<tr><td>5</td><td>Ramp</td><td>550</td><td>Strain and Force</td><td>10°</td></tr>
<tr><td>6</td><td>Cycle</td><td>500</td><td>Strain</td><td>10°</td></tr>
<tr><td>7</td><td colspan="4">For one of the five tibia bone specimen, full ramp testing was performed to assess linearity; additional tests at 300 N, 400 N, 500 N</td></tr>
<tr><td>8</td><td colspan="4">For one of the five tibia bone specimen, tests performed to measure strain with the P3 box (4 channels at a time)</td></tr>
</table>

Table 5 – A summary of the intact tests performed on each of the five intact tibia bone specimens with the relevant parameters stated. Note that the table has been simplified; every row was repeated three times on each specimen.

7.3 Implantation

On completion of the intact tibia testing, the specimens used for the intact testing were implanted with tibial trays and used for the implanted testing. This eliminated any potential variability due to strain gauge placement, specimen preparation, variation in bone geometry and material properties. The five tibia specimens and the single femoral component were implanted with the Stryker Triathlon RTKR components selected during development, using Simplex P surgical bone cement (Stryker, Michigan, USA) according to manufacturer instructions. Simplex P is a Polymethylmethacrylate (PMMA) acrylic bone cement intended for the fixation of a prosthesis to living bone and the subsequent transfer of physiological load. Figure 61 and Figure 62 summarise the process used to implant the components using custom made jigs and the surgical instrumentation, the final femoral component seen in Figure 63.

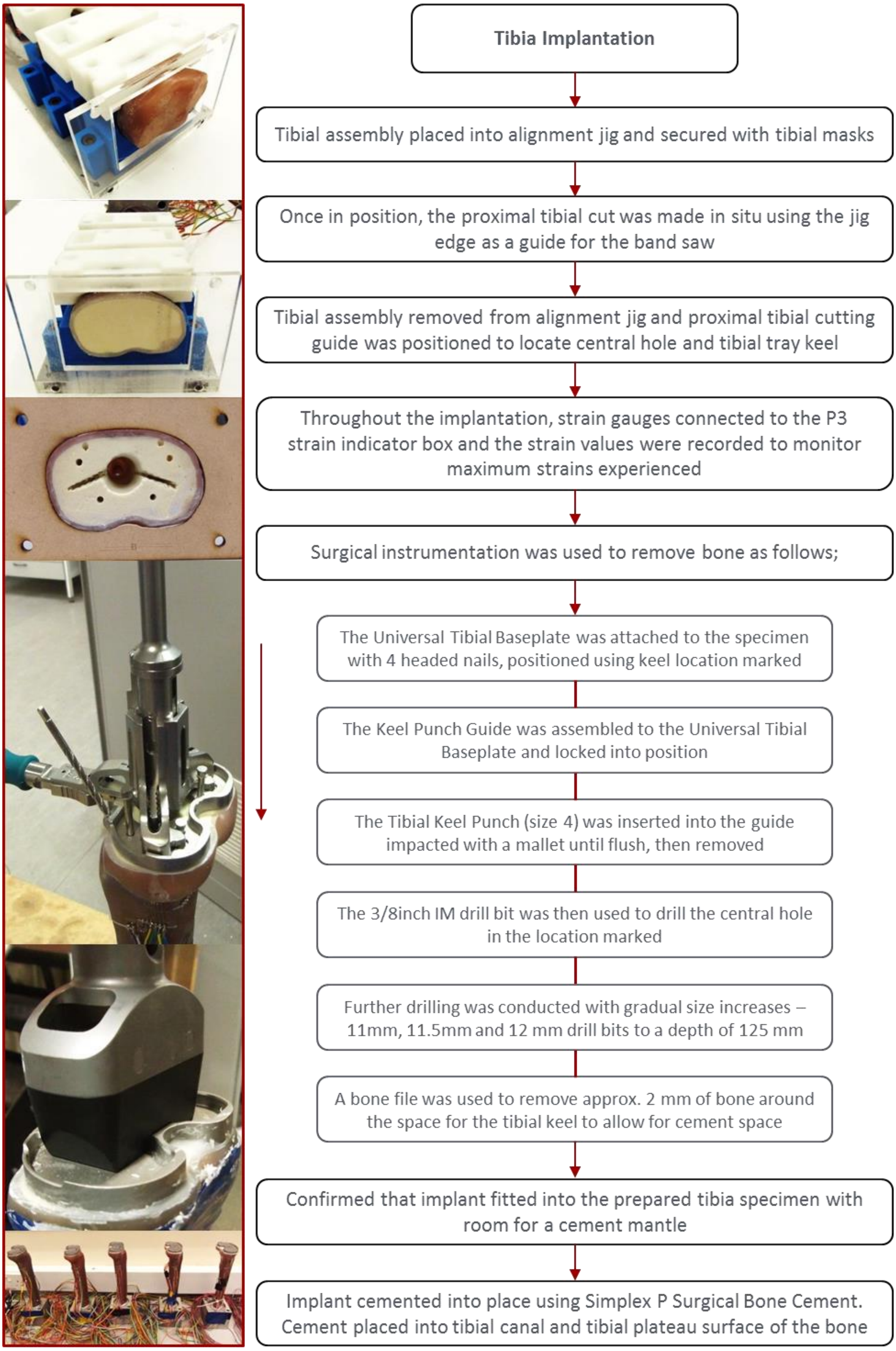

Figure 61 – A summary of the implantation process performed on each of the five tibia specimen between the intact and implanted testing stages

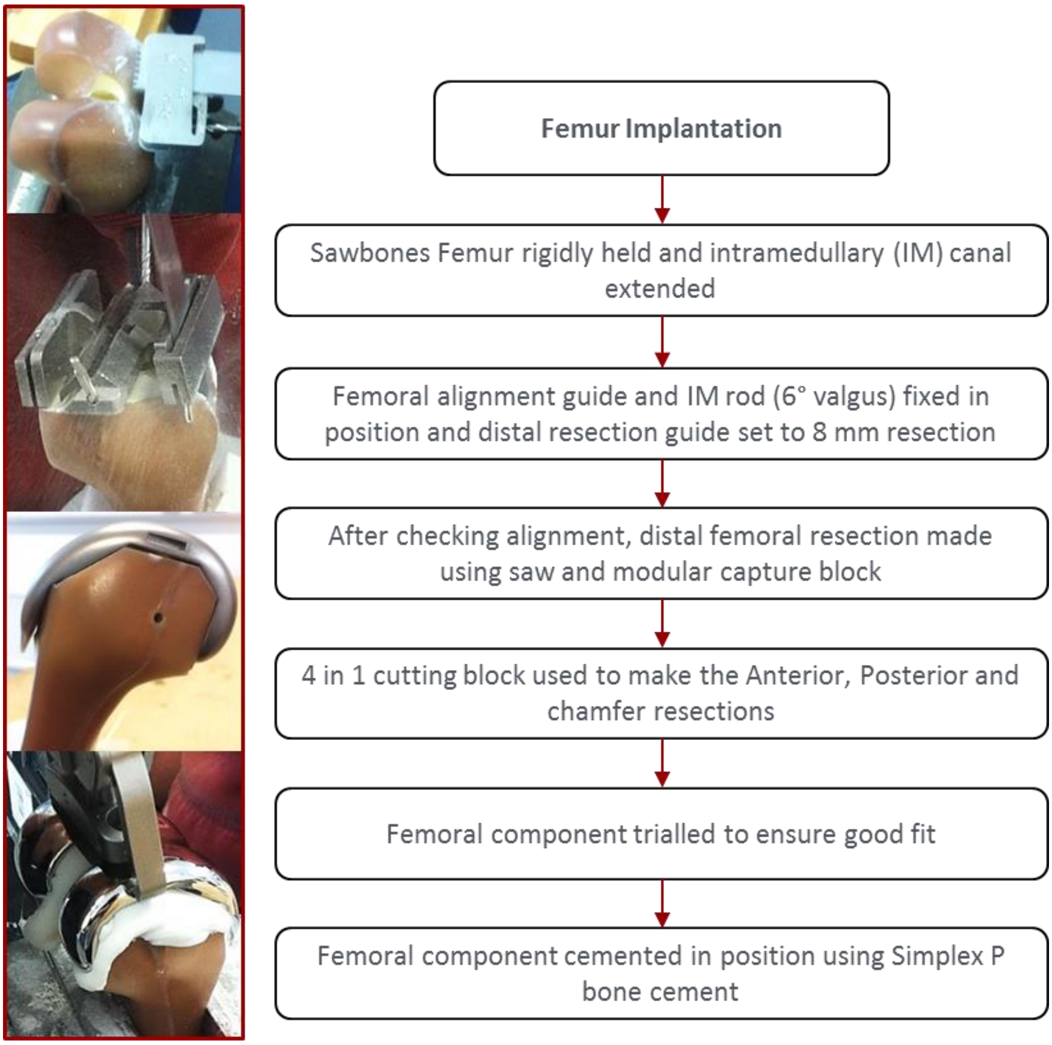

Figure 62 - A summary of the implantation process performed on the Sawbones femur for its use as a loading tool

Figure 63 - The composite femur with an implanted Triathlon component, fixed in the femoral pot for mounting

7.4 Implanted Testing

The experimental procedure carried out for testing the intact specimens was repeated for testing with specimens after they had been implanted with a RTKR as summarised in Figure 64, Table 6 and Figure 65. As with the intact testing, the P3 strain indicator box was also used during some implanted testing to ensure that the strain values recorded with the data acquisition system matched those of the strain indicator box.

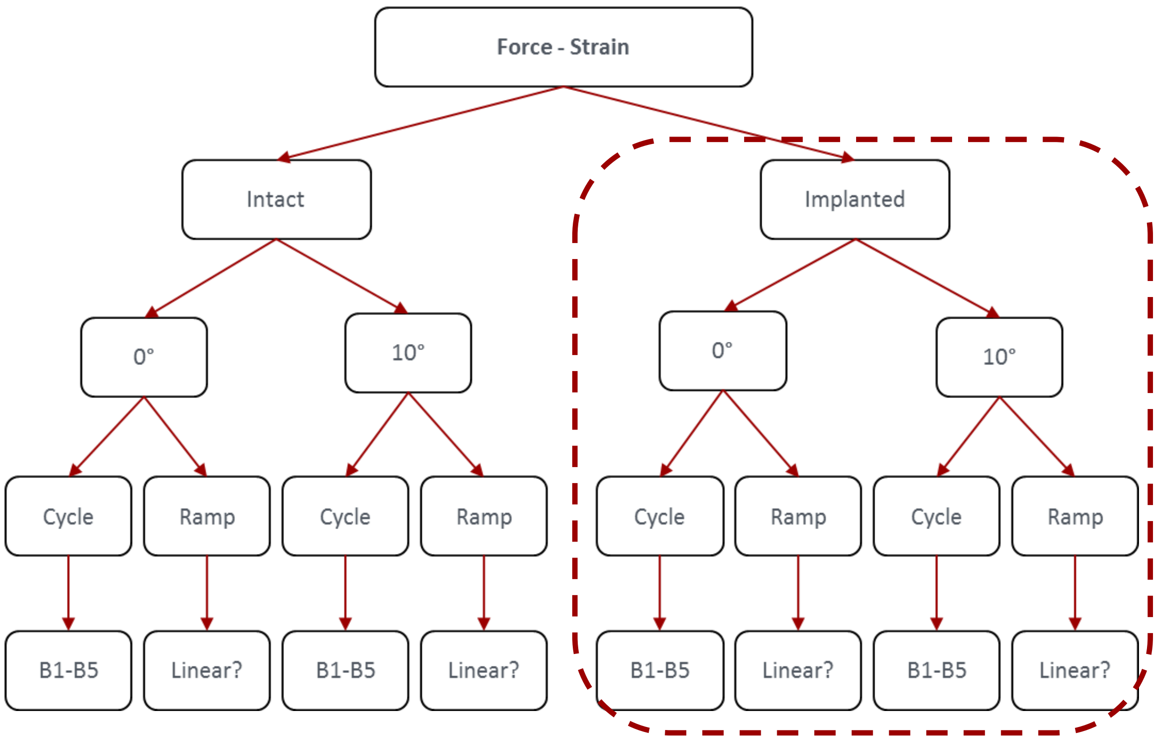

Figure 64 - An overview of the testing performed, highlighting Stage 2: Implanted testing

Test	Load Profile	Load (N)	Sensors	Flexion Angle
Cyclic Loading @ Frequency = 0.5 Hz, Cyclic Preload = 50 N Ramp Loading @ Rate 0.01 kN/s, Ramp Preload = 10 N **3 x repeats** for every test / row				
1	**Ramp**	**550**	**Strain and Force**	**0°**
2	**Cycle**	**500**	**Strain**	**0°**
3	For one of the five tibia bone specimen, full ramp testing was performed to assess linearity; additional tests at 300 N, 400 N, 500 N			
4	For one of the five tibia bone specimen, tests performed to measure strain with the P3 box (4 channels at a time)			
5	**Ramp**	**550**	**Strain and Force**	**10°**
6	**Cycle**	**500**	**Strain**	**10°**
7	For one of the five tibia bone specimen, full ramp testing was performed to assess linearity; additional tests at 300 N, 400 N, 500 N			
8	For one of the five tibia bone specimen, tests performed to measure strain with the P3 box (4 channels at a time)			

Table 6 – A summary of the implanted tests performed on each of the five intact tibia bone specimens with the relevant parameters stated. Note that the table has been simplified; every row was repeated three times on each specimen.

Implanted Testing

↓

Force sensors calibrated and conditioned as described

↓

The PE insert was positioned in the joint space and contact points confirmed by pressure film and force sensors

↓

The Zwick test machine and data acquisition system was prepared for testing

↓

A dummy test was run to ensure all of the strain gauges were producing an adequate output signal – connections checked and fixed if problem with output

↓

Preliminary tests performed to check the proportion of load through the medial and lateral compartments, and the adjustment screws used accordingly to set desired load share

↓

The tests described in Table 4 were run on each specimen in turn until all five specimens had been tested. The trigger was used to start both LabVIEW programmes simultaneously and collect all required data

↓

Rig set up changed to 10° using flexion wedge and placement guides as described

↓

All testing repeated at 10° of flexion

Figure 65 - A summary of the implanted testing process used for each of the five tibia specimen analysed

8 Materials and Methods - Combined Loading

The development of the combined loading rig, use of the prepared specimens and the application of the testing parameters from the tibiofemoral loading methods allowed for the next stage of experiments to be performed. A reliable and repeatable series of tests were established which were capable of assessing the load transfer through a RTKR implanted in composite tibia bones under physiological loading through the tibiofemoral and patellofemoral joints. This chapter outlines the testing protocol observed for the testing of the five implanted Sawbones tibia specimens using the combined loading experimental rig.

8.1 Materials and Methods

The final stage of testing assessed the surface strain under physiological loading in the implanted tibia specimens at both 10° and 25° of flexion as summarised in Figure 66. This allowed a direct comparison of the 10° testing between the two experimental rigs. It also enabled an analysis to be conducted of the effect that a change in flexion angle may have on the strain results. The five implanted bone specimens that had been prepared for the tibiofemoral rig testing were used for the combined loading rig to allow a direct comparison of strain results between the two loading techniques. The same data acquisition equipment was used as in the previous tibiofemoral rig testing. For the 10° and 25° flexion testing, the combined loading rig was mounted and rigidly clamped to the baseplate of the Zwick testing machine in the arrangement depicted in Figure 67. All strain gauges and force sensors were connected to the data acquisition system as described for the tibiofemoral testing.

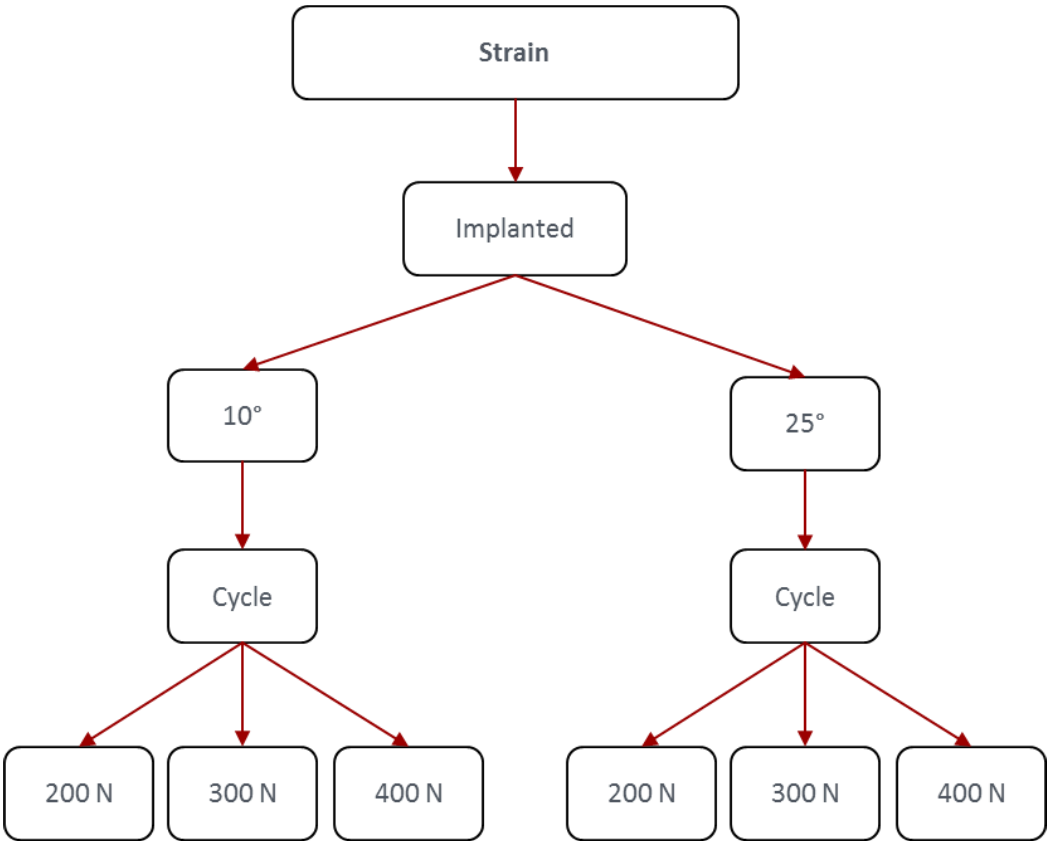

Figure 66 - An overview of the testing performed in the Combined loading rig stage of testing

Each of the five bone samples were then tested in turn according to the testing protocol described in Figure 68. Before applying the required load, each specimen was preloaded to a force of 50N by tightening the turnbuckle simulating the quadriceps tendon. A summary of the tests performed on each specimen can be found in Table 7. A cyclic load profile was used to assess the cortical strain in the tibia across 50 cycles. A ramp load profile was used to determine implant alignment with the pressure film. A total of 24 tests were performed for each specimen at each flexion angle using the testing protocol summarised in Figure 68.

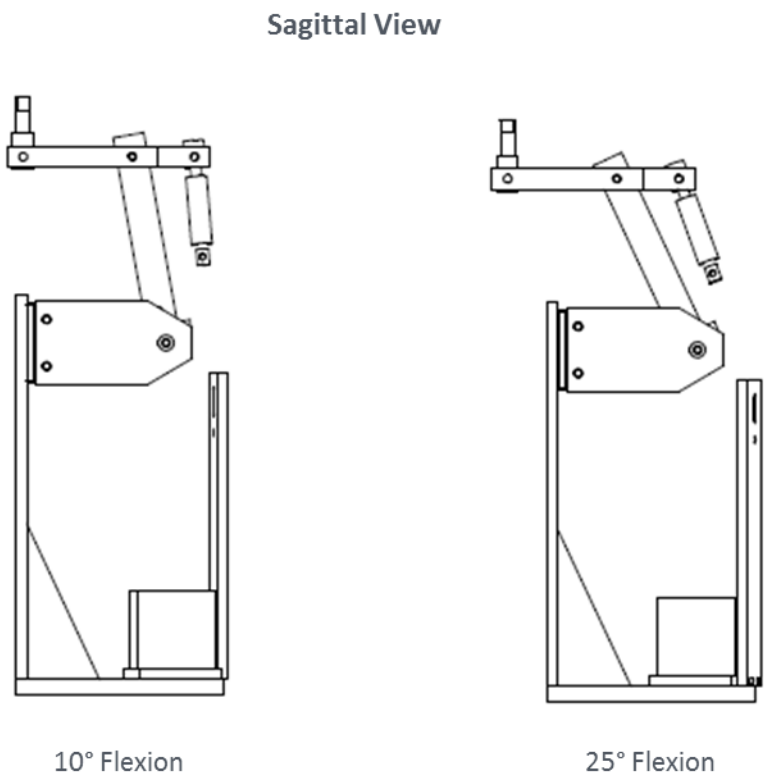

Figure 67 - A sagittal view drawing of the combined loading rig showing the 10° and 25° flexion angles tested

Test	Load Profile	Load (N)	Flexion Angle
Cyclic Loading @ Frequency = 0.5 Hz, Cyclic Preload = 50 N Ramp Loading @ Rate 0.01 kN/s, Ramp Preload = 50 N **3 x repeats** for every test / row			
1	**Ramp**	**500**	**10°**
2	**Cycle**	**200**	**10°**
3	**Cycle**	**300**	**10°**
4	**Cycle**	**400**	**10°**
5	**Ramp**	**500**	**25°**
6	**Cycle**	**200**	**25°**
7	**Cycle**	**300**	**25°**
8	**Cycle**	**400**	**25°**

Table 7 – A summary of the implanted tests performed on each of the five tibia bone specimen with the relevant parameters stated. Note that the table has been simplified; every row was repeated three times on each specimen.

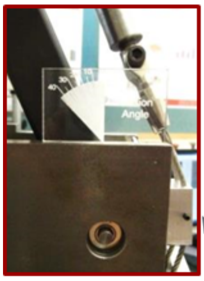

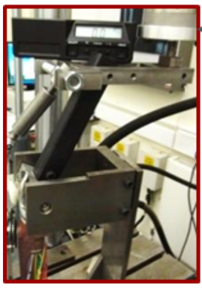

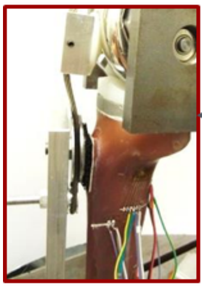

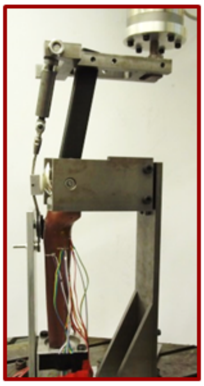

Combined Rig Testing

Samples prepared for testing by flattening the tibial tuberosity and fastening dual lock. Tibia specimen placed in combined rig.

Combined rig set at the required flexion angle, which was confirmed using the flexion angle jig as shown. To achieve the required flexion angle, the rig was shifted around the bed of the Zwick until the femur link reached the correct angle and the lever arm was horizontal.

The tibia axial rotation, femur varus-valgus rotation, anterior-posterior and medial-lateral translations were adjusted to ensure that the implant components were aligned anatomically (verified with pressure film).

Guide plate was attached whilst connecting the dual lock and patella tendon.

Quadriceps tendon Q angle set to 15 degrees.

The height of the patella was set to reflect the anatomical position at each flexion angle and fixed in place with grub screws.

Turnbuckle tightened until the preload in the system reached 50N.

The angle of the quadriceps tendon was measured using an inclinometer. This and the tibial axial rotation was noted for future calculations.

The test was run according to the test parameters in Table 5. Data saved for later manipulation.

All tests shown in Table 5 were performed to complete testing at 10° and 25° flexion at each load, on all five specimen.

Figure 68 - A summary of the implanted combined rig testing process used for each of the five tibia specimen analysed

9 Results

The main results of the testing employing the two test set ups; the tibiofemoral loading rig and combined loading rig, are presented in this chapter. It was important to ensure that the strain gauge results were validated against a benchmark through the strain indicator box and that the compartmental load share was appropriate throughout the testing. The results to assess the effect of RTKR surgery on the tibial strain are presented including the influence of flexion angle. An assessment of the strain results to establish their linearity is included as this may allow extrapolation to higher, more physiological loading levels. Finally an assessment of any difference in strain measurements found between the two applied loading techniques is made.

9.1 Strain Validation

To ensure the accuracy of the strain data acquisition system used, the measured results were compared to the output from a P3 strain indicator (Vishay Precision Group) under identical conditions. The P3 strain indicator box is a portable instrument which functions as a bridge amplifier, strain indicator and digital data logger for four input channels (+/- 1 µstrain resolution, +/- 0.1 % of reading accuracy). The equations used to calculate strain are summarised in Appendix F. A sample of intact testing strain results from each gauge on each rosette was compared with the P3 box before the results were filtered and the principal strain values calculated. The Matlab (MATLAB R2011b., MathWorks., Natick, MA) code analysis applies a low-pass Butterworth filter followed by the built in 'smooth' function. The results displayed in Figure 69 confirm that the data acquisition was suitable to proceed with measurements. Although there were slight discrepancies seen in the comparison, no correction was included in future testing. A check has also been performed to ensure that the Matlab used to analyse the results from the strain gauge rosettes was repeatable, which was confirmed on a sample set of results.

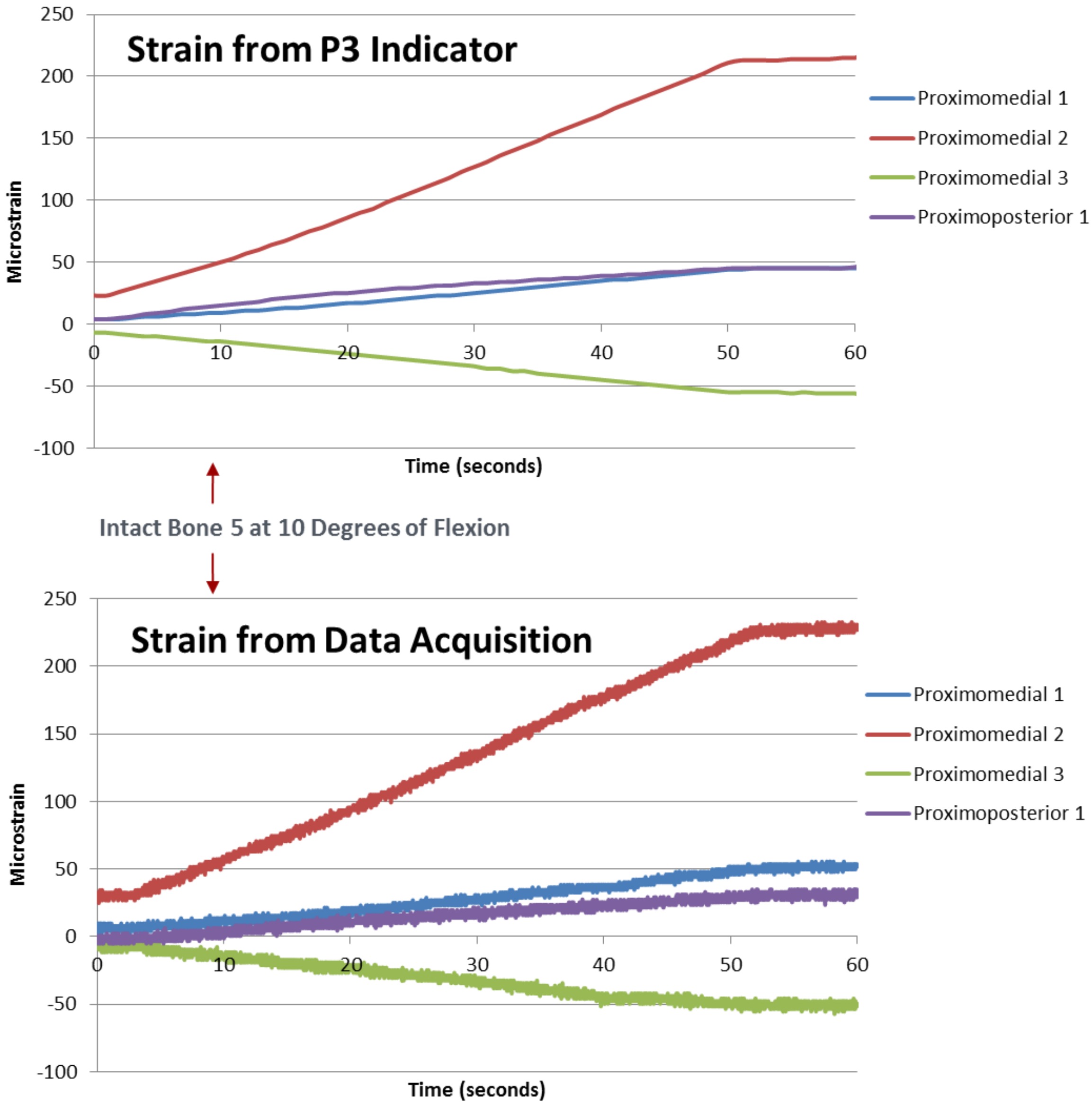

Figure 69 - Results of the comparison between the strain data acquisition used for 15 channels of data to the P3 strain indicator and recorder box. Results shown are an example of four of the channels when testing on the Intact Bone 5 in 10° of flexion.

9.2 Implantation Strains

To ensure that the implantation process did not damage the tibia specimen and affect the strain and loading characteristics during testing of the implanted test specimens, strain measurements were taken during implantation. A selection of the results of these measurements are presented in Figure 70 below and show that strain levels were consistently below 300 µstrain and that some gauges experienced residual strain.

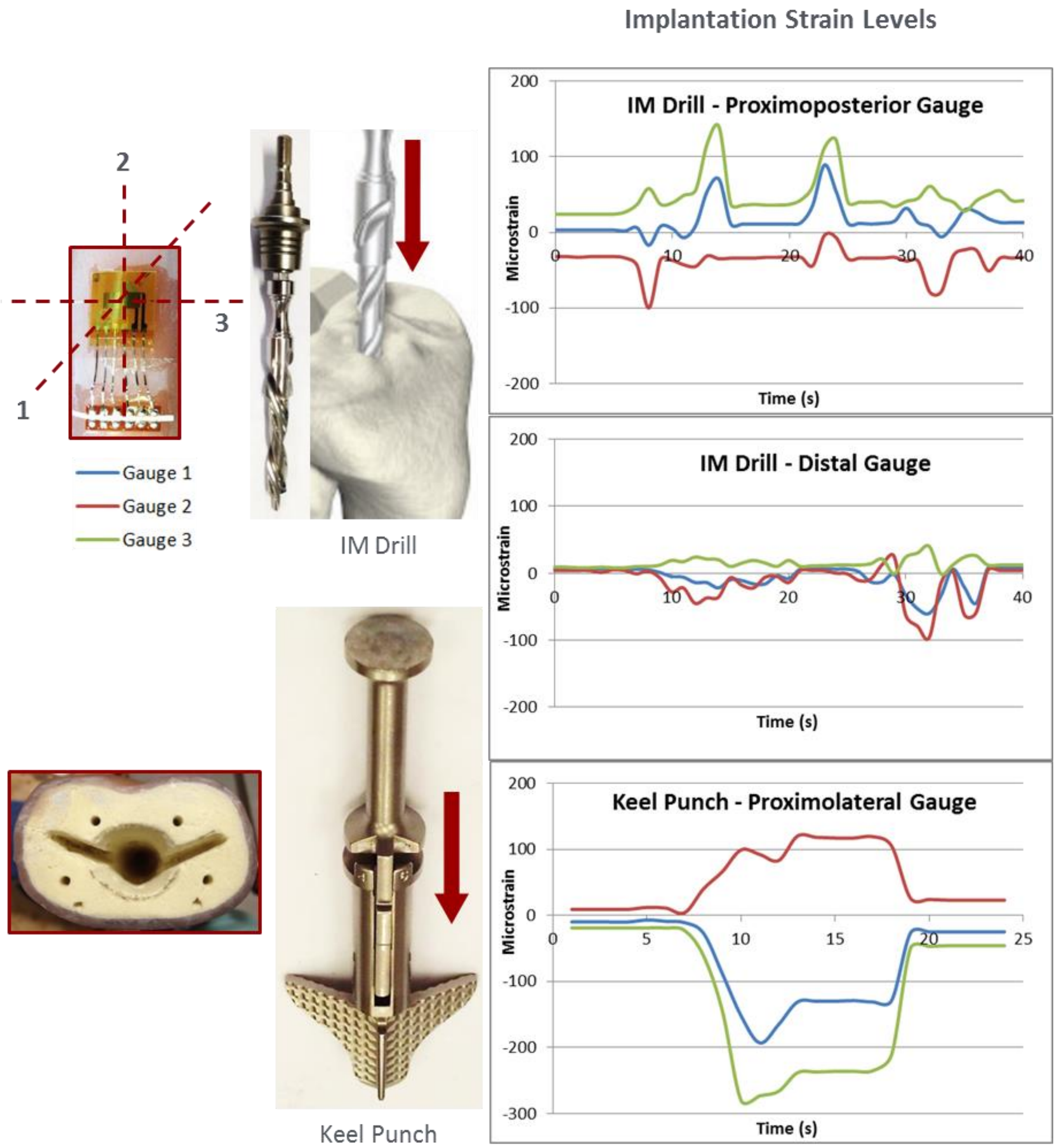

Figure 70 –A selection of the results from the strain gauge measurements taken during implantation (IM Drill - Stryker)

9.3 Compartmental Loading

The Flexiforce sensors were calibrated before the intact testing process and again before the implanted specimen testing on the tibiofemoral rig and the results are shown in Figure 71 and Figure 72. From the results an average calibration factor of 40.05 was calculated using the 'Linest' function in Microsoft Excel to find the gradient of each line which was used for all further analysis of the force test results. The Linest function uses the linear 'least squares' method to calculate a line of best fit of the load and voltage data.

The results from the force sensors summarised in Figure 73 indicate that the compartmental load share is maintained around 60:40 during all of the main testing as desired. These results are analysed in Matlab and averaged to produce the respective charts. The results of this testing validates that the compartmental load assembly within the tibiofemoral rig is capable of producing a physiological load share as measured in instrumented knee components. It also confirms that the following strain analysis is based on physiological compartmental loading.

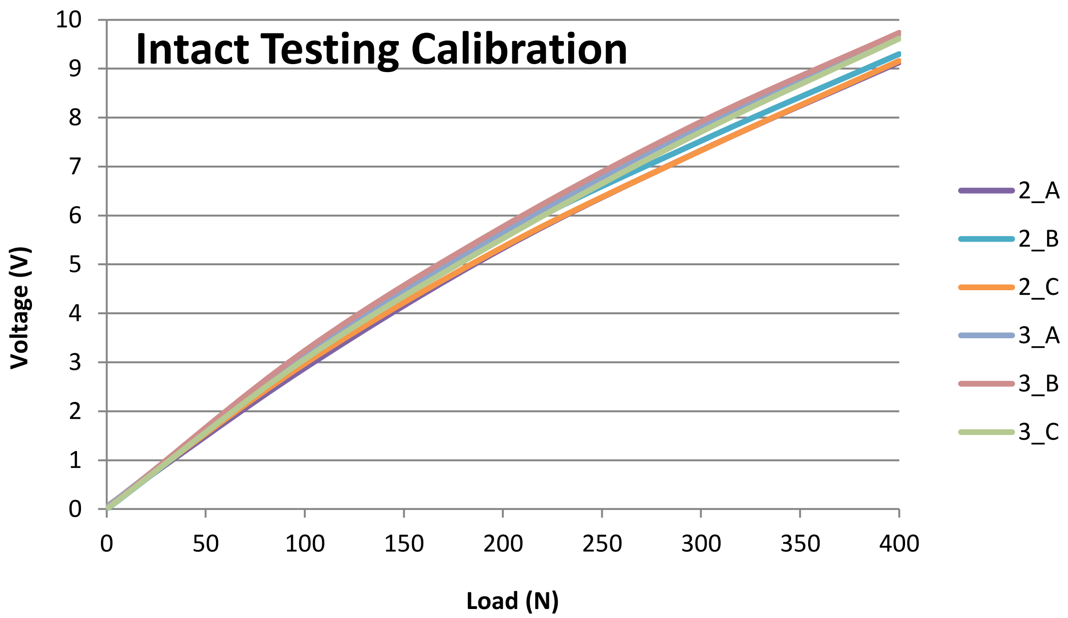

Figure 71 - All results from the calibration of two force sensors (2 and 3) performed prior to the intact testing including three repeats (A-C) of each calibration

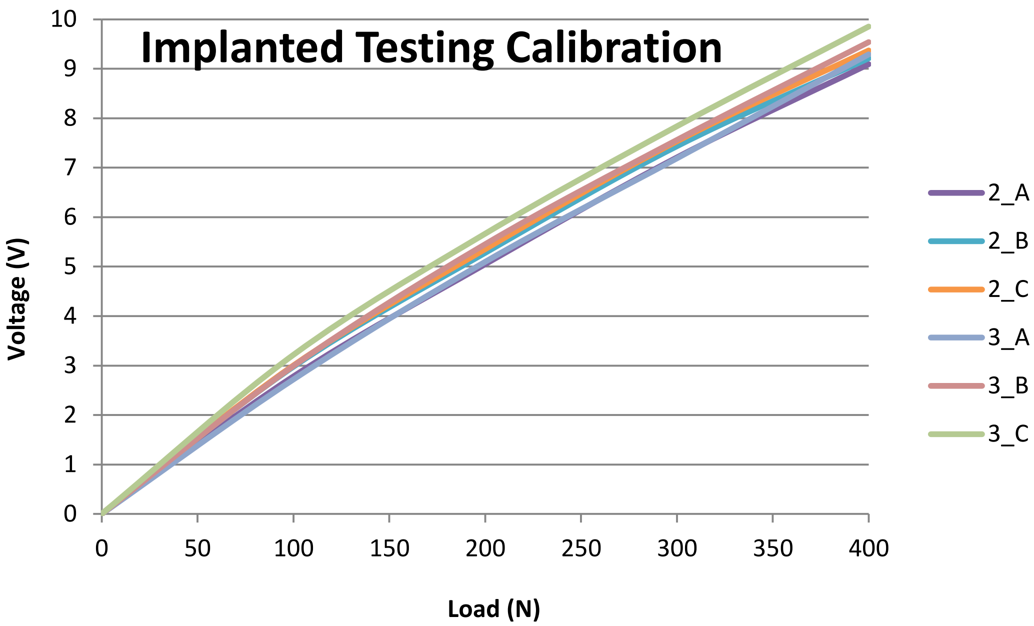

Figure 72 - All results from the calibration of two force sensors (2 and 3) performed after the intact testing and prior to the implanted testing including three repeats (A-C) of each calibration

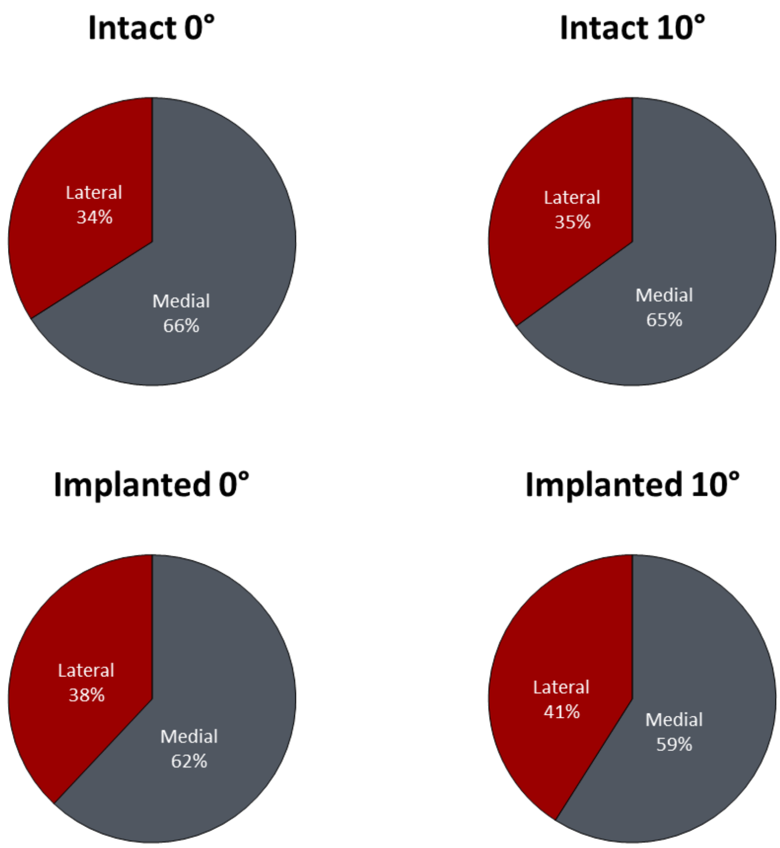

Figure 73 - Charts to illustrate the average medial to lateral load share across the tibial plateau during the tibiofemoral testing

9.4 Effect of RTKR Implant and Flexion Angle – Tibiofemoral Rig (Strain)

The maximum and minimum principal strains were calculated for intact and implanted testing at all gauge locations and flexion angles. This was performed for all five tibia specimen using MATLAB. A within-subjects repeated measures ANOVA test was performed on the four groups of data, as this parametric test is CONSIDERED robust enough to cope with small sample sizes and reduce the threat of outliers. This was followed by a post-hoc paired t-test to establish which comparisons were significantly different, taking a bonferroni correction factor for multiple comparisons into account. The statistics were performed using the software package SPSS 20 (IBM Corp., Armonk, NY, USA) to establish the effect of implantation and flexion angle on the cortical strain at each gauge location. For all statistical tests a p-value of less than 0.0125 indicates statistically significant differences based on the bonferroni correction. The results of this analysis are summarised in Figure 74. The strain values used are the minimum principal strain values as they were largest in amplitude and hence the most dominant strain. These minimum principal strain values were always compressive (negative) strains, with the maximum principal strains being lower in magnitude and tensile (positive). For all analysis, the minimum principal strain values analysed will be referred to as compressive strains. The data displayed is the mean with +/- one standard deviation to give an indication of the variability across the specimens. The direction of strain is shown on the diagram of the specimen and shows that it was consistently within 35° from vertical in the three posterior gauges. For the medial gauges the direction of principal compressive strain was within 20° of the vertical at all times and the lateral gauges were within 35°. The biased compartmental loading towards the medial side coincides with the direction of principal strain offset from vertical. The trend across the results showed the direction of principal compressive strain approaching vertical as the load spread distally.

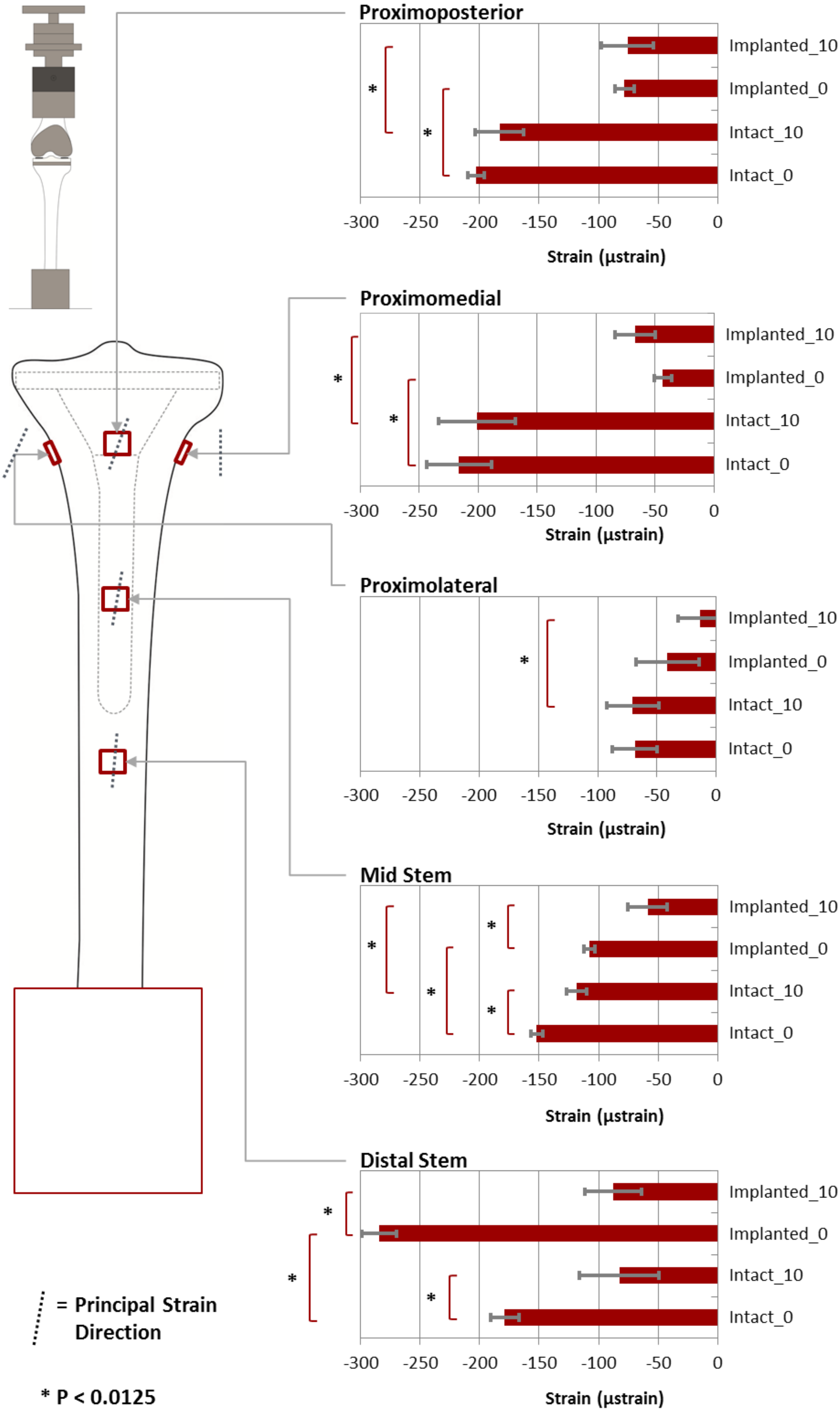

Figure 74 – Results to illustrate the effect on tibial load distribution of a RTKR implant and varying knee flexion angle (posterior view)

9.5 Effect of Flexion Angle – Combined Loading Rig (Strain)

To ensure that the combined loading rig was loading through both compartments, the pressure film used in the tibiofemoral rig was also used in the combined rig to adjust the assembly until it produced the results such as those seen in Figure 75. It was found that after all possible adjustment, the combined rig was biased to loading more on the lateral side compared to the desired 60:40 M:L load distribution. This was a limitation of the combined loading rig and considered during the analysis of the results. Following the main testing phase on the combined loading rig, the maximum and minimum principal strains were calculated for implanted testing at 10° and 25° flexion angles at all gauge locations. Paired t-tests were performed to establish any significant difference between flexion angles. For all statistical tests a p-value of less than 0.05 indicates statistically significant differences. The results of this analysis are summarised in Figure 76. The strain values used were the maximum compressive principal strain values under a 400 N load, as discussed in the previous section. The direction of strain is shown on the diagram of the specimen and shows that it is consistently within 15° from vertical in the three posterior gauges. The trend across the results shows the direction of principal strain approaching vertical as the load spread distally. During testing, the external rotation of the tibia in the first 25° of flexion was noted and compared to that reported in the literature. The difference in external rotation between 10° and 25° of flexion was 4° which coincides with that measured in the natural knee (Browne et al. 2005).

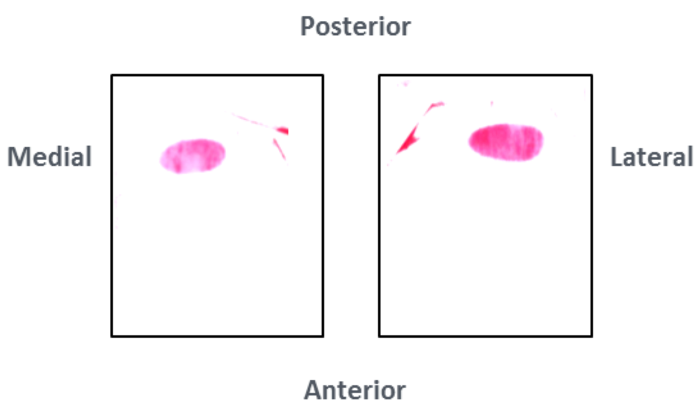

Figure 75 - Example of pressure film results from the combined loading rig

As shown in Figure 76, there were significant differences in compressive strain between 10° and 25° of flexion across all but the proximomedial gauge. At the proximoposterior gauge and mid stem gauge, the mean principal strain at 10° of flexion was significantly higher than that at 25° of flexion ($p < 0.01$). The correlation between the paired samples was strong (0.827 and 0.891 respectively) although limited as there were only 5 samples. At the proximolateral gauge, the mean compressive principal strain at 10° of flexion was also significantly higher than that at 25° of flexion ($p=0.014$). At the distal stem gauge, the mean compressive principal strain at 10° of flexion was again significantly higher than that at 25° of flexion ($p < 0.01$).

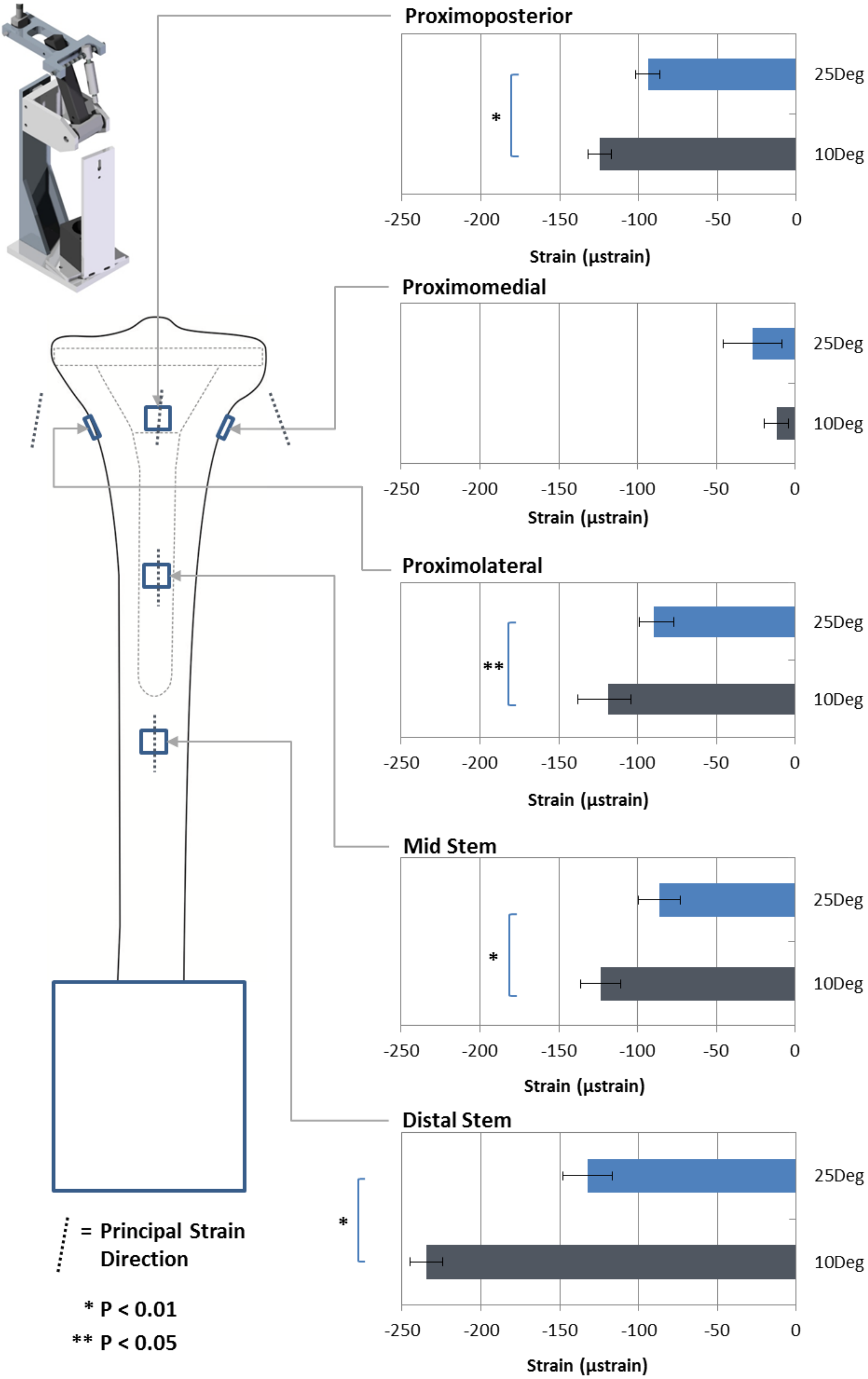

Figure 76 – Indicating the effect of changing the knee flexion angle on the compressive principal strain distribution in implanted tibia specimens (posterior view)

9.6 Regression of Strain

A number of tests under varying applied loads were performed on both loading rigs to allow for the application of regression analysis. The aim was to calculate a regression equation for every scenario of flexion angle and gauge location on the tibiofemoral and combined loading rig to allow the strain at any load to be predicted. This can be performed once the linearity of each data set is established by calculating the correlation coefficient. Linearity can only be proved with more than three load groups and therefore the linearity of the combined loading rig could only be implied through the analysis.

9.6.1 Ramp on TFJ Rig

During the testing on the tibiofemoral rig, further ramp testing was performed on one bone in each scenario to record principal strain values at 300, 400, 500 and 550 N with three repeats of each. This data is analysed in Matlab and used to perform a regression analysis at 0° and 10° of flexion on intact and RTKR implanted bones. Due to the composition of the tibia of cancellous and cortical bone with the addition of cement mantle and implant in the implanted scenario, it was expected that the relationship may be quadratic. For all data, regression analysis were performed for a quadratic fit in an Microsoft Excel spreadsheet and the p-value of the x^2 term was obtained. Where the p-value was significant ($p<0.05$) then the quadratic formula was used. Where the p-value was not significant ($p>0.05$) then the straight line fit was calculated and used instead. An example data set analysed and found to be linear can be seen in Figure 77. An example of a quadratic relationship can be seen in Figure 78. The results of the regression analysis produce a regression equation, which can be used to predict the maximum compressive principal strain at different loads to those tested, are shown in Table 8. From Table 8 it is seen that in all gauges and loading scenarios on the Tibiofemoral rig, the correlation coefficient is indicative of strong linearity.

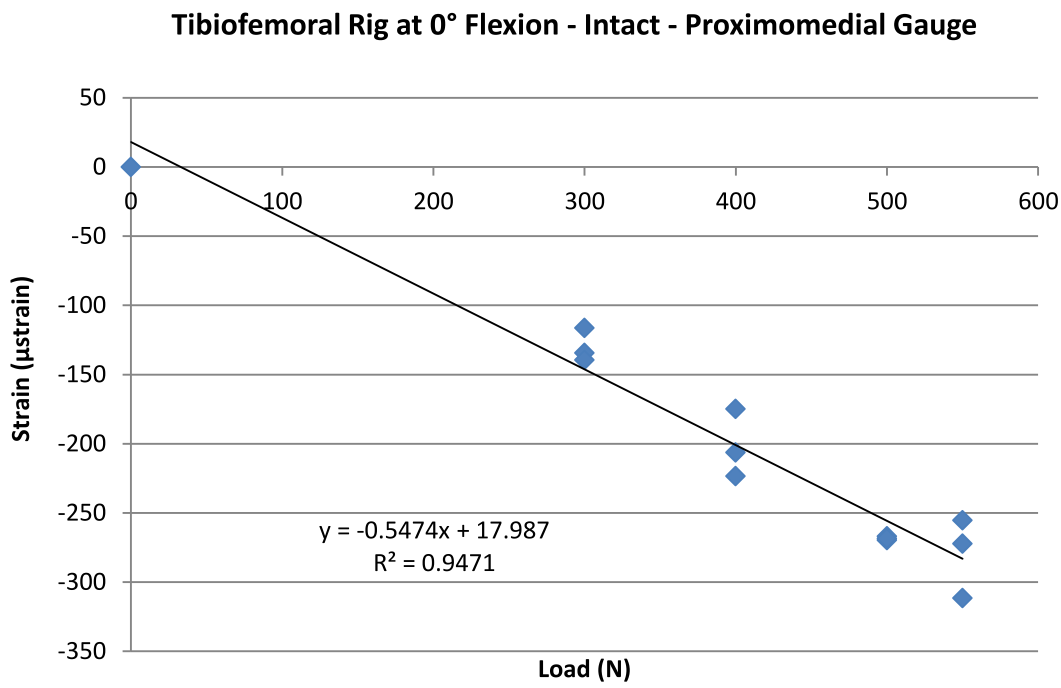

Figure 77 - An example of the graphical results of the linear analysis testing, showing the linear nature of the proximomedial gauge on the intact bone at 0° of flexion. This linearity was proved in the further analysis of the data as described.

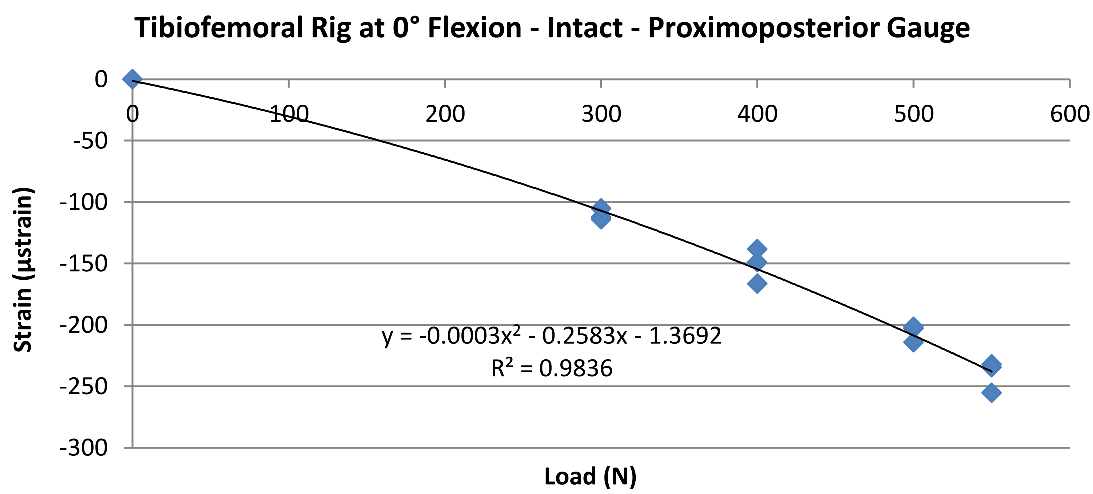

Figure 78 - An example of the graphical results of the quadratic regression analysis testing, showing the proximoposterior gauge on the intact bone at 0° of flexion. The regression results gave a p-value = 0.008 for the x^2 term.

Gauge Location	Correlation Coefficient	Linear Regression Equation For Principal Strain (y)
Intact 0° Flexion		
Proximomed	0.94	y = 17.99 - (0.55*Load)
Proximopost	0.98	y = -1.37- 0.26*Load - 0.00031*Load^2
Proximolat	0.80	y = 0.73 - (0.19*Load)
Mid Stem	0.95	y = 8.91 - (0.3*Load)
Distal Stem	0.89	y = 9.4 - (0.3*Load)
Intact 10° Flexion		
Proximomed	0.98	y = 0.41 - 0.36*Load - 0.00032* Load^2
Proximopost	1	y = -0.085 - 0.29*Load - 0.00023* Load^2
Proximolat	0.93	y = -0.29 - (0.17*Load)
Mid Stem	1	y = -0.13 - 0.19*Load - 0.00012* Load^2
Distal Stem	0.94	y = 8.45 - (0.21*Load)
Implanted 0° Flexion		
Proximomed	1	y = 0.4 - (0.08*Load)
Proximopost	0.99	y = 3.06 - (0.14*Load)
Proximolat	0.98	y = 0.09 - 0.04*Load - 0.00016* Load^2
Mid Stem	0.99	y = 0.92 - 0.16*Load - 0.00011* Load^2
Distal Stem	0.99	y = 2.18 - 0.38*Load - 0.00025* Load^2
Implanted 10° Flexion		
Proximomed	0.91	y = 0.18 - 0.103*Load + 0.0001* Load^2
Proximopost	0.99	y = 0.14 - 0.09*Load -0.00006* Load^2
Proximolat	1	y = 0.24 - 0.006*Load -0.00014* Load^2
Mid Stem	0.99	y = 0.31 - 0.056*Load - 0.0001* Load^2
Distal Stem	0.99	y = 0.66 - 0.086*Load - 0.0001* Load^2

Table 8 – The results of the regression analysis of the tibiofemoral rig including the regression equations which can be used to predict maximum compressive principal strain values at higher loads than those tested.

9.6.2 Combined Loading Rig

Multiple tests under varying applied loads were performed to allow for the application of linear regression analysis. The aim was again to calculate a regression equation for every scenario of flexion angle and gauge location on the combined loading rig to allow the strain at any load to be predicted. The results were analysed in Matlab which produced principal strain values for three repeats of three load values, at each location under 10° and 25° of flexion on every tibia specimen. The linearity of each set of tests is assessed by calculating the correlation coefficient using the method described during the tibiofemoral analysis. For all but four of the fifty data sets completed with the combined loading rig, the correlation coefficient is between 0.9 and 1 indicating strong linearity. As discussed, this linearity is implied as only three load groups were tested, but it produces a good indication and allows the linear regression analysis to continue.

The slope and best fit was calculated for all data, with their respective standard errors, using the same Linest function in excel. The weighting of each tibia specimen was then calculated followed by the weighted average across all bones and uncertainty of the principal strain measurements using the equations shown below. This was done across all data sets including all five tibia samples at five gauge locations for the three repeats at 200 N, 300 N and 400 N. The results of the weighted average calculations can be found in Table 9 and Table 10. Due to the strength of the five sets of data for each load scenario and the ability to calculate a weighted average, simple linear regression was performed. The weighted average gradients were used to describe the linear regression equation which can be used to predict the maximum compressive principal strain at different loads to those used in testing.

Weighted average from Taylor 1997

Firstly the weights, w_i, are calculated using the standard errors of each measurement for i = 1 to N number of repeated measures;

$$w_i = \frac{1}{{\sigma_{Ei}}^2}$$

Then the weighted average is found by combining the sum of the weight multiplied by the measurement E;

$$E_{w-ave} = \frac{\sum_{i=1}^{N} w_i E_i}{\sum w_i}$$

Finally, the uncertainty of the weighted average is calculated;

$$\sigma_{w-ave} = \frac{1}{\sqrt{\sum_{i=1}^{N} w_i}}$$

Gauge Location	Weighted Average of Gradient	Uncertainty	Weighted Average of Intercept	Uncertainty	Linear Regression Equation For Principal Strain (y)
Proximomed	0.10	0.002	-1.42	0.646	y = (0.10*Load) – 1.42
Proximopost	-0.33	0.007	9.57	2.028	y = 9.57 - (0.33*Load)
Proximolat	-0.31	0.006	7.12	1.666	y = 7.12- (0.31*Load)
Mid Stem	-0.32	0.007	9.56	2.062	y = 9.56 - (0.32*Load))
Distal Stem	-0.62	0.016	22.50	4.634	y = 22.5 - (0.62*Load)

Table 9 – Results of the linear regression analysis for 10° of knee flexion on the combined loading rig

Gauge Location	Weighted Average of Gradient	Uncertainty	Weighted Average of Intercept	Uncertainty	Linear Regression Equation For Principal Strain (y)
Proximomed	-0.01	0.001	-0.26	0.310	y = (-0.01*Load) - 0.26
Proximopost	-0.25	0.006	7.37	1.696	y = 7.37 - (0.25*Load)
Proximolat	-0.24	0.005	5.64	1.464	y = 5.64 - (0.24*Load)
Mid Stem	-0.21	0.004	4.72	1.175	y = 4.72 - (0.21*Load))
Distal Stem	-0.31	0.005	5.48	1.531	y = 5.48 - (0.31*Load)

Table 10 - Results of the linear regression analysis for 25° of knee flexion on the combined loading rig

9.7 Effect of Applied Loading

An important part of the investigation in this research aimed to compare the tibial strain results produced by the tibiofemoral and combined loading rigs, when using the same specimens under the same loading conditions. This allows assessment of the inclusion of the patellofemoral joint during testing of knee implant components. The equivalent loading between rigs was the 550 N loading through the tibiofemoral rig and 200 N of load applied through the combined loading rig as described in the methods section. The maximum and minimum principal strains were calculated for implanted testing on both rigs at all gauge locations at the 10° flexion angle tested on both set-ups. This was performed for all five tibia specimen using Matlab. Paired t-tests were performed at each location using SPSS to establish the effect of experimental rig set-up on the cortical strain at each gauge location. For all statistical tests a p-value of less than 0.05 indicates statistically significant differences. The strain values compared are the minimum principal strain values as they were largest in amplitude and will be referred to as the maximum compressive principal strain. As it was not possible to measure the compartmental loading at this stage in the combined loading rig, the results of the proximomedial and proximolateral strain gauges were not analysed as it was not considered a fair comparison. The results of this analysis are summarised in Figure 79. No significant difference was found with the addition of the patellofemoral joint loading in any of the three posterior gauge locations. There was a trend for the principal strain to decrease in the proximoposterior section of the bone specimens ($p = 0.058$).

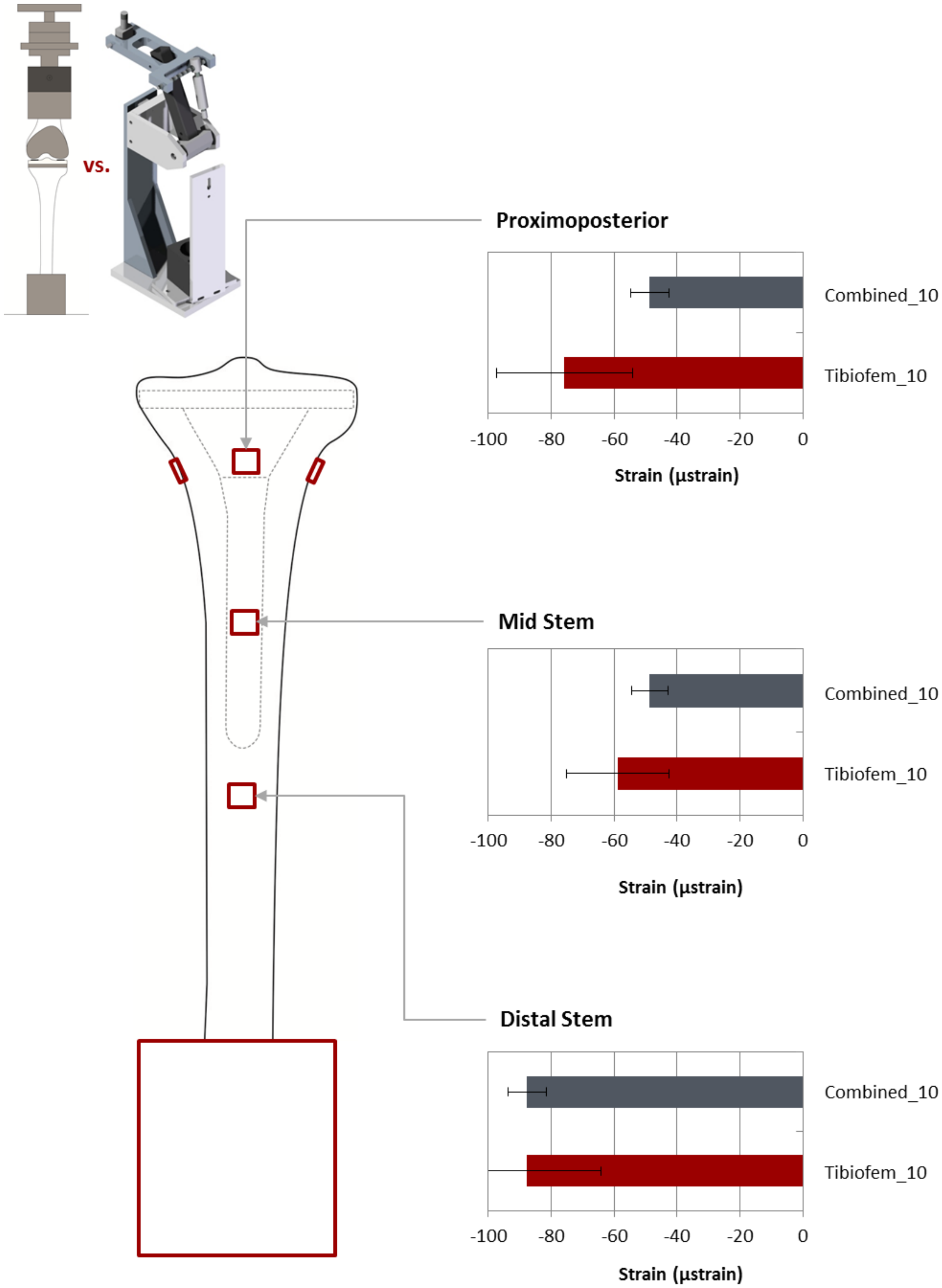

Figure 79 – Results to display the comparison of strain distribution through the tibia between the two equivalent applied loading techniques at 10° of knee flexion (posterior view)

10 Discussion

The overall aim of this research was to develop and investigate methods for determining the load transfer and strain distribution in composite tibia specimens under varying applied loading conditions, with and without an implanted RTKR. The results from all validation and calibration testing illustrate that the recorded strain distribution and compartmental force measurements provided accurate data for analysis of the experiments. The results from the strain indicator box correlate with the same strain gauge amplitudes measured by the data acquisition system used, as shown in Figure 69, and the manipulation in Matlab was repeatable. The calibration of the Tekscan force sensors used to assess compartmental loading is presented in Figure 71 and Figure 72. After calibration, a strict protocol prior to each test was followed to ensure correct conditioning of the sensors.

10.1 Implantation Strains

During the implantation procedure of the revision tibial component, the results recorded from the strain gauge rosettes demonstrate that the bone specimens were not exposed to abnormally high strains which may have influenced the strain measurements during testing. From Figure 70 it is clear that the maximum strain levels experienced were less than 300 µstrain when impacting the keel punch. This level of strain has been measured in the cortical bone in past studies including that by Lanyon et al who were the first to measure bone strains in vivo (Lanyon et al. 1975). The results of their study recorded maximum principal strains greater than 300 µstrain during walking and increasing to over 800 µstrain whilst running. These were the results from a strain gauge rosette placed at the mid shaft of the tibia, but they give a good indication of the tibial response to normal loading. More recent studies also indicate similar tibial strain levels for walking including that of Burr based on Lanyon’s work (Burr et al. 1996) and the extensive publications from Milgrom through the 2000 decade (including Milgrom et al. 2000). In a literature search to establish if these findings correlated with other studies, there appears to be no published papers discussing the strain levels experienced during the implantation process. The implantation strain measurements reported in this study are therefore useful in confirming that the results from implanted testing were not compromised by the implantation process. They also give an appreciation of the levels of strain that the bone might be subjected to during implantation in surgery. The residual strain seen in some of the gauges is an interesting observation from this experiment which was unexpected and is generally not considered during surgery. This permanent strain after removal of the tool is likely to be due to the change in structure of the tibia after bone removal and indicates some degree of plastic deformation; this would be interesting to investigate further in the future.

10.2 Compartmental Loading

The results from the Tekscan force sensors obtained during testing confirm that the adjustable knee alignment system provided the desired physiological compartmental load distribution of approximately 60:40 proportion medial to lateral seen in Figure 73. Although this did fluctuate on the medial side between 59% to 66%, the literature search showed that this ratio typically varied from 55:45 to 75:25 (Green et al. 2002, Mundermann et al. 2008, Reilly et al. 1982). Ensuring that the knee was aligned to more closely replicate physiological compartmental loading provided confidence in the validity of the strain distribution results. A preliminary investigation into the effect of the compartmental load on strain recorded at the distal tibia demonstrated a strong relationship between the compartmental load in the knee joint and the load distribution through the tibia. It was therefore important to monitor compartmental loading during testing. This was particularly true for the proximomedial and proximolateral gauges which were more likely to be influenced by the compartmental load transfer through the tibial plateau. Further investigation into the direct effect of altering the compartmental load on the medial and lateral gauges would be a valuable addition to this research. This would examine possible implications of surgical malalignment effects in RTKR.

10.3 Effect of RTKR Component

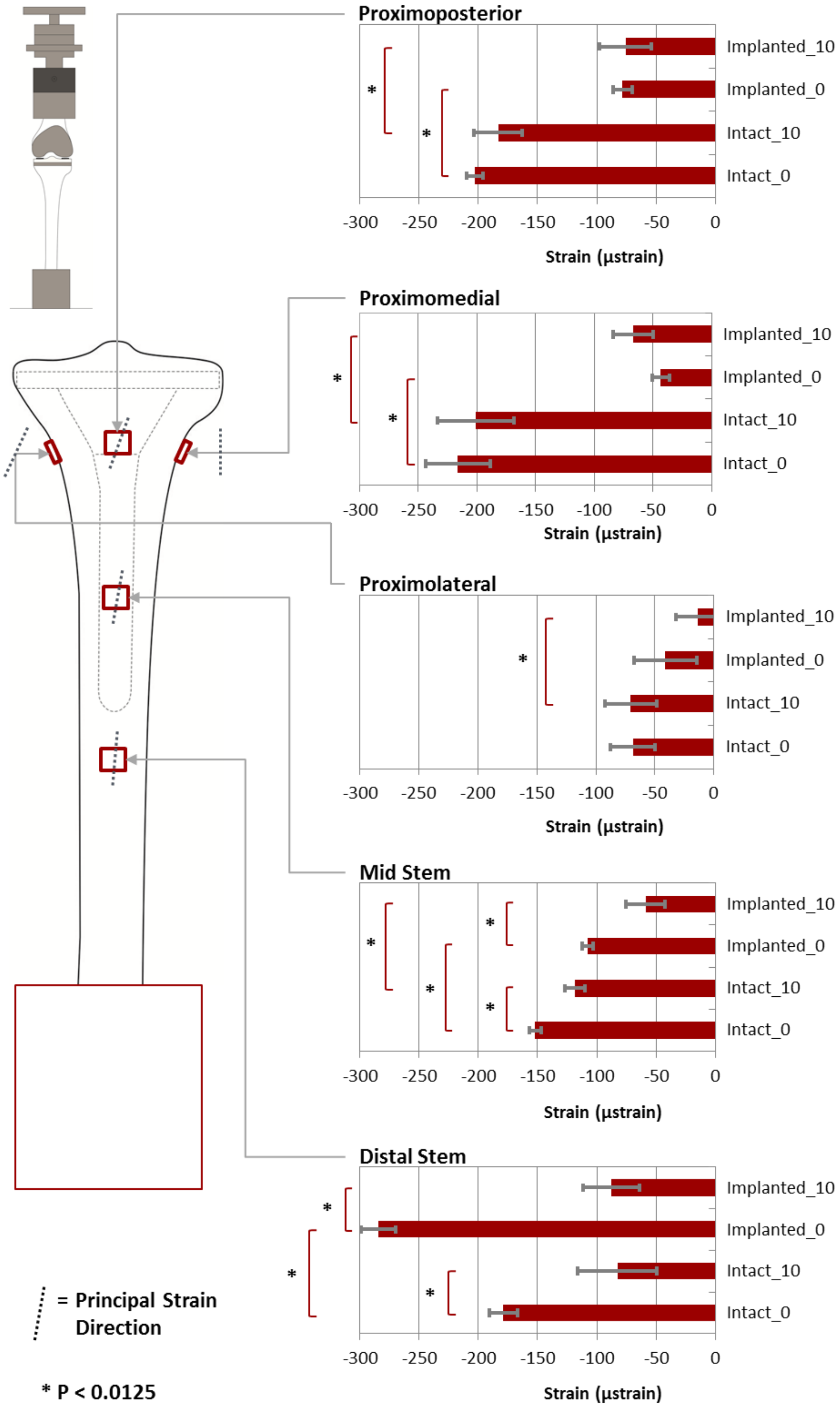

Figure 80 – A duplicate of Figure 74 results for ease of reference, which illustrate the effect on tibial load distribution of a RTKR implant and varying knee flexion angle

The results from the comparison of cortical strain distribution through intact and implanted tibias demonstrated significant differences between the two states as illustrated in Figure 80. In general, principal compressive strains were higher in the intact tibia in the areas measured than they were after implantation of the revision tibial component. The exception to this is at the distal stem gauge where the maximum compressive principal strain experienced in the implanted tibias under the 550 N loading was 285 µstrain during axial (0°) loading. This is significantly higher than that measured in the intact bone (179 µstrain, $p < 0.0125$). These results agree with previous studies that have found high strain areas just below the stem tip (Chong et al. 2011 and Completo et al. 2008a) and are similar to the strain value predicted in basic calculations during development (359.7 µstrain in Section 6.8). It is likely that in the samples studied, the physiological load applied in the proximal region of the tibial condyles is largely transferred distally through the stem tip of the revision component. Such concentrated load is reflected in the significant increase in concentrated compressive strain levels in the distal cortical bone and is likely to be the cause of pain reported by some RTKR patients.

The concentration of compressive strain in the distal region of the tibia is a result of reduced load being transferred in the proximal tibia. The strain in all three proximal gauges is significantly reduced post implantation at both flexion angles except for the proximolateral gauge at 0° flexion. This significant reduction in compressive strain proximally between the intact and implanted tibias supports the concept of proximal strain shielding. The load is effectively being bypassed away from the proximal bone which could lead to bone resorption if the strain levels are not adequate to encourage bone remodelling in this area. Is important to note that the low measured strain levels are associated with an applied load of only 550 N, which is a lower load than that associated with typical activities of daily living. However, the strain gauge rosettes are positioned far enough away from the tray that it is likely the localised areas directly underneath the tray may experience even lower compressive strains than those measured.

The consequence of the relatively rigid tibial tray and stem combination can lead to different levels of load share in the way in which load is transferred through the tibia. In this particular fully cemented revision component, it seems that the main load transfer is through the stem tip. A possible way to improve the load transfer could be to investigate novel designs where the tray and stem are able to slide relative to each other. This could allow the tray to transfer load by compression on the tibial plateau and the stem to accommodate the flexural loads. Future work could aim to produce some prototypes of these novel designs and repeat the full testing protocol to compare the strain distribution results.

At the mid stem level, the results from the posterior gauge also yielded significantly higher principal compressive strains in the intact bone compared to after implantation at both flexion angles. This reduction in compressive strains at the mid stem after implantation correlates with the theory of the load bypassing the proximal bone and transferring more distally. The trend of the strain values at the posterior mid stem level compared to the posterior gauge in the more proximal location also altered after implantation. The principal compressive strain values at the mid stem were lower than the proximoposterior and proximomedial gauges in the intact tibia, but were slightly increased after implantation. This indicates a shift in load transfer distally with implantation, which correlates with the results found when comparing the proximal to distal gauges.

The medial and lateral gauges at the proximal tibia level confirm the relationship between greater load transfer on the medial side with a correspondingly greater strain below the tibial plateau on that side. This pattern is more consistent in the intact bone compared to the implanted bone however, but this is likely to be related to the greater reduction in proximal strain seen post implantation. On close inspection, the intact load share is greater than the 60:40 medial to lateral produced at the tibiofemoral joint but consistent between flexion angles (76:24 and 74:26). The load share in the implanted specimens has great variation between flexion angles with a 51:49 share at 0° of flexion and 83:17 at 10° of flexion. This may be attributed to the flexural rigidity of the tibial tray and the uniform structure of the intact composite bones which is likely to be disrupted by RTKR implantation.

The directions of compressive strains experienced through the tibia are predominantly axial which is consistent with the axial direction of the external loading. As displayed in Figure 80 with the dashed lines, the direction of the principal compressive strains on all of the posterior gauges is inclined towards the medial side as expected with the greater compartmental load through the medial condyle. These findings are consistent with the medial bias of the compartmental loading and with that expected in the natural knee. Importantly, the natural trabecular architecture of the tibia, with its arched network from the condylar joint surface as seen in Figure 8 allows for such strain patterns. In the tibial component, the design of the keel below the tibial tray may overcome the off centre loading.

The results of this section of the research should help to inform future implant design to improve understanding of how load is transferred through the tibia. The specific design to adjust for physiological loading also highlights the importance of incorporating the compartmental load share into pre-clinical assessment techniques.

10.4 Effect of Flexion Angle

The results from the tibiofemoral rig shown in Figure 80 indicate that a change in knee flexion from 0° to 10° generated significant reductions in the principal compressive strain magnitudes at the mid and distal stem location for both the intact and implanted bone specimens ($p<0.0125$). No significant differences in strain were found between flexion angles in the three proximal gauges before or after implantation. Such results indicate that knee flexion has a greater effect in the more distal areas than it does proximally, with the pattern maintained after RTKR. This is likely to be due to a combination of reasons including 10° flexion which has a horizontal load component and the possibility that the contact point between femur and tibia in the A-P direction may move with 10° of flexion. The effect of introducing a horizontal force component instead of a pure vertical force reduces the vertical component whilst also slightly counteracting the compressive forces with the horizontal bending moment in the opposite direction. The 10° loading is therefore effectively superimposing a tensile strain on the distal tibia that has the overall effect of reducing the compressive strain. This is likely to show in the more distal gauges due to the increased distance from the point of loading. Moving the tibiofemoral point of contact in the A-P direction may contribute to the strain reduction seen by changing the moment arm. These significant differences experienced at only a 10° change in knee flexion emphasises the need for testing at higher flexion angles to assess the effect on strain distribution.

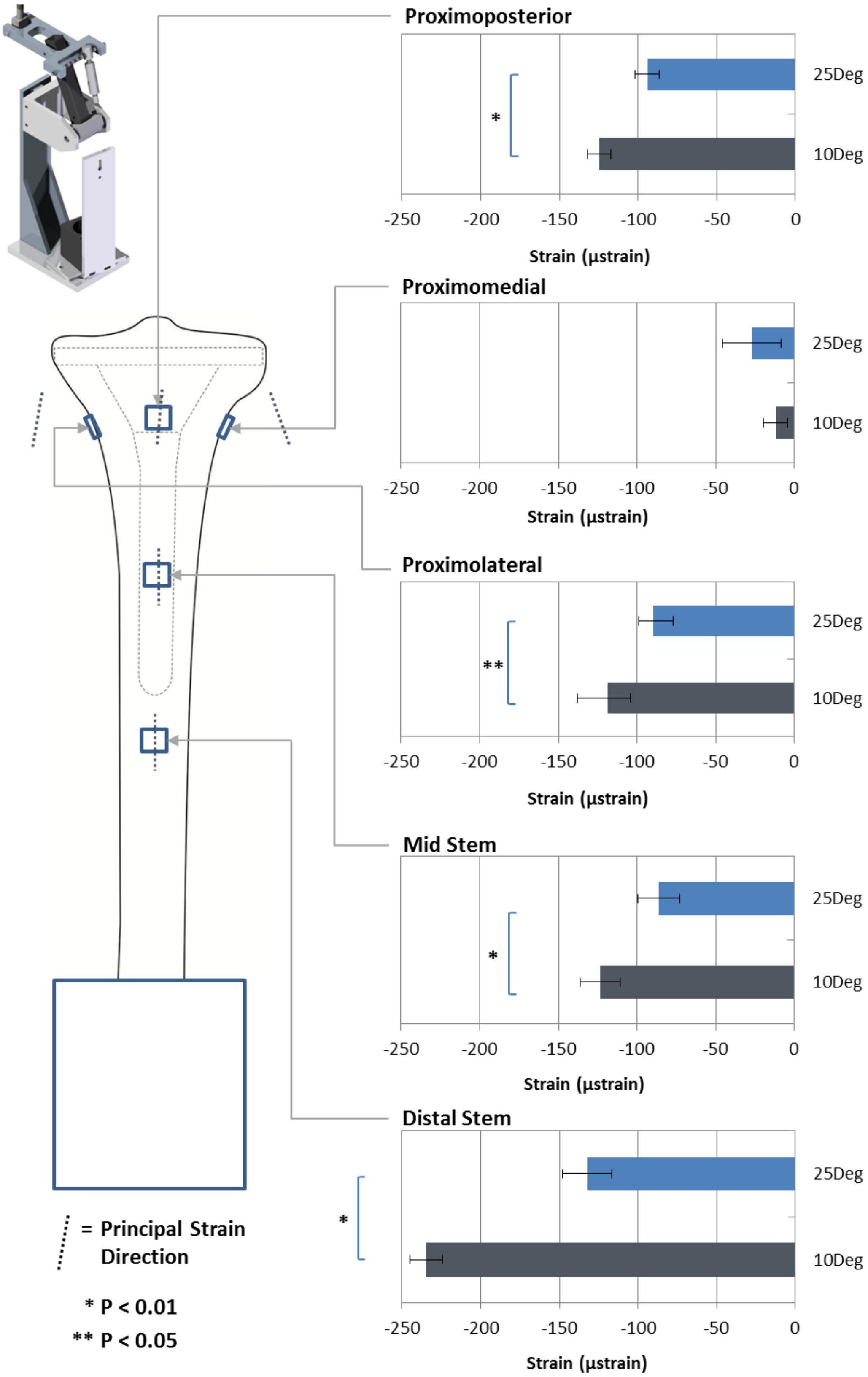

Figure 81 – A duplicate of Figure 76 for ease of reference, which illustrates the effect of changing the knee flexion angle on the compressive principal strain distribution in implanted tibia specimens

The results from the combined loading rig (Figure 81) display significant differences in the tibial strain pattern between 10° and 25° of flexion. There is a significant decrease in strain in the proximoposterior, mid stem and distal locations with increasing flexion angle. The reduction in compressive strain is more profound in the strain gauge locations moving from the proximal to distal tibia. For example, at the mid stem location, a 30.3 % reduction in principal strain is experienced between 10° and 25° flexion. At the distal stem, this strain decrease was found to be an average of 43.5%. This correlates with the results found on the tibiofemoral rig where there was also a decrease in strain with greater knee flexion (0° to 10°). This confirms that at low knee flexion angles within the screw-home arc and beginning of the functional arc, there is a trend for reduced strain as knee flexion increases; particularly in the distal region. These findings follow the same pattern of reduced strain with increased flexion as found through further testing on the combined loading rig. This study tested flexion at 10, 20, 30 and 40° and concluded that principal strains decreased as the flexion angle increased (Thomas 2015).

The overall strain patterns found when testing the implanted tibia specimens on the combined loading rig are similar to those of the tibiofemoral loading rig. Further analysis of this will be made during the direct comparison of equivalent loads between the rigs, but some obvious trends appear from the data presented in Figure 81 at the highest load tested. The compressive strain magnitude is greatest at the distal stem area which importantly agrees with results from the tibiofemoral rig and confirms the theory of stress concentrations leading to end of stem pain. In addition, the strain in the distal region are the same for both loading rigs which correlates with Saint-Venant's Principle whereby the distance of the stem tip gauge from the load application is sufficient to not be affected by the way that the load is applied (Love 2013). The principal compressive strain levels recorded at the proximomedial rosette are much lower than those at the proximolateral and all other gauges, as expected due to the compartmental loading bias on the lateral side. Ideally this would have been overcome in the combined loading rig using a similar compartment loading and alignment system as in tibiofemoral rig; however this was beyond the scope of the research and should be incorporated into the rig in the future. These results do interestingly enhance the research and discussion regarding the relationship between the compartmental load application at the condyles and the load distribution through the tibia.

The directions of principal compressive strain on the posterior surface of the tibia are along the long axis of the bone. The direction of principal strain in the sagittal plane is angled from the posterior of the tibia which coincides with the results from the pressure film displaying slightly posterior loading (Figure 75).

10.5 Effect of Applied Loading

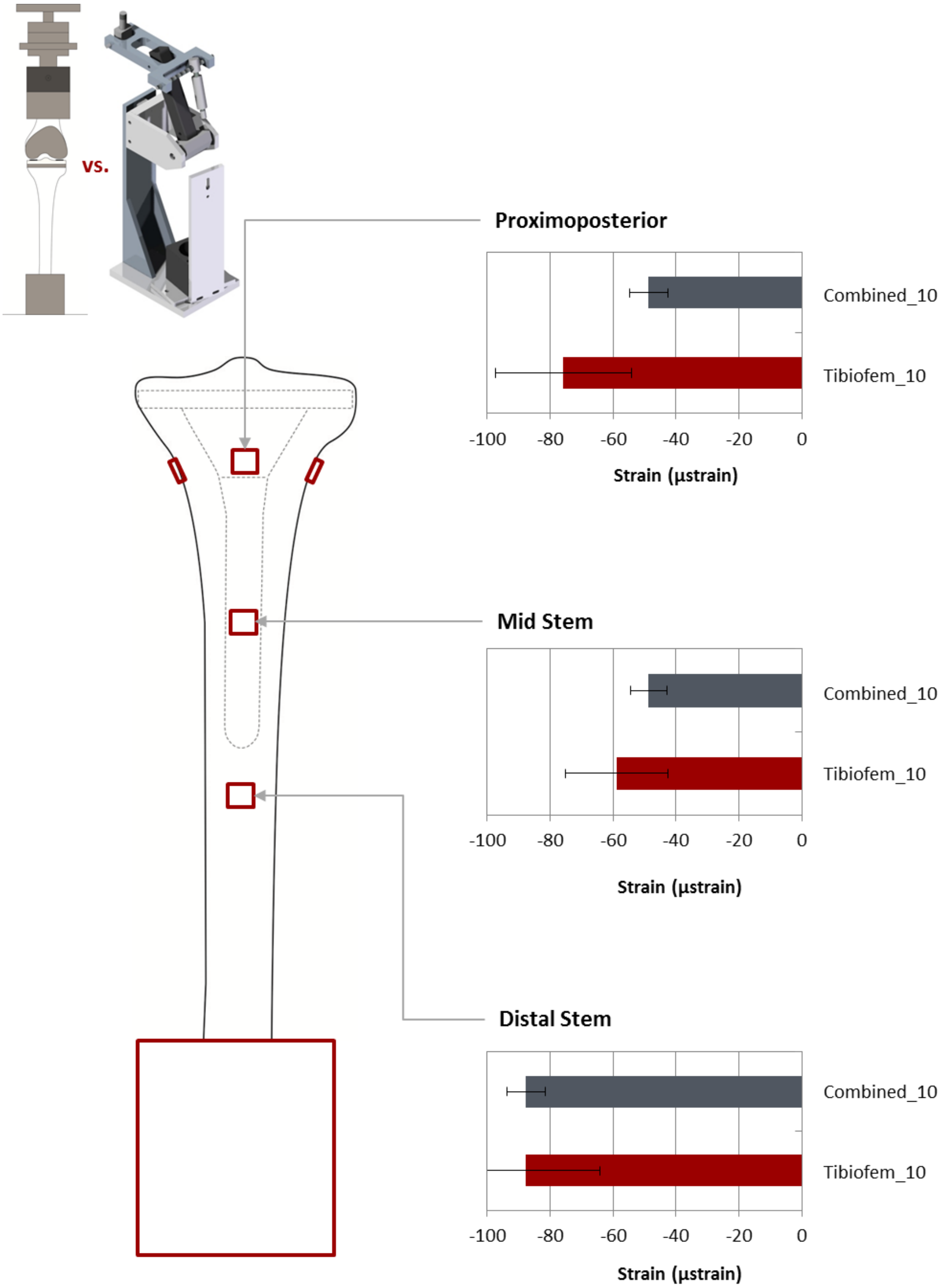

Figure 82 - A duplicate of Figure 80 for ease of reference, to display the comparison of strain distribution through the tibia between the two equivalent applied loading techniques at 10° of knee flexion

The results of the direct comparison of the applied loading rigs indicate that at 10° the proximal strain is lower in the combined rig compared to the tibiofemoral rig; however the difference is not statistically significant for the small knee flexion angle. The trend for the principal strain to decrease with the inclusion of the patellofemoral joint was strongest in the proximoposterior of the bone ($p = 0.058$). This reduction is likely to be due to the patella tendon force acting to oppose the bending effect of the tibiofemoral force at this small flexion angle. This analysis was performed for 10° of flexion only which is the beginning of the functional arc of motion due to the limitations of the tibiofemoral rig. At higher flexion angles, the patellofemoral reaction load increases significantly relative to the tibiofemoral load, in addition to the change in direction of the tibiofemoral reaction force. This will have a significant effect on tibial strains, as shown in the 25° flexion results, so it is recommended that testing at higher flexion angles should be performed in the combined loading rig in future. The direct comparison of the applied loading again illustrates the general trend of strain distribution through the tibia being concentrated distally at the stem tip.

The effect of overestimating the strain levels by excluding the patellofemoral joint is likely to introduce problems when assessing areas of strain shielding, rather than areas of high strain. This is because the adverse strain concentrations are likely to be lower than predicted in the traditional tibiofemoral rigs, whereas the areas of bone that are subjected to low strain levels may actually experience even less. It is possible that the inclusion of the patellofemoral joint may change the strain pattern significantly in the proximal tibia, however more strain gauge rosettes in this area are required to assess this appropriately.

10.6 Results Extrapolation

From the results of the regression analysis, the strain distribution through the tibia can be predicted for any applied load value. This allows further understanding and comparison with the literature at physiological load levels, and also has the potential to predict potential areas of strain peaks with high loading activities. Using the regression equations for the tibiofemoral rig, the principal compressive strain at the five gauge locations have been calculated for intact and implanted tibia as shown in Table 11. The 2030 N load is based on that used in a previous study (Completo et al. 2012). The 5165 N load is to provide an indication of the maximum strains experienced as this has been found to be the maximum load through the knee, measured whilst slow jogging (Bergmann et al. 2014). Comparing these predictions with published literature which used a similar loading technique with press fit revision tibia components show similar magnitudes of compressive principal strain were measured, however in general the predicted values were greater than those published. This is likely to be related to the quadratic curve fitted to the results. Assessing the maximum strain estimated in the tibia indicates that the compressive strain results are much above the suggested 1500 µstrain value for normal bone remodelling. Such findings encourage the requirement for testing at higher loads to confirm the prediction. If the strain levels are accurate, then the effect on the bone remodelling process may be a cause of stem end pain or failure of the RTKR.

Gauge Location	Linear Regression Equation For Principal Strain (y)	Principal Compressive Strain at 2030 N	Literature Estimation (Completo et al. 2012) (µstrain)	Principal Compressive Strain at 5165 N (µstrain)
Implanted 0° Flexion				Based on Bergmann et al. 2014
Proximomed	y = 0.4 - (0.08*Load)	-162	-125	-413
Proximopost	y = 3.06 - (0.14*Load)	-281	-140	-720
Proximolat	y = 0.09 - 0.04*Load - 0.00016* Load^2	-740	-140	-4475
Mid Stem	y = 0.92 - 0.16*Load - 0.00011* Load^2	-777	N/A	-3760
Distal Stem	y = 2.18 - 0.38*Load - 0.00025* Load^2	-1799	-1300	-8630
Implanted 10° Flexion				
Proximomed	y = 0.18 - 0.103*Load + 0.0001* Load^2	203		2136
Proximopost	y = 0.14 - 0.09*Load - 0.00006* Load^2	-430		-2065
Proximolat	y = 0.24 - 0.006*Load - 0.00014* Load^2	-589	N/A	-3766
Mid Stem	y = 0.31 - 0.056*Load - 0.0001* Load^2	-525		-2957
Distal Stem	y = 0.66 - 0.086*Load - 0.0001* Load^2	-586		-3111

Table 11 – Compressive strain at five locations produced from a selection of physiological loads with the tibiofemoral joint rig, including how it compares to published research using a similar loading technique

The linear regression equations for the implanted tibia in the combined loading rig have been used to predict the corresponding compressive strains seen in Table 12. The estimation demonstrates similar strain patterns to the tibiofemoral rig results; high compressive strain in the distal region and spread through the proximal and mid stem regions at 10° flexion. The compressive strain values are higher than the results from the tibiofemoral rig because the load transmitted through the tibiofemoral joint is actually higher than the load stated which was that placed on the Zwick. The compressive strain values at 5165 N are also higher than 1500 µstrain in the distal tibia as discussed with regard to the tibiofemoral rig results.

Gauge Location	Linear Regression Equation For Principal Strain (y)	Principal Compressive Strain at 2030 N (µstrain)	Principal Compressive Strain at 5165 N (µstrain)
10° Flexion			
Proximomed	y = (0.10*Load) – 1.42	202	515
Proximopost	y = 9.57 - (0.33*Load)	-660	-1695
Proximolat	y = 7.12- (0.31*Load)	-622	-1594
Mid Stem	y = 9.56 - (0.32*Load))	-640	-1643
Distal Stem	y = 22.5 - (0.62*Load)	-1236	-3180
25° Flexion			
Proximomed	y = (-0.01*Load) - 0.26	-21	-52
Proximopost	y = 7.37 - (0.25*Load)	-500	-1284
Proximolat	y = 5.64 - (0.24*Load)	-482	-1234
Mid Stem	y = 4.72 - (0.21*Load))	-422	-1080
Distal Stem	y = 5.48 - (0.31*Load)	-624	-1596

Table 12 - Compressive strain at five locations for the implanted tibia produced from physiological loading using the combined loading rig

10.7 Limitations

There are a number of limitations to this research that should be considered when interpreting the effect of the results obtained. The physiological loading rigs are simplified arrangements of a complex in vivo situation. This includes the static loading nature of both experimental rigs which may not replicate the physiological situation as accurately as a dynamic loading rig because they only consider the kinetic forces rather than kinetic and kinematic combined. The use of composite bone models, only one muscle action and the absence of ligamentous structures meant that the influence of the properties of natural bone, multiple muscle action and soft tissue structures in the knee joint were not taken into account. As the soft tissues contribute to load transfer through the knee, it is predicted that the strain distribution results may have been affected. A recent computational study of a unicompartmental knee replacement model did however show that there were no significant differences in tibial strain with the inclusion of muscle forces acting on the tibia (Pegg et al. 2012).

The loading scenarios tested were also limited to relatively low loads and small flexion angles. The maximum load applied to either rig was 550 N which is not fully representative of the physiological loads experienced in vivo. This was addressed by testing at increments to allow linear regression models to be calculated so that extrapolation could be used to predict compressive principal strain results from any applied load. The small flexion angles tested on the tibiofemoral rig, within the screw-home arc of knee flexion, was a limitation within this rig. This limitation was addressed in the combined loading rig which was developed to allow testing at greater flexion angles and inclusion of the patellofemoral joint which will be adapted further in future work to reach beyond 25° of flexion.

The strain measurement using five strain gauge rosettes does constrain the understanding of the load distribution across the full tibial surface. This was managed by using digital image correlation to identify any strain peaks on the tibial surface that were not covered by the location of the strain gauge rosettes. The results of this preliminary full surface strain study were useful but the complex geometry of the tibia meant further analysis was limited. Although it is accepted that the cortical bone strain does give an indication of how the load is transmitted in the cancellous bone surrounding the implant. Using this experimental data to validate an FEA model would allow a computational method to analyse the internal strains in the cancellous bone which cannot be achieved experimentally.

This research has developed a robust experimental testing protocol for evaluating tibial components in RTKR although this was limited to testing of a single type of implant. The focus was on the development of the methodology for future pre-clinical testing, which in the future could be used to evaluate other RTKR designs as well as stem geometry, stem length and fixation methods.

11 Conclusions

This research has involved the development and evaluation of a robust experimental test protocol for pre-clinical evaluation of RTKR tibial components. A tibiofemoral loading rig has been designed and tested which allows determination of the strain distribution in the tibia produced by the implantation of RTKR components. The importance of monitoring the strains experienced during implantation and the compartmental loading produced during physiological testing was considered. Within the rig development, a significant analysis of the differences in strain distribution caused by the implantation of a commonly used RTKR component compared to an intact composite tibia was performed. It was found that the addition of a revision knee component reduced the principal compressive strains throughout the proximal tibia whilst significantly increasing the distal strain at the stem tip. This is in line with reported strain shielding in the proximal tibia and end of stem pain due to a distal strain concentration. The analysis has also allowed the prediction of strain levels at the five tibial locations for any load applied to intact or implanted composite tibias. This could be used for future pre-clinical evaluation of tibial components, particularly to address the reported problems associated with their current design.

A combined loading rig was developed to address the limitation of traditional static knee loading rigs which do not include load transfer of the patellofemoral joint. The presence of a functioning patellofemoral joint also allowed simulation of greater knee flexion angles to measure the effect of increased flexion on the load transfer pattern in the tibia. Both experimental rigs found that an increase in flexion angle produced a decrease in compressive strain, particularly in the more distal tibia. If current implant testing is performed at 0°, this means that the strain distribution results will not be representative of those associated with flexion.

A study to assess the difference in load distribution through the tibia under applied loading from the tibiofemoral rig compared to the combined loading rig was performed. A comparison of the results between these two loading rigs indicated that the principal compressive strain in the tibia decreased with the inclusion of the patellofemoral joint, although the preliminary results were not statistically significant at the low flexion angle of 10°. The inclusion of both knee joints in the combined loading rig produced a similar strain pattern in the tibia as the results from the tibiofemoral rig. This adds further weight to the concept of proximal strain shielding and high strain in the distal stem tip region. The results strengthen the requirement for improved tibial component design which should try to reduce the proportion of load that is transferred straight through the stem tip. To avoid adverse bone remodelling, the physiological load through the knee should be evenly distributed through the tibia. This research enables prediction of strain levels at the locations tested for any load applied and there is the potential in the future to expand this for a range of flexion angles with any implant design. This will allow the assessment of RTKR components under more physiological conditions, improving understanding of the force pattern in the tibial regions surrounding the implant. The more realistic loading methodology developed will aid evaluation of component design features such as stem design, geometry, length, fixation type and the design of the junction between stem and tray.

12 Further Work

The research performed has generated ideas to expand the study and follow some additional areas of interest. Further measurement and analysis of the compressive strain magnitudes experienced during implantation would improve understanding of its effect on the tibia. No published studies have explored this area and it is considered very important to the entire revision surgery process.

An expansion of the RTKR components tested in this research would be useful to further assess the experimental test protocol. This covers many aspects of RTKR including the implantation and testing of alternative RTKR components to the Stryker Triathlon used here. It would also be interesting to assess the effect on strain distribution from using trabecular metal cones as their prevalence increases. The literature review suggests that bone loss has a significant impact on clinical decision making during RTKR surgery and is likely to alter strain distribution in the tibia. Levels of bone loss seen clinically were not replicated for this testing due to the need for reproducible specimens during the development of the testing protocol. Further work could assess how the compressive strain results are affected when taking bone loss replication into account. Based on the strain distribution results seen using the Stryker Triathlon implant as a guide for improvement, an important extension of the work would be to design and manufacture prototypes of the tibial components to address the strain shielding and strain concentrations. These could then be tested using the experimental protocol and the strain distribution results compared to evaluate any improvements in tibial component design.

The development of a FE model which replicates the tibiofemoral experimental rig has the potential to assess different implant designs and changes to the stem length, stem diameter and material for example. The experimental data from this research is currently being used in a follow up PhD study to validate a FE model with realistic loading, which will allow some computational studies to be employed to evaluate different stem designs.

The development of the combined loading rig will allow more physiological testing of revision tibial knee components, however further development of the rig could improve its range of testing. Some of these developments have already been made with the guidance of the author through an undergraduate research project to increase the allowable flexion angle of testing. Further to this, the design could be improved to reach higher flexion angles and therefore replicate a wider scope of activities. It will be interesting to be able to assess if the effect of the patellofemoral joint continues to increase with flexion as predicted in the discussion section.

This flexion testing may also allow extrapolation of results to predict the tibial load distribution at any angle of flexion. These results coupled with the existing linear equations from this research will allow estimation of the strain distribution at any load and flexion angle, therefore capable of reproducing any activity of daily living. A main limitation of the combined loading rig was that it was not capable of adjustment of the compartmental loading to ensure that the proportion was physiological. Further work should adapt the rig to allow such adjustment following the assertion that this research makes regarding the effect of compartmental load share on tibial strain distribution.

13 References

aap Implantate AG., 2011. Annual Report. Berlin.

Aglietti, P., Insall, J.N. & Cerulli, G., 1983. Patellar pain and ingongruence.1. Measurements of incongruence. Clinical Orthopaedics and Related Research, 176), pp. 217-224.

Al Nazer, R., Lanovaz, J., Kawalilak, C., Johnston, J.D. & Kontulainen, S., 2012. Direct in vivo strain measurements in human bone-A systematic literature review. J. Biomech., 45(1), pp. 27-40.

Albrektsson, B.E.J., Ryd, L., Carlsson, L.V., Freeman, M.A.R., Herberts, P., Regner, L. & Selvik, G., 1990. The effect of a stem on the tibial component of knee arthroplasty – a roentgen stereophotogrammetric study of uncemented tibial components in the freeman-samuelson knee arthroplasty. Journal of Bone and Joint Surgery-British Volume, 72(2), pp. 252-258.

Aquilant Orthopaedics., 2015. All Products [Online]. Basingstoke. Available: http://www.aquilantorthopaedics.com/products/products_by_all.asp?idSpecialism=70 [Accessed 22nd June 2015].

Au, A.G., Raso, V.J., Liggins, A.B. & Amirfazli, A., 2007. Contribution of loading conditions and material properties to stress shielding near the tibial component of total knee replacements. J. Biomech., 40(6), pp. 1410-1416.

Australian Orthopaedic Association., 2014. Revision Hip and Knee Arthroplasty Supplementary Report. National Joint Replacement Registry. Australia.

Barrack, R.L., Rorabeck, C., Burt, M. & Sawhney, J., 1999. Pain at the end of the stern after revision total knee arthroplasty. Clinical Orthopaedics and Related Research, 367), pp. 216-225.

Barrack, R.L., Stanley, T., Burt, M. & Hopkins, S., 2004. The effect of stem design on end-of-stem pain in revision total knee arthroplasty. The Journal of Arthroplasty, 19(7, Supplement 2), pp. 119-124.

Bartel, D.L., Burstein, A.H., Santavicca, E.A. & Insall, J.N., 1982. Performance of the tibial component in total knee replacement – conventional and revision designs. J. Bone Joint Surg.-Am. vol., 64(7), pp. 1026-1033.

Beckmann, J., Luring, C., Springorum, R., Kock, F.X., Grifka, J. & Tingart, M., 2011. Fixation of revision TKA: a review of the literature. Knee Surgery Sports Traumatology Arthroscopy, 19(6), pp. 872-879.

Bennett, J.E., Li, G., Foreman, K., Best, N., Kontis, V., Pearson, C., Hambly, P. & Ezzati, M., 2015. The future of life expectancy and life expectancy inequalities in England and Wales: Bayesian spatiotemporal forecasting. The Lancet.

Bergmann, G., Bender, A., Graichen, F., Dymke, J., Rohlmann, A., Trepczynski, A., Heller, M.O. & Kutzner, I., 2014. Standardized Loads Acting in Knee Implants. PLoS One, 9(1), p. 12.

Bertin, K.C., Freeman, M.A.R., Samuelson, K.M., Ratcliffe, S.S. & Todd, R.C., 1985. Stemmed revision arthroplasty for aseptic loosening of total knee replacment. Journal of Bone and Joint Surgery-British Volume, 67(2), pp. 242-248.

Biomet, 2015. Knees [Online]. Bridgend, Wales. Available: http://www.biomet.co.uk/medhome-uk/knee [Accessed 22nd June 2015].

Bono, J.V. & Scott, R.D., 2005. Revision Total Knee Arthroplasty. New York: Springer.

Bourne, R.B., Chesworth, B., Davis, A., Mahomed, N. & Charron, K., 2010. Comparing Patient Outcomes After THA and TKA Is There a Difference? Clinical Orthopaedics and Related Research, 468(2), pp. 542-546.

Bourne, R.B. & Finlay, J.B., 1986. The influence of tibial component intramedullary stems and implant cortex contact on the strain distribution of the proximal tibia following total knee arthroplasty – an in vitro study. Clinical Orthopaedics and Related Research, 208), pp. 95-99.

Britton, J.R. & Prendergast, P.J., 2005. Preclinical testing of femoral hip components: An experimental investigation with four prostheses. J. Biomech. Eng.-Trans. ASME, 127(5), pp. 872-880.

Brooks, P.J., Walker, P.S. & Scott, R.D., 1984. Tibial component fixation in deficient tibial bone stock. Clinical Orthopaedics and Related Research, 184), pp. 302-308.

Browne, C., Hermida, J.C., Bergula, A., Colwell, C.W. & D'Lima, D.D., 2005. Patellofemoral forces after total knee arthroplasty: effect of extensor moment arm. Knee, 12(2), pp. 81-88.

Bugbee, W.D., Ammeen, D.J. & Engh, G.A., 2001. Does implant selection affect outcome of revision knee arthroplasty? The Journal of Arthroplasty, 16(5), pp. 581-585.

Burns, A.W.R., Bourne, R.B., Chesworth, B.M., MacDonald, S.J. & Rorabeck, C.H., 2006. Cost effectiveness of revision total knee arthroplasty. Clinical Orthopaedics and Related Research, 446), pp. 29-33.

Burr, D.B., Milgrom, C., Fyhrie, D., Forwood, M., Nyska, M., Finestone, A., Hoshaw, S., Saiag, E. & Simkin, A., 1996. In vivo measurement of human tibial strains during vigorous activity. Bone, 18(5), pp. 405-410.

Chang, T.W., Yang, C.T., Liu, Y.L., Chen, W.C., Lin, K.J., Lai, Y.S., Huang, C.H., Lu, Y.C. & Cheng, C.K., 2011. Biomechanical evaluation of proximal tibial behavior following unicondylar knee arthroplasty: modified resected surface with corresponding surgical technique. Medical engineering & physics, 33(10), pp. 1175-82.

Chong, D.Y.R., Hansen, U.N., van der Venne, R., Verdonschot, N. & Amis, A.A., 2011. The influence of tibial component fixation techniques on resorption of supporting bone stock after total knee replacement. J. Biomech., 44(5), pp. 948-954.

Completo, A., Duarte, R., Fonseca, F., Simoes, J.A., Ramos, A. & Relvas, C., 2013. Biomechanical evaluation of different reconstructive techniques of proximal tibia in revision total knee arthroplasty: An in-vitro and finite element analysis. Clinical biomechanics, 28(3), pp. 291-298.

Completo, A., Fonseca, F. & Simões, J.A., 2008a. Strain shielding in proximal tibia of stemmed knee prosthesis: Experimental study. J. Biomech., 41(3), pp. 560-566.

Completo, A., Fonseca, F., Simões, J.A., Ramos, A. & Relvas, C., 2012. A new press-fit stem concept to reduce the risk of end-of-stem pain at revision TKA: A pre-clinical study. The Knee, 19(5), pp. 537-542.

Completo, A., Rego, A., Fonseca, F., Ramos, A., Relvas, C. & Simoes, J.A., 2010. Biomechanical evaluation of proximal tibia behaviour with the use of femoral stems in revision TKA: An in vitro and finite element analysis. Clinical biomechanics, 25(2), pp. 159-165.

Completo, A., Simões, J.A. & Fonseca, F., 2009. Revision total knee arthroplasty: The influence of femoral stems in load sharing and stability. The Knee, 16(4), pp. 275-279.

Completo, A., Simões, J.A., Fonseca, F. & Oliveira, M., 2008b. The influence of different tibial stem designs in load sharing and stability at the cement–bone interface in revision TKA. The Knee, 15(3), pp. 227-232.

Conditt, M.A., Parsley, B.S., Alexander, J.W., Doherty, S.D. & Noble, P.C., 2004. The optimal strategy for stable tibial fixation in revision total knee arthroplasty. J. Arthroplast., 19(7), pp. 113-118.

Cowin, S.C., 2001. Bone Mechanics Handbook. Second Edition. USA: CRC Press.

Cristofolini, L. & Viceconti, M., 2000. Mechanical validation of whole bone composite tibia models. J. Biomech., 33(3), pp. 279-288.

D'Lima, D.D., Patil, S., Steklov, N., Slamin, J.E. & Colwell, C.W., 2006. Tibial forces measured in vivo after total knee arthroplasty. J. Arthroplast., 21(2), pp. 255-262.

D'Lima, D.D., Townsend, C.P., Arms, S.W., Morris, B.A. & Colwell, C.W., 2005. An implantable telemetry device to measure intra-articular tibial forces. J. Biomech., 38(2), pp. 299-304.

de Beer, J. & Leone, J., 2005. Proximal tibial bone defects in total knee arthroplasty: Biomechanical assessment of tibial tray fixation. Journal of Bone & Joint Surgery, British Volume, 87-B(SUPP I), pp. 17-18.

Dennis, D.A., 2007. A Stepwise Approach to Revision Total Knee Arthroplasty. The Journal of Arthroplasty, 22(4), pp. 32-38.

DePuy Synthes Institute., 2014. Knee Revision Solutions: X-Ray Case Book. Indiana, USA.

Dorr, L.D., 2002. Revision total knee arthroplasty: An overview. Clinical Orthopaedics and Related Research, 404(pp. 143-144.

Eckhoff, D.G., Bach, J.M., Spitzer, V.M., Reinig, K.D., Bagur, M.M., Baldini, T.H., Rubinstein, D. & Humphries, S., 2003. Three-dimensional morphology and kinematics of the distal part of the femur viewed in virtual reality - Part II. J. Bone Joint Surg.-Am. vol., 85A(pp. 97-104.

Fehring, T.K., Odum, S., Olekson, C., Griffin, W.L., Mason, J.B. & McCoy, T.H., 2003. Stem fixation in revision total knee arthroplasty - A comparative analysis. Clinical Orthopaedics and Related Research, 416), pp. 217-224.

Finlay, J.B., Bourne, R.B. & McLean, J., 1982. A technique for the in vitro measurement of principal strain in the human tibia. J. Biomech., 15(10), pp. 723-739.

Freeman, M.A.R., 2001. How the knee moves. Curr. Orthop., 15(6), pp. 444-450.

Frost, H.M., 1991. A new direction for osteoporosis research – a review and proposal. Bone, 12(6), pp. 429-437.

Fuchs-Winkelmann, S., El-Zayat, B., Heyse, T.J., Fanciullacci, N., Chevalier, Y. & Innocenti, B., 2012. Numerical Analysis of stem length and fixation technique in a hinged TKA. Orthopaedic Research Society. California.

Gofton, W.T., Tsigaras, H., Butler, R.A., Patterson, J.J., Barrack, R.L. & Rorabeck, C.H., 2002. Revision total knee arthroplasty - Fixation with modular stems. Clinical Orthopaedics and Related Research, 404), pp. 158-168.

Gray, H.A., Taddei, F., Zavatsky, A.B., Cristofolini, L. & Gill, H.S., 2008. Experimental validation of a finite element model of a human cadaveric tibia. J. Biomech. Eng.-Trans. ASME, 130(3), p. 9.

Green, G.V., Berend, K.R., Berend, M.E., Glisson, R.R. & Vail, T.P., 2002. The effects of varus tibial alignment on proximal tibial surface strain in total knee arthroplasty - The posteromedial hot spot. J. Arthroplast., 17(8), pp. 1033-1039.

Haas, S.B., Insall, J.N., Montgomery, W. & Windsor, R.E., 1995. Revision total knee arthroplasty with use of modular components with stems inserted without cement. J. Bone Joint Surg.-Am. vol., 77A(11), pp. 1700-1707.

Haidukewych, G.J. & Service, B., 2012. Contemporary Bone Loss Management Options for Revision Total Knee Arthroplasty. Seminars in Arthroplasty, 23(1), pp. 39-41.

Heiner, A.D., 2008. Structural properties of fourth-generation composite femurs and tibias. J. Biomech., 41(15), pp. 3282-3284.

Heyligers, I.C., van Haaren, E.H. & Wuisman, P., 2001. Revision knee arthroplasty using impaction grafting and primary implants. J. Arthroplast., 16(4), pp. 533-537.

Hollister, A.M., Jatana, S., Singh, A.K., Sullivan, W.W. & Lupichuk, A.G., 1993. The axes of rotation of the knee. Clinical Orthopaedics and Related Research, 290), pp. 259-268.

Huiskes, R., Weinans, H., Grootenboer, H.J., Dalstra, M., Fudala, B. & Slooff, T.J., 1987. Adaptive bone-remodeling theory applied to prosthetic-design analysis. J. Biomech., 20(11–12), pp. 1135-1150.

Jazrawi, L.M., Bai, B., Kummer, F.J., Hiebert, R. & Stuchin, S.A., 2001. The effect of stem modularity and mode of fixation on tibial component stability in revision total knee arthroplasty. J. Arthroplast., 16(6), pp. 759-767.

Jensen, C., Petersen, M., Schrøder, H. & Lund, B., 2012. Bone mineral density changes of the proximal tibia after revision total knee arthroplasty. A randomised study with the use of porous tantalum metaphyseal cones. International orthopaedics, 36(9), pp. 1857-1863.

Jonkers, I., Sauwen, N., Lenaerts, G., Mulier, M., Van der Perre, G. & Jaecques, S., 2008. Relation between subject-specific hip joint loading, stress distribution in the proximal femur and bone mineral density changes after total hip replacement. J. Biomech., 41(16), pp. 3405-3413.

Kaufman, K.R., Kovacevic, N., Irby, S.E. & Colwell, C.W., 1996. Instrumented implant for measuring tibiofemoral forces. J. Biomech., 29(5), pp. 667-671.

Kessler, O., Lacatusu, E., Sommers, M.B., Mayr, E. & Bottlang, M., 2006. Malrotation in total knee arthroplasty: effect on tibial cortex strain captured by laser-based strain acquisition. Clinical biomechanics, 21(6), pp. 603-609.

Kimpton, C.I., Crocombe, A.D., Bradley, W.N. & Gavin Huw Owen, B., Analysis of Stem Tip Pain in Revision Total Knee Arthroplasty. The Journal of Arthroplasty.

Kurtz, S., Ong, K., Lau, E., Mowat, F. & Halpern, M., 2007. Projections of primary and revision hip and knee arthroplasty in the United States from 2005 to 2030. J. Bone Joint Surg.-Am. vol., 89A(4), pp. 780-785.

Kurtz, S.M., Ong, K.L., Lau, E., Widmer, M., Maravic, M., Gomez-Barrena, E., de Pina Mde, F., Manno, V., Torre, M., Walter, W.L., de Steiger, R., Geesink, R.G., Peltola, M. & Roder, C., 2011. International survey of primary and revision total knee replacement. International orthopaedics, 35(12), pp. 1783-9.

Kurtz, S.M., Ong, K.L., Lau, E., & Bozic, K. J., 2014. Impact of the Economic Downturn on Total Joint Replacement Demand in the United States. J. Bone Joint Surg.-Am. vol., 96(8), pp. 624-630.

Kuster, M.S., Wood, G.A., Stachowiak, G.W. & Gachter, A., 1997. Joint load considerations in total knee replacement. Journal of Bone and Joint Surgery-British Volume, 79B(1), pp. 109-113.

Kutzner, I., Heinlein, B., Graichen, F., Bender, A., Rohlmann, A., Halder, A., Beier, A. & Bergmann, G., 2010. Loading of the knee joint during activities of daily living measured in vivo in five subjects. J. Biomech., 43(11), pp. 2164-2173.

Labey, L., Vander Sloten, J., Van Audekercke, R. & Van der Perre, G., 2000. Bone strains and anterior lift-off, measured with three alternative designs of tibial components of TKA. J. Mater. Sci.-Mater. Med., 11(7), pp. 443-448.

Lanyon, L.E., Hampson, W.G.J., Goodship, A.E. & Shah, J.S., 1975. Bone deformation recorded in vivo from strain gauges attached to human tibial shaft. Acta Orthopaedica Scandinavica, 46(2), pp. 256-268.

Lee, R.W., Volz, R.G. & Sheridan, D.C., 1991. The role of fixation and bone quality on the mechanical stability of tibial knee components. Clinical Orthopaedics and Related Research, 273), pp. 177-183.

Levitz, C.L., Lotke, P.A. & Karp, J.S., 1995. Long-term changes in bone-mineral density following total knee replacement. Clinical Orthopaedics and Related Research, 321), pp. 68-72.

Lonner, J.H., Lotke, P.A., Kim, J. & Nelson, C., 2002. Impaction grafting and wire mesh for uncontained defects in revision knee arthroplasty. Clinical Orthopaedics and Related Research, 404), pp. 145-151.

Love, A.E.H., 2013. A Treatise on the Mathematical Theory of Elasticity. Cambridge University Press.

Lundberg, H.J., Foucher, K.C., Andriacchi, T.P. & Wimmer, M.A., 2012. Direct comparison of measured and calculated total knee replacement force envelopes during walking in the presence of normal and abnormal gait patterns. J. Biomech., 45(6), pp. 990-996.

Mabry, T.M. & Hanssen, A.D., 2007. The Role of Stems and Augments for Bone Loss in Revision Knee Arthroplasty. The Journal of Arthroplasty, 22(4, Supplement), pp. 56-60.

Mabry, T.M., Vessely, M.B., Schleck, C.D., Harmsen, W.S. & Berry, D.J., 2007. Revision Total Knee Arthroplasty With Modular Cemented Stems: Long-Term Follow-Up. The Journal of Arthroplasty, 22(6, Supplement), pp. 100-105.

Malinzak, R.A., Small, S.R., Rogge, R.D., Archer, D.B., Oja, J.W., Berend, M.E. & Ritter, M.A., 2014. The Effect of Rotating Platform TKA on Strain Distribution and Torque Transmission on the Proximal Tibia. J. Arthroplast., 29(3), pp. 541-547.

Mann, K.A., 2014. Peri-implant bone strains and micro-motion following in vivo service : A postmortem retrieval study of 22 tibial components from total knee replacements. Journal of Orthopaedic Research, 32(3), pp. 355-361.

Manopoulos, P., Havet, E., Pearce, O., Lardanchet, J.F. & Mertl, P., 2012. Mid- to long-term results of revision total knee replacement using press-fit intramedullary stems with cemented femoral and tibial components. Journal of Bone and Joint Surgery-British Volume, 94B(7), pp. 937-940.

Maradit-Kremers, H., Crowson, C.S., L., R.D., Jiranek, W.A. & Berry, D.J., 2014. Prevalence of Total Hip (THA) and Total Knee (TKA) Arthroplasty in the United States. AAOS Annual Meeting.

Meireles, S., Completo, A., Simoes, J.A. & Flores, P., 2010. Strain shielding in distal femur after patellofemoral arthroplasty under different activity conditions. J. Biomech., 43(3), pp. 477-484.

Microport Orthopaedics., 2015. Knees: ADVANCE® Stemmed Medial-Pivot [Online]. Tennessee, USA. Available: http://www.ortho.microport.com/Physicians/products/knees/ADVANCEStemmedMedialPivotandRevisionKneeSystem.asp [Accessed 22nd June 2015].

Milgrom, C., Finestone, A., Simkin, A., Ekenman, I., Mendelson, S., Millgram, M., Nyska, M., Larsson, E. & Burr, D., 2000. In vivo strain measurements to evaluate the strengthening potential of exercises on the tibial bone. Journal of Bone and Joint Surgery-British Volume, 82B(4), pp. 591-594.

Mizuno, Y., Kumagai, M., Mattessich, S.M., Elias, J.J., Ramrattan, N., Cosgarea, A.J. & Chao, E.Y.S., 2001. Q-angle influences tibiofemoral and patellofemoral kinematics. Journal of Orthopaedic Research, 19(5), pp. 834-840.

Moreland, J.R., Bassett, L.W. & Hanker, G.J., 1987. Radiographic analysis of the axial alignment of the lower-extremity. J. Bone Joint Surg.-Am. vol., 69A(5), pp. 745-749.

Morrison, J.B., 1970. The Mechanics of the knee joint in relation to normal walking. J. Biomech., 3(1), pp. 51.

Mundermann, A., Dyrby, C.O., D'Lima, D.D., Colwell, C.W. & Andriacchi, T.P., 2008. In vivo knee loading characteristics during activities of daily living as measured by an instrumented total knee replacement. Journal of Orthopaedic Research, 26(9), pp. 1167-1172.

Murray, P.B., Rand, J.A. & Hanssen, A.D., 1994. Cemented long-stem revision total knee arthroplasty. Clin Orthop Relat Res., 309), pp. 116-123.

Nagamine, R., Miura, H., Inoue, Y., Urabe, K., Matsuda, S., Okamoto, Y., Nishizawa, M. & Iwamoto, Y., 1998. Reliability of the anteroposterior axis and the posterior condylar axis for determining rotational alignment of the femoral component in total knee arthroplasty. J Orthop Sci, 3(4), pp. 194-198.

National Joint Registry for England, W.a.N.I., 2009. Prostheses used in hip and knee replacement procedures 2008.

National Joint Registry for England, W.a.N.I., 2010. Prostheses used in hip and knee replacement procedures 2009.

National Joint Registry for England, W.a.N.I., 2011. Prostheses used in hip, knee and ankle replacement procedures 2010.

National Joint Registry for England, W.a.N.I., 2012. Prostheses used in hip, knee and ankle replacement procedures 2011.

National Joint Registry for England, W.a.N.I., 2013a. 10th Annual Report 2013.

National Joint Registry for England, W.a.N.I., 2013b. Prostheses used in hip, knee, ankle, elbow and shoulder replacement procedures 2012.

National Joint Registry for England, W.a.N.I., 2014a. 11th Annual Report 2014.

National Joint Registry for England, W.a.N.I., 2014b. Prostheses used in hip, knee, ankle, elbow and shoulder replacement procedures 2013.

Nazarian, D.G., Mehta, S. & Booth, R.E., 2002. A comparison of stemmed and unstemmed components in revision knee arthroplasty. Clinical Orthopaedics and Related Research, 404, pp. 256-262.

Nelson, C.L., Gioe, T.J., Cheng, E.Y. & Thompson, R.C., 2003a. Implant selection in revision total knee arthroplasty. J. Bone Joint Surg. Am. vol., 85A, pp. 43-51.

Nelson, C.L., Lonner, J.H., Rand, J.A. & Lotke, P.A., 2003b. Strategies of stem fixation and the role of supplemental bonegraft in revision total knee arthroplasty. J. Bone Joint Surg. Am. vol., 85A, pp. 52-57.

Noble, P.C., Conditt, M.A., Cook, K.F. & Mathis, K.B., 2006. The John Insall Award - Patient expectations affect satisfaction with total knee arthroplasty. Clinical Orthopaedics and Related Research, 452, pp. 35-43.

Nordin, M. & Frankel, V.H., 2001. Basic Biomechanics of the Musculoskeletal System. Lippincott Williams & Wilkins.

Office for National Statistics., 2015. Theme: Population [Online]. Available: http://ons.gov.uk/ons/taxonomy/index.html?nscl=Population [Accessed 19th September 2015].

Ostermeier, S. & Stukenborg-Colsman, C., 2011. Quadriceps force after TKA with femoral single radius. Acta orthopaedica, 82(3), pp. 339-343.

Palastanga, N., Field, D. & Soames, R.W., 2002. Anatomy and Human Movement: Structure and Function. Oxford: Butterworth-Heinemann.

Parsley, B.S., Sugano, N., Bertolusso, R. & Conditt, M.A., 2003. Mechanical alignment of tibial stems in revision total knee arthroplasty. The Journal of Arthroplasty, 18, Supplement(0), pp. 33-36.

Pegg, E.C., Walter, J., Mellon, S.J., Pandit, H.G., Murray, D.W., D'Lima, D.D., Fregly, B.J. & Gill, H.S., 2013. Evaluation of factors affecting tibial bone strain after unicompartmental knee replacement. Journal of Orthopaedic Research, 31(5), pp. 821-828.

Peters, C.L., Erickson, J., Kloepper, R.G. & Mohr, R.A., 2005. Revision total knee arthroplasty with modular components inserted with metaphyseal cement and stems without cement. J. Arthroplast., 20(3), pp. 302-308.

Politis, A.N., Siogkas, G.K., Gelalis, I.D. & Xenakis, T.A., 2013. Patterns of stress distribution at the proximal femur after implantation of a modular neck prosthesis. A biomechanical study. Clinical biomechanics, 28(4), pp. 415-422.

Putzer, D., Mayr, E., Haid, C., Reinthaler, A. & Nogler, M., 2011. Impaction bone grafting A laboratory comparison of two methods. Journal of Bone and Joint Surgery-British Volume, 93B(8), pp. 1049-1053.

Radnay, C.S. & Scuderi, G.R., 2006. Management of bone loss - Augments, cones, offset stems. Clinical Orthopaedics and Related Research, 446), pp. 83-92.

Rastetter, B.R., 2014. Development of a finite element model for the tibial component of revision total knee replacement. Thesis (MSc). University of Bath, Bath.

Rath, E. & Richmond, J.C., 2000. The menisci: basic science and advances in treatment. Br. J. Sports Med., 34(4), pp. 252-257.

Rawlinson, J.J., Peters, L.E., Campbell, D.A., Windsor, R., Wright, T.M. & Bartel, D.L., 2005. Cancellous bone strains indicate efficacy of stem augmentation in constrained condylar knees. Clinical Orthopaedics and Related Research, 440), pp. 107-116.

Reilly, D., Walker, P.S., Bendov, M. & Ewald, F.C., 1982. Effects of tibial components on load-transfer in the upper tibia. Clinical Orthopaedics and Related Research, 165), pp. 273-282.

Sadoghi, P., Liebensteiner, M., Agreiter, M., Leithner, A., Böhler, N. & Labek, G., Revision Surgery After Total Joint Arthroplasty: A Complication-Based Analysis Using Worldwide Arthroplasty Registers. The Journal of Arthroplasty.

Sah, A.P., Shukla, S., Della Valle, C.J., Rosenberg, A.G. & Paprosky, W.G., 2011. Modified Hybrid Stem Fixation in Revision TKA is Durable at 2 to 10 Years. Clinical Orthopaedics and Related Research, 469(3), pp. 839-846.

Sawbones Europe AB., 2015. Sawbones Biomechanical Test Materials Catalogue. Sweden.

Schindler, O.S., 2012. Basic kinematics and biomechanics of the patellofemoral joint Part 2: The patella in total knee arthroplasty. Acta Orthop. Belg., 78(1), pp. 11-29.

Schindler, O.S. & Scott, W.N., 2011. Basic kinematics and biomechanics of the patello-femoral joint Part 1: The native patella. Acta Orthop. Belg., 77(4), pp. 421-431.

Scott, C.E.H. & Biant, L.C., 2012. The role of the design of tibial components and stems in knee replacement. Journal of Bone & Joint Surgery, British Volume, 94-B(8), pp. 1009-1015.

Scott, C.E.H., Eaton, M.J., Nutton, R.W., Wade, F.A., Pankaj, P. & Evans, S.L., 2013. Proximal tibial strain in medial unicompartmental knee replacements - A biomechanical study of implant design. Bone Joint J., 95B(10), pp. 1339-1347.

Sculco, T.P. & Choi, J.C., 1998. The role and results of bone grafting in revision total knee replacement. Orthopedic Clinics of North America, 29(2), pp. 339.

Shannon, B.D., Klassen, J.F., Rand, J.A., Berry, D.J. & Trousdale, R.T., 2003. Revision total knee arthroplasty with cemented components and uncemented intramedullary stems. The Journal of Arthroplasty, 18, Supplement(0), pp. 27-32.

Shiers, L.G.P., 1954. Arthroplasty of the knee - preliminary report of a new method. Journal of Bone and Joint Surgery-British Volume, 36(4), pp. 553-560.

Smith and Nephew PLC., 2014. Orthopaedic Reconstruction [Online]. London. Available: http://www.smith-nephew.com/uk/products/orthopaedic-reconstruction/ [Accessed 22nd June 2015].

Stambough, J.B., Clohisy, J.C., Barrack, R.L., Nunley, R.M. & Keeney, J.A., 2014. Increased risk of failure following revision total knee replacement in patients aged 55 years and younger. Bone Joint J., 96B(12), pp. 1657-1662.

Stanmore Implants Worldwide., 2015. METS Modular Implant System [Online]. Elstree, UK. Available: http://www.stanmoreimplants.com/mets-modular-system.php [Accessed 22nd June 2015].

Steens, W., Loehr, J.F., Wodtke, J. & Katzer, A., 2008. Morselized bone grafting in revision arthroplasty of the knee: a retrospective analysis of 34 reconstructions after 2-9 years. Acta orthopaedica, 79(5), pp. 683-688.

Stolk, J., Verdonschot, N. & Huiskes, R., 2001. Hip-joint and abductor-muscle forces adequately represent in vivo loading of a cemented total hip reconstruction. J. Biomech., 34(7), pp. 917-926.

Stryker Orthopaedics., 2015. Orthopaedic Products [Online]. New Jersey, USA. Available: http://www.stryker.com/en-us/products/Orthopaedics/index.htm [Accessed 22nd June 2015].

Sugru., 2015. What is Sugru? [Online]. London, UK. Available: https://sugru.com/about [Accessed 19th September 2015].

Sztefek, P., Vanleene, M., Olsson, R., Collinson, R., Pitsillides, A.A. & Shefelbine, S., 2010. Using digital image correlation to determine bone surface strains during loading and after adaptation of the mouse tibia. J. Biomech., 43(4), pp. 599-605.

Tang, Q., Zhou, Y., Yang, D., Xu, H. & Liu, Q., 2010. The Offset of the Tibial Shaft from the Tibial Plateau in Chinese People. J. Bone Joint Surg.-Am. vol., 92A(10), pp. 1981-1987.

Taylor, J.R., 1997. An Introduction to Error Analysis: The Study of Uncertainties in Physical Measurements. University Science Books.

Taylor, W.R., Heller, M.O., Bergmann, G. & Duda, G.N., 2004. Tibio-femoral loading during human gait and stair climbing. Journal of Orthopaedic Research, 22(3), pp. 625-632.

The Engineering Toolbox., 2015. Tensile Modulus - Modulus of Elasticity or Young's Modulus - for some common Materials [Online]. Available: http://www.engineeringtoolbox.com/young-modulus-d_417.html [Accessed 19th September 2015].

The Health and Social Care Information Centre., 2010. Provisional Monthly Patient Reported Outcome Measures (PROMs) in England. April 2009 – April 2010: Pre- and postoperative data: Experimental statistics.

Thomas, R., 2015. Biomechanics of the Knee Joint. Thesis (MEng). University of Bath, Bath.

Thongtrangan, I., Yoon, P. & Saleh, K.J., 2003. Bone reconstruction in revision total knee arthroplasty. Seminars in Arthroplasty, 14(3), pp. 152-158.

Toms, A.D., Barker, R.L., Jones, R.S. & Kuiper, J.H., 2004. Current concepts review - Impaction bone-grafting in revision joint replacement surgery. J. Bone Joint Surg.-Am. vol., 86A(9), pp. 2050-2060.

United States Census Bureau., 2015. US and World Population Clock [Online]. Washington DC, USA. Available: http://www.census.gov/popclock/ [Accessed 19th September 2015].

van Loon, C.J.M., Buma, P., Maleijt, M., van Kampen, A. & Veth, R.P.H., 2000. Morsellized bone allografting in revision total knee replacement - a case report with a 4-year histological follow-up. Acta Orthopaedica Scandinavica, 71(1), pp. 98-101.

Waide, V., Cristofolini, L., Stolk, J., Verdonschot, N. & Toni, A., 2003. Experimental investigation of bone remodelling using composite femurs. Clinical biomechanics, 18(6), pp. 523-536.

Weber, W.E. & Weber, E., 1992. Mechanics of the Human Walking Apparatus. Springer-Verlag.

Whaley, A.L., Trousdale, R.T., Rand, J.A. & Hanssen, A.D., 2003. Cemented long-stem revision total knee arthroplasty. The Journal of Arthroplasty, 18(5), pp. 592-599.

Whittaker, J.P., Dharmarajan, R. & Toms, A.D., 2008. The management of bone loss in revision total knee replacement. Journal of Bone and Joint Surgery-British Volume, 90B(8), pp. 981-987.

Zhao, D., Banks, S.A., D'Lima, D.D., Colwell, C.W. & Fregly, B.J., 2007. In vivo medial and lateral tibial loads during dynamic and high flexion activities. Journal of Orthopaedic Research, 25(5), pp. 593-602.

Zimmer, 2014. Knee Replacement Products [Online]. Indiana, USA. Available: http://www.zimmer.co.uk/medical-professionals/products/knee.html [Accessed 22nd June 2015].

Appendix A - Stem Manufacture

It was important to ensure that the final testing with original Stryker Triathlon tibial trays and in-house manufactured stems was an adequate reflection of what would have been seen with full original tibial component assemblies. The material selected to use for the manufactured stems was stainless steel 316 (200 GPa), as this had a similar Young's modulus to the medical grade cobalt chrome used in the original stem (220 GPa). The manufactured stems were created as replicas of the original stem using precision engineering. The five manufactured and single original stem was then weighed. The mass of each stem is displayed in Table 13, showing minimal differences in the material used between the manufactured stems and the original stem. This alludes to the precision of manufacture and it is likely that the greater mass of the original stem is due to the slightly higher density of the material.

Stem	Mass (g)
Stryker - Original	85.4
Manufactured 1	82.9
Manufactured 2	83.2
Manufactured 3	83.3
Manufactured 4	82.1
Manufactured 5	83.0

Table 13 - Mass of original and manufactured stems taken before implantation into the composite bone

Appendix B – Meniscus Compression Tests

An investigation to select the most appropriate meniscus substitute from two sample options was performed. This compared the mechanical properties of 70 Durometer and 80 Durometer Sorbothane to the natural meniscus. Compression tests were performed using an Instron test machine (Instron 5965, Buckinghamshire, UK) and a test method set up on the BlueHill 3.0 materials testing software. The parameters used are summarised in Table 14.

Test Type	Test		End of Test
	Control Mode	Displacement Rate	Load Limit
Compression	Extension Ramp	0.5 mm/min	500 N

Table 14 - Compression test parameters used during the Sorbothane materials testing

The 70 Durometer Sorbothane sample, 56.5 mm in diameter, was placed on the test bed and loaded four times, followed by the 80 Durometer tests with 4 repeats. The samples were then given 15 minutes to rest and the test procedure was repeated so that a total of 16 tests were performed on two samples. All output results were recorded and saved for manipulation. The output results from the compression testing produced values for the load applied and extension of the samples in response to such load. These values could be converted into stress-strain values as the cross sectional area and original length of the specimens were known constants. All materials produced a similar response to load with a linear elastic section, as shown in the graphs of Figure 83 and Figure 84.

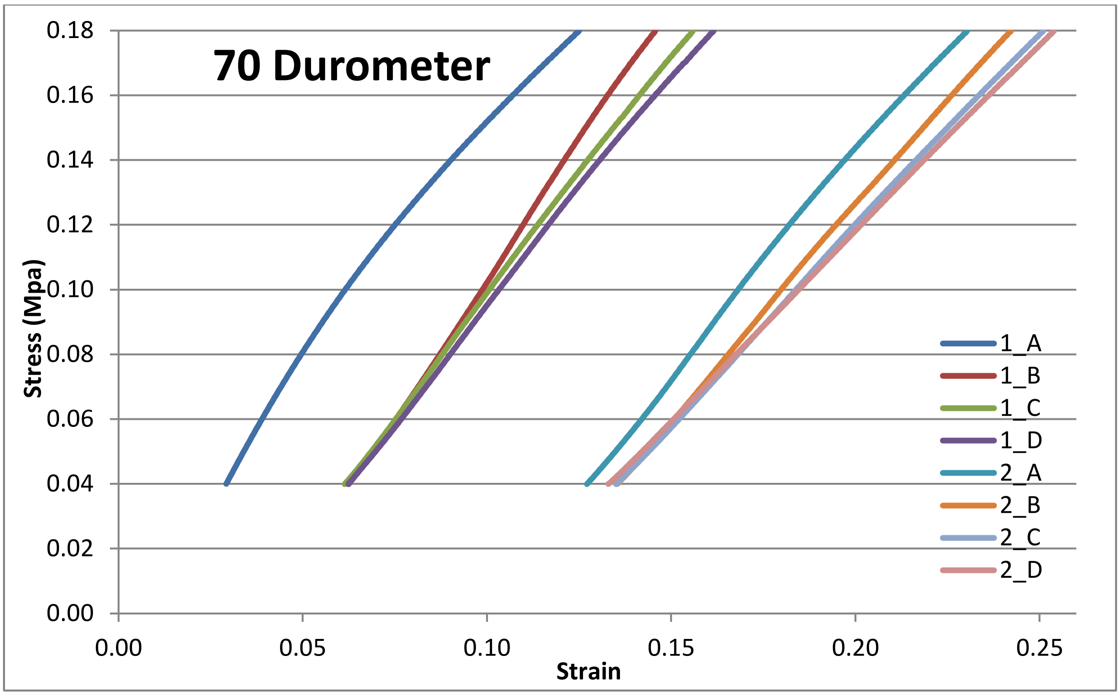

Figure 83 - A graph to display the linear elastic portion of the results of the compression testing of the 70 Durometer Sorbothane across all eight tests performed. Group 1 consecutive testing was followed by a 15 minute pause and then Group 2 consecutive testing.

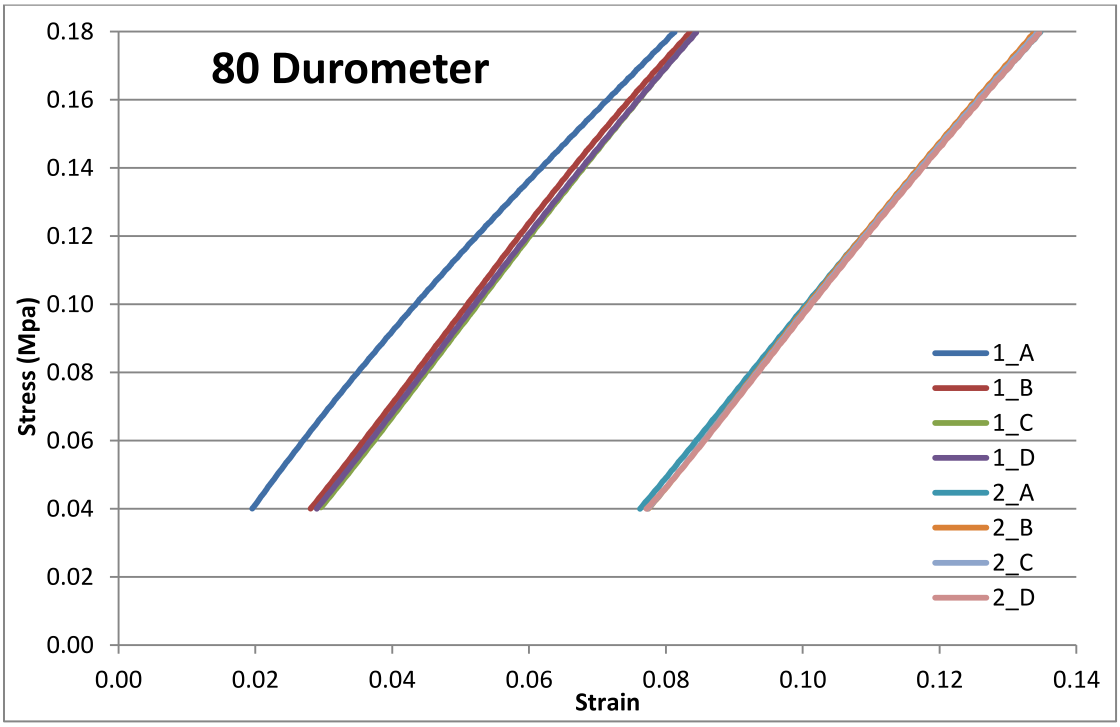

Figure 84 - A graph to display the linear elastic portion of the results of the compression testing of the 80 Durometer Sorbothane across all eight tests performed. Group 1 consecutive testing was followed by a 15 minute pause and then Group 2 consecutive testing.

The LINEST function in Excel was used to estimate the gradient of each line which corresponded to the Young's modulus for the specimens. These are summarised in Table 15.

70 Durometer		80 Durometer	
Test	Young's Modulus (MPa)	Test	Young's Modulus (MPa)
1_A	1.43	1_A	2.24
1_B	1.73	1_B	2.56
1_C	1.50	1_C	2.58
1_D	1.44	1_D	2.55
2_A	1.39	2_A	2.40
2_B	1.32	2_B	2.50
2_C	1.22	2_C	2.48
2_D	1.17	2_D	2.47
Average	**1.40**	**Average**	**2.47**

Table 15 – The Young's modulus of the two varieties of Sorbothane, calculated from the results of the compression testing and averaged across all samples

Overall the modulus of the 70 Durometer Sorbothane was an average of 1.40 MPa and the 80 Durometer Sorbothane a 2.47 MPa average. Scott et al. 2013 state that the Young's modulus of cartilage lies between 0.31 to 1.13 MPa. It was therefore decided that the 70 Durometer Sorbothane was the most appropriate to use as a substitute meniscus in this research.

Appendix C – BORS Poster

The Effect of Altering the Medial to Lateral Load Transfer Through the Knee Joint in TKA

SJ Wright, S Gheduzzi, AW Miles

Department of Mechanical Engineering, University of Bath, UK

centre for orthopaedic biomechanics

Introduction

The use of instrumented tibial components in Total Knee Arthroplasty (TKA) has demonstrated that the compartmental load share across the tibial condyles changes during daily living activities [1]. Compartmental load share is rarely measured directly in experimental studies that assess load transfer through the tibia. No reported experimental studies have assessed how the compartmental load share may affect the load distribution through the tibia after TKA. Pre-clinical assessments should strive towards replicating compartmental loading conditions if they are found to affect loading through the tibia.

The aim of this study was to develop a method to measure the compartmental load share across the tibial condyles of a TKA *in vitro*. The investigation employed force sensors to measure compartmental load and strain gauges to provide the cortical strains in a composite tibia as an indication of load transfer through the bone. This method will be used in future studies to investigate the effect of varying the compartmental loading on the strain levels through the tibia.

Methods

- Two force sensors were selected (Flexiforce A201, Tekscan) to measure force through each tibial condyle. These were conditioned to 110% of their maximum load five times as recommended by the manufacturer and then calibrated.
- A performance evaluation of the sensors was conducted using a range of surface geometries including TKA components. An axial load was applied in 50 N increments to a maximum of 400 N and results were recorded for three test repeats.
- A test rig was developed to allow the adjustment of the medial and lateral load share in the tibial condyles by altering the ab/adduction of the femoral loading component (Figure 1).

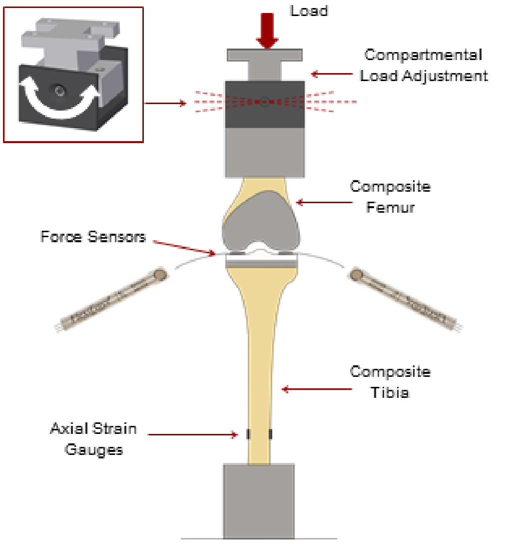

Figure 1: The test rig capable of adjustment of the ad/abduction of the femoral component and application of load to the tibial condyles.

- A composite tibia and femur (4th Generation, Sawbones, #3401 and #3403) was prepared and implanted with Stryker Universal Triathlon components (Size 4, 100 mm Tibial Stem Length) according to surgical protocol.
- Two strain gauges were bonded on the medial and lateral side of the distal tibia to measure cortical strain (Vishay: J2A-13-S109M-350).
- The femur and tibia were positioned relative to each other using an alignment jig. The force sensors were placed in the condyles between TKA components and used to set the compartmental load share to 40:60% (Medial:Lateral).
- The medial and lateral compartmental forces and cortical strains were recorded under a 400 N load applied by a hydraulic test machine.

Results

The force sensor performance testing recorded a mean combined load of 422.3 N with a standard deviation of 5.8 N (1.4%) when the applied load was 400 N. This average force equates to a 5.6% error from the sensor.

The results from the preliminary testing into the effect on tibial load transfer are summarised in Figure 2. When the load share measured by the force sensors was 40:60% (Medial:Lateral), the strain measured in the distal tibia was found to have similar proportions between the medial and lateral sides (70 and 100 microstrain).

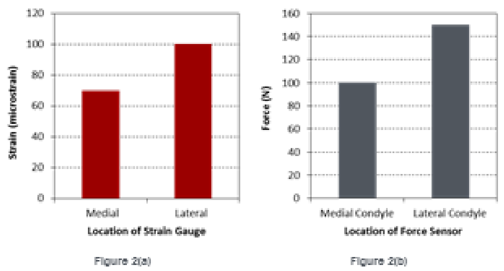

Figure 2: Illustrating the medial and lateral strain measured at the distal end of the composite tibia (a) when subjected to measured force through the knee joint (b)

Conclusions

The force sensor evaluation results show that it is possible to use force sensors to precisely (1.4% SD) and accurately (5.6% error) measure the load share across the tibial condyles in a composite tibia implanted with TKA components.

The initial study to gauge what effect this share has on the load transferred distally through the tibia highlighted how closely related these factors are with the 40:60% compartmental load share transferring to the distal tibia.

The study demonstrates that it is possible to measure the medial to lateral compartmental load share through the knee joint. It indicates that this spread of load may have an effect on the strain distribution in the tibia. All future testing should account for this due to its affect on tibial load distribution and its potential clinical significance in TKA.

References:

1. Mundermann, A., et al. In vivo knee loading characteristics during activities of daily living as measured by an instrumented total knee replacement. J Orthop Res., 2008. 26(9): 1167-72.

Corresponding Author: S.J.Wright@bath.ac.uk

UNIVERSITY OF BATH

Figure 85 – British Orthopaedic Research Society (BORS) Poster presenting the preliminary study using the novel compartmental load assembly and the effect of adjusting the load on the strain distribution

Appendix D – Combined Loading Rig

The final detailed assembly drawings of the combined loading rig are shown below.

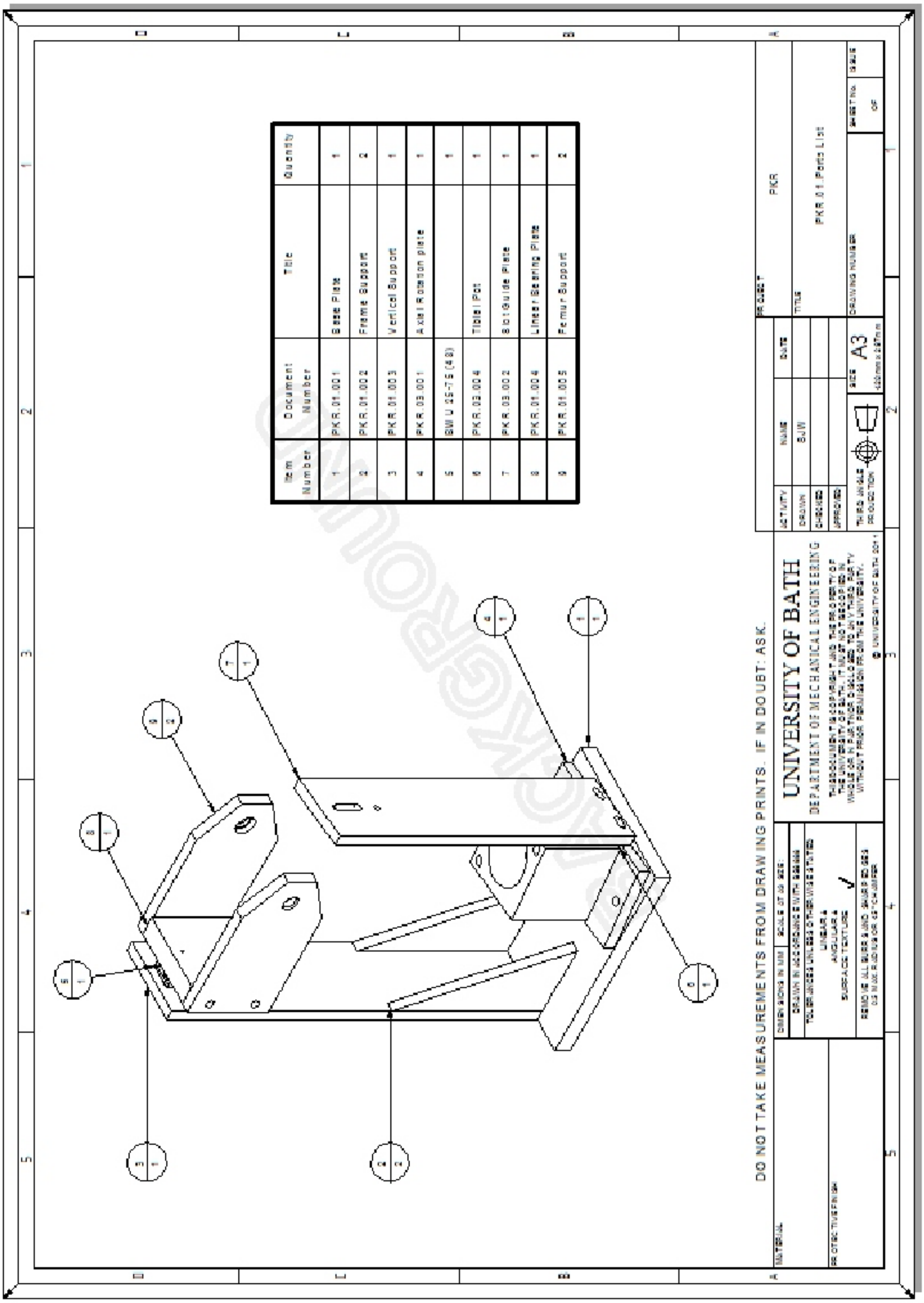

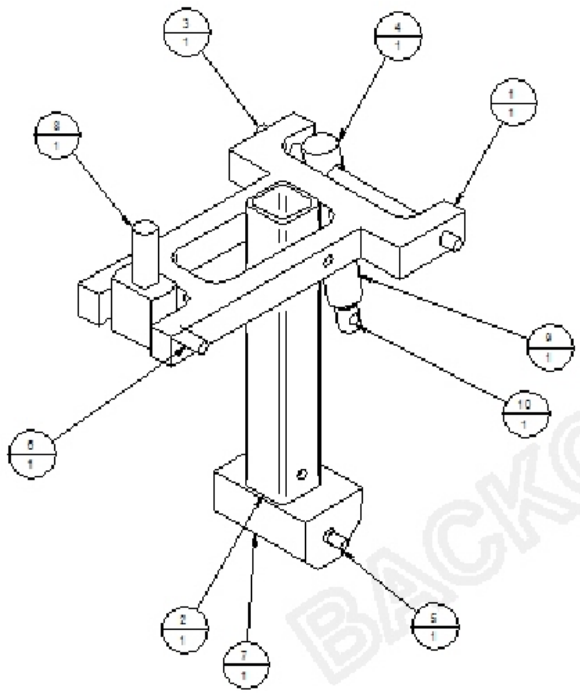

Item Number	Document Number	Title	Quantity
1	PKR.02.001	Lever Arm	1
2	PKR.02.003	Femur Link	1
3	PKR.02.010	Quad Shaft	1
4	PKR.02.004	Q-Angle Adapter	1
5	PKR.02.008	Femur Mount Shaft	1
6	PKR.02.009	Zick Adapter Shaft	1
7	PKR.02.007	Femur Mount	1
8	PKR.02.002	Zwick Adapter	1
9	PKR.02.005	Turnbuckle Body	1
10	PKR.02.006	Turnbuckle Distal Adapter	1

DO NOT TAKE MEASUREMENTS FROM DRAWING PRINTS. IF IN DOUBT: ASK.

MATERIAL

PROTECTIVE FINISH

DIMENSIONS IN MM | SCALE 1:1 | SIZE

DRAWN IN ACCORDANCE WITH BS8888

TOLERANCES UNLESS OTHERWISE STATED

LINEAR ±
ANGULAR ±
SURFACE TEXTURE ✓

REMOVE ALL BURRS AND SHARP EDGES
0.5 MAX. RADIUS OR 45° CHAMFER

UNIVERSITY OF BATH
DEPARTMENT OF MECHANICAL ENGINEERING

ACTIVITY	NAME	DATE
DRAWN	SJW	
CHECKED		
APPROVED		

THIRD ANGLE PROJECTION

SIZE A3
420mm x 297mm

PROJECT
PKR

TITLE
PKR.02 Parts List

DRAWING NUMBER

SHEET No. OF

ISSUE

Appendix E – Strain Gauge Bonding

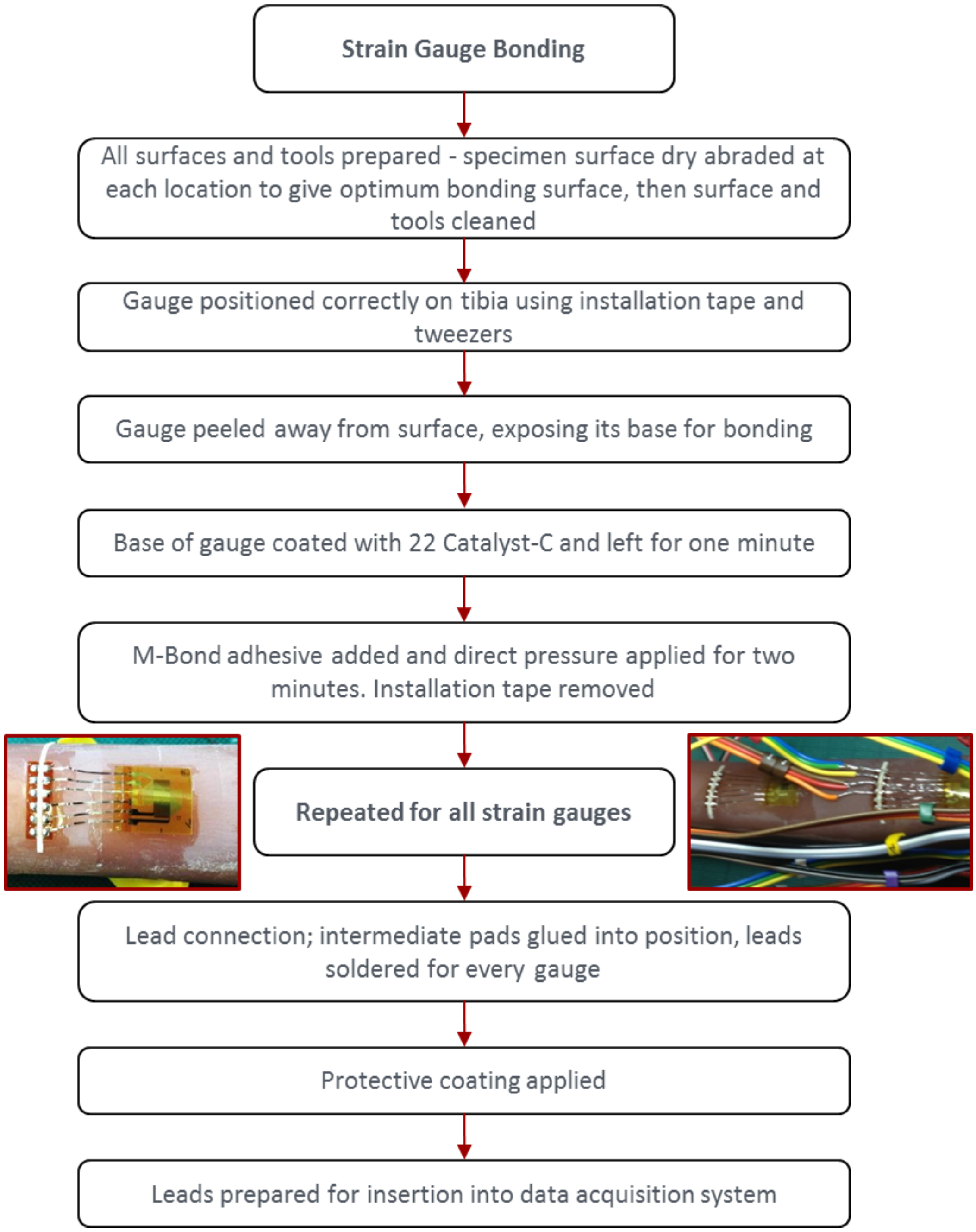

Figure 86 – A summary of the process of strain gauge bonding used for five strain gauge rosettes on each of the five tibia specimen

Appendix F – Strain Calculations

To convert the strain gauge voltage output reading to Strain (Ɛ);

$$Ɛ = 4\ x\ \left(\frac{V_0}{V_S}\right)\ x\ \left(\frac{1}{S}\right)$$

Where;

$$V_0 = Output\ of\ the\ bridge\ before\ the\ amplifier = \frac{Rdn}{Amp\ Gain}$$

$$Rdn = Recorded\ voltage\ reading\ from\ LabVIEW$$

$$Amp\ Gain = 1000$$

$$VS = Supply\ Voltage = 5\ V$$

$$S = Gauge\ Factor = 2.1$$

The convert the reading from the three gauges in each rosette principal minimum and maximum strains;

$$\varepsilon_{P,Q} = \left(\frac{\varepsilon_1 + \varepsilon_3}{2}\right) \pm \frac{1}{\sqrt{2}} \sqrt{(\varepsilon_1 - \varepsilon_2)^2 + (\varepsilon_2 - \varepsilon_3)^2}$$

$$\theta = \frac{1}{2} \tan^{-1}\left(\frac{\varepsilon_1 - 2\varepsilon_2 + \varepsilon_3}{\varepsilon_1 - \varepsilon_3}\right)$$

Where;

$Ɛ_1$, $Ɛ_2$, $Ɛ_3$ are the output strains from each gauge of a rosette

$Ɛ_P$ and $Ɛ_Q$ are the maximum and minimum principal strains

θ is the direction of principal strain

Publications

The following publications have been made related to this research in addition to the two journal articles which are in progress.

Wright, S.J., Gheduzzi, S and Miles, A. W. 'Traditional or novel knee loading techniques: A comparison of in vitro strain distribution in composite tibias following revision total knee replacement (RTKR)'. International Society for Technology in Arthroplasty 28th Annual Congress, Vienna; September 2015. Abstract accepted for Oral Presentation.

Wright, S.J., Gheduzzi, S and Miles, A. W. 'Tibial Strain Distribution following RTKR Surgery using Precise Compartmental Physiological Loading'. European Society of Biomechanics 21st Congress, Prague; July 2015. Oral Presentation. *See Abstract below.*

Wright, S.J., Gheduzzi, S and Miles, A. W. 'The Effect of Altering the Medial to Lateral Load Transfer through the Knee Joint in TKA'. British Orthopaedic Research Society Annual Meeting, UK; June 2014. Poster Presentation. *See Appendix C.*

Wright, S.J., Holsgrove, T., Forder, J and Miles, A. W. 'The Effect of Implanting a Revision Tibial Knee Component on the Surface Strain of the Tibia: An In Vitro Analysis using Digital Image Correlation'. 7th World Congress of Biomechanics, Boston; July 2014. Poster Presentation.

Tibial Strain Distribution following RTKR Surgery using Precise Compartmental Physiological Loading

European Society of Biomechanics 2015

Accepted abstracted for Oral Presentation

Introduction

The implantation of stemmed tibial components during revision total knee replacement (RTKR) surgery is believed to alter the strain distribution through the tibia and lead to proximal bone resorption and patient reported pain at the stem tip. Additionally, the in vivo use of instrumented tibial components has demonstrated that the compartmental load share across the tibial condyles changes during daily living activities [Mundermann, 2008]. Despite this, compartmental load share is not directly measured or controlled in experimental studies that assess load transfer through the tibia.

The aim of this study was to assess the load distribution through the tibia before and after implantation of RTKR components, whilst monitoring compartmental load distribution. An experimental rig was developed that replicated physiological loading through the knee, including a method to measure and control the compartmental load share across the tibial condyles. The investigation employed force sensors to measure compartmental load and strain gauges to provide the cortical strains in a composite tibia as an indication of load transfer through the bone. This investigation will further understanding of the effect of stemmed tibial components on the strain levels through the tibia and guide future implant designs to improve patient outcomes.

Methods

An experimental rig was developed to replicate knee loading conditions and allow the adjustment of the compartmental load share in the tibial condyles (Figure 1). Five composite tibias (4th Generation Sawbones) were prepared with five strain gauge rosettes (HBM) and tested under physiological loading. The loading through the medial and lateral compartments was measured using two force sensors in the condyles (Tekscan) and adjusted prior to each test. The cortical strains were recorded under a 500 N load applied at 0° and 10° of flexion by a hydraulic test machine. The five tibias were then implanted with Stryker Triathlon components according to surgical protocol and testing was repeated.

Results

Preliminary test results verified the use of the force sensors to measure the load share and illustrated the relationship between compartmental loading and strain distribution through the tibia.

The strain gauge results were processed to calculate the principal strain values and averaged across the five specimens. An example of the results for a single gauge is presented in Figure 2. The implantation of a tibial component produced a significant reduction in strain in the three proximal gauges and at the mid stem region (Within Subjects ANOVA $p<0.0125$). There was also a significant increase in strain at the stem tip with 0° flexion after implant insertion.

Discussion

The significant reduction in strain in the proximal tibia aligned with the proximal bone resorption that has been reported post-RTKR. The increase in strain around the stem tip correlates with the pain that can be reported by patients after surgery. These results should guide future implant design to improve how load is transferred through the tibia and advance clinical outcomes. The specific design to adjust for physiological loading also highlights the importance of incorporating the compartmental load share into pre-clinical assessment techniques.

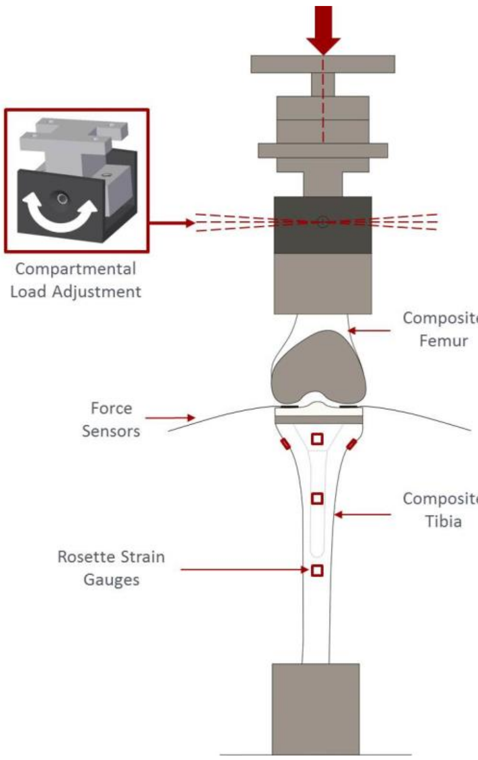

Figure 1: The experimental rig capable of physiological loading through the knee with a RTKR to measure the strain distribution through the tibia.

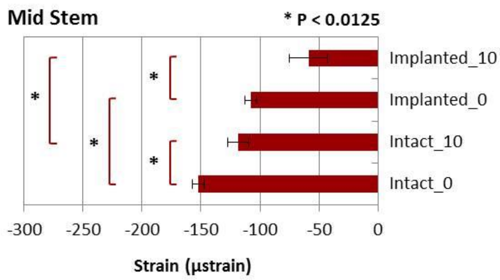

Figure 2: This example shows the principal strain measured at the mid stem gauge averaged across all five specimens during four loading scenarios.

References

Mundermann, A., *et al*. J Orthop Res, 26(9): 1167-72, 2008